Exchange-correlation functionals from ab initio potentials

Giuseppina Menconi

Exchange-Correlation Functionals from *ab initio* Potentials

Giuseppina Menconi

Graduate Society

Department of Chemistry

University of Durham

2002

A thesis submitted in partial fulfillment of the requirements for the degree of Doctor of Philosophy

Abstract

An accurate description of the exchange-correlation energy is central to density functional theory (DFT). In this thesis a series of exchange-correlation functionals are developed using new approaches based on exchange-correlation potentials and enhancement factors. The functionals are assessed for a wide range of molecular properties.

Chapter 1 describes Hartree Fock theory, introducing the key concepts of exchange and correlation. Chapter 2 describes the fundamental ideas of DFT and the implementation of Kohn-Sham theory. Chapter 3 describes a new approach for determining exchange-correlation functionals solely from *ab initio* potentials. A series of functionals are developed and assessed. Chapter 4 investigates the performance of one of these functionals, which provides particularly high quality structural predictions. A challenging benchmark of sulfur-containing compounds and a new benchmark of diatomic molecules are considered. Results are assessed in terms of the enhancement factor. In Chapter 5, the enhancement factor is used to develop new functionals that satisfy several exact physical conditions. The potential energy curve of the Helium dimer is investigated, since this is known to be sensitive to the enhancement factor. In Chapter 6 a series of hybrid functionals are determined. Particular attention is paid to their performance for chemical reactions and the relationship of these results to self-interaction errors. Chapter 7 investigates a new definition of the exchange-correlation charge (hole), which is directly related to the exchange-correlation potential. The first such calculations on molecular systems are presented. Concluding remarks are presented in Chapter 8.

Acknowledgments

I would like to express my sincere gratitude to Dr. David J. Tozer for his supervision and constant encouragement during the period of my research in Durham. Special thanks goes to Dr. Philip Wilson, whose help has been very important and to Dr. Lydia Heck, who has been always ready to assist me with computational matters.

I would like to thank all the friends of the theoretical chemistry groups in rooms CG207 and CG209, for having made my time in Durham so enjoyable.

A very special thank-you goes to my family and to Paolo for their constant support.

Declaration

The material contained within this thesis has not previously been submitted for a degree at the University of Durham or any other university. The research reported within this thesis has been conducted by the author unless indicated otherwise.

To my family

Contents

List of Figures

List of Tables

Chapter 1

Theoretical background

In this chapter, following a brief discussion of the Schrödinger equation and the Born-Oppenheimer approximation, we describe in detail the Hartree-Fock approximation, as it contains many of the features of density functional theory (DFT), which is the subject of this thesis. We describe how to derive and solve the Hartree-Fock equations. We introduce the concept of a basis set, explaining the reasons for their introduction in practical calculations. We introduce the concepts of exchange and correlation, presenting an overview of the correlated methods that we will utilize in the following chapters.

1.1 The Schrödinger equation

According to quantum mechanics, any problem in the structure of matter is covered by the solutions of the Schrödinger partial differential equation [1]-[3]. In atomic units ($e = \hbar = m_e = 4\pi\epsilon_0 = 1$)

$$\hat{H}\Psi = E\Psi \tag{1.1}$$

where $\hat{H}$ is the Hamiltonian differential operator, which contains the kinetic and potential energy operators of the nuclei and electrons

$$\hat{H} = -\sum_A \frac{\nabla_A^2}{2M_A} - \sum_i \frac{\nabla_i^2}{2} - \sum_{iA} \frac{Z_A}{r_{iA}} + \sum_{i>j} \frac{1}{r_{ij}} + \sum_{A>B} \frac{Z_A Z_B}{R_{AB}}. \tag{1.2}$$

This is the non-relativistic Hamiltonian, appropriate for relatively light atoms. E is the numerical value of the energy of the states, that is the energy relative to a state where the constituent particles are infinitely separated and at rest. Ψ is the wavefunction, which depends on the cartesian coordinates of all the particles and also on their spin coordinates. It contains all the information that can be known about the system.

In order to solve the Schrödinger equation it is necessary to impose boundary conditions. The wavefunction must be well-behaved everywhere; it must decay to zero at infinity for an atom or a molecule; it must obey appropriate periodic boundary conditions for a solid. There are many acceptable independent solutions for a given system, corresponding to different stationary states, and the state with the lowest energy is termed the ground state.

1.1.1 The Born-Oppenheimer approximation

The first approximation used to simplify the Schrödinger equation is the Born-Oppenheimer approximation [4], which is regarded as accurate and simple. Its underlying assumption is to consider the significant difference between the mass of the nuclei and the mass of the electrons. The nuclei, as compared to the rapidly moving electrons, move slowly. We can therefore consider the electrons as moving in a field of fixed nuclei; the problem can then be reduced to a separate nuclear and electronic problem. The electronic Schrödinger equation is

$$\hat{H}_e \Psi_e = E_e \Psi_e \tag{1.3}$$

where the electronic Hamiltonian $\hat{H}_e$ is

$$\hat{H}_e = -\sum_i \frac{\nabla_i^2}{2} - \sum_{iA} \frac{Z_A}{r_{iA}} + \sum_{i>j} \frac{1}{r_{ij}} \tag{1.4}$$

Ψ_e in Eq.(1.3) represents the wavefunction describing the motion of the electrons; it depends explicitly on the electronic coordinates and parametrically on the nuclear coordinates. This means that for different arrangements of

the nuclei, the wavefunction Ψ_e is a different function of the electronic coordinates. The total electronic energy, E_e is then the sum of the electronic energy and the nuclear-nuclear repulsion energy. The variation of E_e with nuclear coordinates defines the potential energy surface (PES).

1.2 The Hartree-Fock approximation

The cornerstone among the conventional wavefunction-based quantum chemical methods is the Hartree-Fock approximation [5, 6], which forms the basis for more accurate approximations including the effects of electron correlation. The wavefunction must be antisymmetric with respect to the interchange of space and spin coordinates of any pair of electrons (Pauli principle). Hence, the simplest approximation, which defines Hartree-Fock theory, is a single determinant (Slater determinant) [7].

$$\Psi_{\text{HF}}(\mathbf{x}_1, \mathbf{x}_2, \cdots, \mathbf{x}_N) = \frac{1}{\sqrt{N!}} \begin{vmatrix} \chi_1(\mathbf{x}_1) & \chi_2(\mathbf{x}_1) & \cdots & \chi_N(\mathbf{x}_1) \\ \chi_1(\mathbf{x}_2) & \chi_2(\mathbf{x}_2) & \cdots & \chi_N(\mathbf{x}_2) \\ \vdots & \vdots & & \vdots \\ \chi_1(\mathbf{x}_N) & \chi_2(\mathbf{x}_N) & \cdots & \chi_N(\mathbf{x}_N) \end{vmatrix} \tag{1.5}$$

This is an antisymmetrized product of N-orthonormal one-electron spin orbitals $\chi_i(\mathbf{x}_i)$, each composed of a spatial orbital $\varphi_i(\mathbf{r})$, and one of two orthonormal spin functions $\alpha(s)$, $\beta(s)$. The prefactor in front of the determinant normalizes the wavefunction. The antisymmetric nature of the wavefunction is ensured by the property of the determinant for which a change of two rows or columns i and j changes the sign, which corresponds to an interchange of the space-spin coordinates of the electrons i and j. The central idea of the Hartree-Fock method is to find the set of spin orbitals $\{\chi_i\}$ that minimize the electronic energy by applying the variational principle and maintaining, as a constraint, that the spin orbitals remain orthonormal.

The expectation value of the electronic Hamiltonian is the Hartree-Fock

energy E_{HF}

$$E_{\text{HF}} = \langle \Psi_{\text{HF}} | \hat{H} | \Psi_{\text{HF}} \rangle = \sum_{i=1}^{N} (i|\hat{h}|i) + \frac{1}{2} \sum_{i,j=1}^{N} [(ii|jj) - (ij|ji)] \tag{1.6}$$

where we use the integral notation

$$(p|\hat{h}|q) = \int \chi_p(\mathbf{x}) \left(-\frac{1}{2}\nabla^2 - \sum_{iA} \frac{Z_A}{r_{iA}} \right) \chi_q(\mathbf{x}) d\mathbf{x} \tag{1.7}$$

$$(pq|rs) = \int \int \frac{\chi_p(\mathbf{x})\chi_q(\mathbf{x})\chi_r(\mathbf{x}')\chi_s(\mathbf{r}')}{|\mathbf{x} - \mathbf{x}'|} d\mathbf{x} d\mathbf{x}' \tag{1.8}$$

assuming real orbitals. The first term in Eq.(1.6) is the sum of the kinetic energy and the nuclear-electron attraction. The next term is the classical repulsion for the electron density and the last term is the exchange energy.

The exchange energy arises entirely from the antisymmetric nature of the wavefunction. Two electrons of like spin cannot be at the same point in space. Hence, the probability reduces as the two electrons approach each other, causing a lowering of the energy. In other words, each electron is surrounded by an exchange hole, also known as a Fermi hole [8, 9].

An important aspect of Eq.(1.6) is the issue of self-interaction. When $i = j$, there is an unphysical behaviour, in that the Coulomb term would represent the interaction of the charge distribution with itself. However the expression for the exchange energy is exactly the same and so cancels. This is not achieved in practical density functional theory (See Chapter 2). Minimizing Eq.(1.6) with respect to the variations

$$\chi_i \rightarrow \chi_i + \delta\chi_i \tag{1.9}$$

subject to the constraint that the spin orbitals remain orthonormal

$$\langle \chi_i | \chi_j \rangle = \delta_{ij} \tag{1.10}$$

gives the Hartree-Fock equations

$$\hat{F}\chi_i = \sum_j \varepsilon_{ij}\chi_j \tag{1.11}$$

where ε_{ij} is the matrix of Lagrange multipliers. This can then be transformed via a unitary transformation to the usual canonical form

$$\hat{F}\chi_i = \varepsilon_i\chi_i \tag{1.12}$$

where the Lagrange multipliers ε_i are orbital energies and the Fock operator $\hat{F}$ is a one-electron operator

$$\hat{F}(\mathbf{x}_1) = -\frac{1}{2}\nabla_1^2 - \sum_A^M \frac{Z_A}{r_{1A}} + \hat{J}(\mathbf{x}_1) - \hat{K}(\mathbf{x}_1). \tag{1.13}$$

The first two terms represent the kinetic energy operator and the potential operator, which describes the attraction of a single electron by the nuclei. The other two are the Coulomb $\hat{J}$ and the exchange $\hat{K}$ operators defined by

$$\hat{J}(\mathbf{x}_1)\chi_i(\mathbf{x}_1) = \left[\sum_j \int \chi_j(\mathbf{x}_2)\frac{1}{r_{12}}\chi_j(\mathbf{x}_2)d\mathbf{x}_2\right]\chi_i(\mathbf{x}_1) \tag{1.14}$$

$$\hat{K}(\mathbf{x}_1)\chi_i(\mathbf{x}_1) = \sum_j \int \chi_j(\mathbf{x}_2)\frac{1}{r_{12}}\chi_i(\mathbf{x}_2)d\mathbf{x}_2\chi_j(\mathbf{x}_1) \tag{1.15}$$

It is important to point out the different nature of these two operators. The effect of the exchange operator on the spin orbital $\chi_i(\mathbf{x}_1)$ depends on the value of χ_i throughout all of space. For this reason it is termed *non-multiplicative*. All others operators in Eq.(1.13) are instead multiplicative; their values depend only on the value of χ_i at $\mathbf{x}_1$. The Hartree-Fock method formally scales as N^4 with the size of the system.

1.2.1 Koopmans' theorem

A physical interpretation for the Lagrange multipliers ε_i introduced in the minimization procedure is obtained from the Koopmans' theorem [10]. We consider the energy of a system in which one electron is removed from the orbital k and assume that the system does not relax. At this point the energy expressions for the two systems (closed-shell and open-shell after the electron removal) would be

$$E_N = \sum_{i=1}^{N}(i|\hat{h}|i) + \frac{1}{2}\sum_{i=1}^{N}\sum_{j=1}^{N}(ii|jj) - (ij|ji) \tag{1.16}$$

$$E_{N-1}^{k} = \sum_{i=1}^{N-1}(i|\hat{h}|i) + \frac{1}{2}\sum_{i=1}^{N-1}\sum_{j=1}^{N-1}(ii|jj) - (ij|ji). \tag{1.17}$$

Subtracting the two energies

$$E_N - E_{N-1}^{k} = (k|\hat{h}|k) + \frac{1}{2}\sum_{i=1}^{N}(ii|kk) - (ik|ki) + \frac{1}{2}\sum_{j=1}^{N}(kk|jj) - (kj|jk) \tag{1.18}$$

since the last two terms are identical, the energy difference becomes

$$E_N - E_{N-1}^{k} = (k|\hat{h}|k) + \sum_{i=1}^{N}(kk|ii) - (ki|ik) = \varepsilon_k \tag{1.19}$$

The theorem proves that within the Hartree Fock approximation the orbital energy ε_k is an approximation to minus the ionization energy associated with the removal of an electron from the orbital χ_k. See Chapter 2 for a discussion of Koopmans' theorem in density functional theory.

1.2.2 Unrestricted Hartree-Fock (UHF)

In the unrestricted Hartree-Fock method, the spin orbitals are not constrained to have the same spatial form

$$\chi_i(\mathbf{x}) = \begin{cases} \varphi_i^{\alpha}(\mathbf{r})\alpha(s) \\ \varphi_i^{\beta}(\mathbf{r})\beta(s) \end{cases} \tag{1.20}$$

We use an unrestricted formalism for all the open-shell calculations in this thesis. To define φ_i^{α} and φ_i^{β} we substitute the spin orbitals into the Hartree Fock equations and integrate over the spin functions. The resulting equations are

$$\hat{F}^{\alpha}\varphi_i^{\alpha} = \varepsilon_i^{\alpha}\varphi_i^{\alpha} \tag{1.21}$$

$$\hat{F}^{\beta}\varphi_i^{\beta} = \varepsilon_i^{\beta}\varphi_i^{\beta} \tag{1.22}$$

where

$$\hat{F}^{\alpha}(\mathbf{x}_1) = h(\mathbf{x}_1) + J^{\alpha}(\mathbf{x}_1) + J^{\beta}(\mathbf{x}_1) - K^{\alpha}(\mathbf{x}_1) \tag{1.23}$$

The electrons of spin α experience a Coulomb interaction $J^{\alpha} + J^{\beta}$ due to all the electrons and an exchange interaction $-K^{\alpha}$ arising from each of the spin α electrons. The Fock operator for the β spin is

$$\hat{F}^{\beta}(\mathbf{x}_1) = h(\mathbf{x}_1) + J^{\alpha}(\mathbf{x}_1) + J^{\beta}(\mathbf{x}_1) - K_i^{\beta}(\mathbf{x}_1) \tag{1.24}$$

Equations (1.21)-(1.22) are coupled ($\hat{F}^{\alpha}$ depends on the occupied β orbitals and viceversa) hence they must be solved in an iterative procedure.

1.2.2.1 The Pople-Nesbet equations

To solve the unrestricted Hartree-Fock equations it is necessary to introduce a basis set expansion for the unrestricted molecular orbitals φ_i^{α} and φ_i^{β}

$$\varphi_i^{\alpha} = \sum_{\mu} C_{\mu i}^{\alpha} \eta_{\mu} \tag{1.25}$$

$$\varphi_i^{\beta} = \sum_{\mu} C_{\mu i}^{\beta} \eta_{\mu} \tag{1.26}$$

where η_{μ} is a set of one-electron basis functions. Substituting into Eq.(1.21)-(1.22) we obtain

$$\sum_{\mu} (\hat{F}^{\alpha} - \varepsilon_i^{\alpha}) C_{\mu i}^{\alpha} \eta_{\mu} = 0 \tag{1.27}$$

$$\sum_{\mu} (\hat{F}^{\beta} - \varepsilon_i^{\beta}) C_{\mu i}^{\beta} \eta_{\mu} = 0 \tag{1.28}$$

Multiplying Eq.(1.27)-(1.28) on the left by a function $\eta_{\lambda}(\mathbf{r})$ and integrating over the spatial coordinates gives the Pople-Nesbet equations [11]

$$\sum_{\mu} F_{\lambda\mu}^{\alpha} C_{\mu i}^{\alpha} = \varepsilon_i^{\alpha} \sum_{\mu} S_{\lambda\mu} C_{\mu i}^{\alpha} \tag{1.29}$$

$$\sum_{\mu} F_{\lambda\mu}^{\beta} C_{\mu i}^{\beta} = \varepsilon_i^{\beta} \sum_{\mu} S_{\lambda\mu} C_{\mu i}^{\beta} \tag{1.30}$$

Equations (1.29)-(1.30) can be rewritten in matrix form as

$$\mathbf{F}^{\alpha}\mathbf{C}^{\alpha} = \mathbf{S}\mathbf{C}^{\alpha}\varepsilon^{\alpha} \tag{1.31}$$

$$\mathbf{F}^{\beta}\mathbf{C}^{\beta} = \mathbf{S}\mathbf{C}^{\beta}\varepsilon^{\beta} \tag{1.32}$$

where $\mathbf{S}$ is the basis function overlap matrix and $\mathbf{F}$ is the matrix representation of the Fock operator in the basis η_{μ}. The procedure to solve them is iterative. It starts with a guess for the $\mathbf{F}^{\alpha}$ and $\mathbf{F}^{\beta}$ matrices; once Eq.(1.31)-(1.32) are solved, new values for $\mathbf{C}^{\alpha}$ and $\mathbf{C}^{\beta}$ are obtained. The process stops only when self-consistency is achieved.

1.2.3 Restricted Hartree-Fock (RHF)

In a restricted formalism the α and β spin orbitals are constrained to have the same spatial part

$$\chi_i(\mathbf{x}) = \begin{cases} \varphi_i(\mathbf{r})\alpha(s) \\ \varphi_i(\mathbf{r})\beta(s) \end{cases} \tag{1.33}$$

The corresponding closed-shell Fock operator has the form

$$\hat{F}(\mathbf{x}_1) = h(\mathbf{x}_1) + 2J(\mathbf{x}_1) - K(\mathbf{x}_1) \tag{1.34}$$

and the closed-shell spatial Hartree-Fock equation is

$$\hat{F}\varphi_i = \varepsilon_i\varphi_i \tag{1.35}$$

1.2.3.1 The Roothaan-Hall equations

As in unrestricted Hartree-Fock, basis sets must be introduced. The corresponding equations are written as

$$\sum_{\mu}(F_{\lambda\mu} - \varepsilon_i S_{\lambda\mu})C_{\mu i} \tag{1.36}$$

or in matrix form

$$\mathbf{FC} = \mathbf{SC}\varepsilon. \tag{1.37}$$

These are the Roothaan-Hall equations [12, 13].

1.3 One-electron basis sets

It is therefore necessary to expand the molecular orbitals φ_i in terms of a set of basis functions η_μ to solve the Hartree-Fock equations. This procedure is exact only if the set of basis functions is complete. From a computational point of view this is impractical. However, in order to get high quality results, large basis sets are necessary.

In general, in the majority of the wavefunction-based methods, the set of basis functions η_μ is chosen to consist of gaussian-type orbitals (GTO) [14]

rather than Slater-type orbitals (STO) [15]. Gaussian-type orbitals have the general form

$$\eta^{\mathrm{GTO}}(\mathbf{r}) = Nx^l y^m z^n \exp(-\alpha r^2) \tag{1.38}$$

where N is a normalization factor ($\langle \eta_\mu | \eta_\mu \rangle = 1$), α is the orbital exponent which determines the amplitude of the function and $L = l + m + n$ describes the character of the GTO function. Slater-type orbitals, instead, are represented as

$$\eta^{\mathrm{STO}}(\mathbf{r}) = Nr^{n-1} \exp(-\xi r) Y_{lm}(\theta, \varphi) \tag{1.39}$$

where n is the principal quantum number, the orbital exponent is ξ and Y_{lm} constitutes the spherical harmonics that describe the angular part of the function.

The reason for the high applicability of GTO basis sets is their low computational cost with respect to STO basis sets [14]. However, from a physical point of view, the STO basis functions are more natural since the simple exponential mimics perfectly the exact orbitals of hydrogenic atoms. They have the correct cusp behaviour for $r \to 0$ and the proper exponential decay for $r \to \infty$. In order to get the same accuracy as with the STO, it is common practice to introduce the contracted-gaussian type orbitals [16]-[18], where several primitive gaussian functions are linearly combined to give a contracted function

$$\eta_\tau^{\mathrm{CGF}}(\mathbf{r}) = \Sigma_a^A d_{\tau a} \eta_a^{\mathrm{GTO}}(\mathbf{r}) \tag{1.40}$$

In this way it is possible to derive appropriate values for $d_{\tau a}$ so that a CGF basis function is as similar as possible to an STO [19, 20].

Different kinds of GTO are commonly used in electronic structure calculations, and they assume different names according to the nature of the functions involved. Minimal-basis set employs enough functions to contain all the electrons of the neutral atoms. By doubling or tripling the number of basis functions we obtain double zeta (DZ) or triple zeta (TZ) basis sets which, in general, provide a better description of how the electrons are

distributed in bonding regions.

Basis sets can also include higher angular momentum functions, namely polarization functions. For calculations that do not include correlation effects, the introduction of the first set of such functions is by far the most important since they introduce all the charge polarization effects. If methods including electron correlation are used, higher angular momentum functions are essential to obtain an accurate description of the electron-electron cusp.

Finally, we mention the concept of basis set superposition error (BSSE). If a calculation is performed on a system comprising of two fragments, then one of the fragments can artificially lower its energy by using the basis function on the other fragment. The conceptually simplest way to eliminate the BSSE is to use extremely large basis sets when these kinds of calculations are performed. However, this leads to very large and computationally expensive calculations. The approximate way to correct this error is to use the counterpoise (CP) correction [21], which approximates the BSSE error as the difference between monomer energies with the regular basis and the energies calculated with the full set of basis functions of the whole complex.

1.4 The correlation energy

The correlation energy is defined as the difference between the exact non-relativistic, Born-Oppenheimer ground state energy E_0 and the Hartree Fock energy [22] which, due to the variational principle, is always an upper bound

$$E_{\mathrm{C}} = E_0 - E_{\mathrm{HF}} \tag{1.41}$$

The correlation energy arises from the instantaneous repulsion of the electrons and it has traditionally been divided into two contributions. The first one is dynamic correlation (short-range) which is related to the reduction of the wavefunction when two electrons get close to each other [23]. This phenomenon is not accounted for in the Hartree-Fock method since each

electron experiences only an electrostatic potential spatially averaged over all the other electrons. The electrons get too close to each other.

The second contribution is non-dynamical correlation (long-range), also known as left-right correlation, which can be understood as the correlation effect which makes the electrons move to separate atoms as a molecule dissociates. In Hartree-Fock theory, such a phenomenon is not represented since the chosen Slater determinant can fail to describe properly the ground state of the molecule when there are different determinants with a very similar energy. Consider the H_2 molecule. The RHF scheme computed at the equilibrium distance provides a good approximation; the correlation error, which is mainly due to dynamic correlation, is small. However, when the molecule dissociates [24], the correlation energy error gets large, despite the fact that the dynamic correlation goes to zero. This is non-dynamical correlation.

A simple way to overcome this incorrect dissociation problem is to apply the UHF. This solution would lead to an exact description of this long range behaviour, but at the same time it will change the ground state of the molecule. It will no longer be a singlet, but a mixture of a singlet and a triplet. Therefore the exact behavior of the energy must be considered a consequence of the fact that the UHF wavefunction breaks the inversion symmetry axis of the molecule and puts an electron with spin up at one nucleus and the second one with opposite spin at the other nucleus [25]. In the same manner as for the exchange interaction, the correlation interaction generates a hole surrounding each electron, known as coulomb hole or correlation hole [26].

Within DFT the exchange and left-right correlation energies are naturally linked in local exchange approximation (See Chapter 3).

1.5 Post Hartree-Fock methods

The correlation energy is therefore a measure of the error in the Hartree-Fock approximation. For a system of many interacting electrons, the exact wavefunction can never be represented by a single determinant. It is therefore necessary to apply more sophisticated correlated methods. We now turn our attention towards two popular correlated methods: Møller-Plesset perturbation theory (MP) and the coupled cluster approximation (CC), both of which will be used later in this thesis.

1.5.1 Møller-Plesset perturbation theory

Møller-Plesset perturbation theory [28] has traditionally been very popular in quantum chemistry. Many levels of theory can be calculated. We will focus our attention on the second order corrections (MP2) since for the properties on which we are interested MP2 covers the most important correlation effects [29].

In Møller-Plesset theory, correlation effects are introduced stepwise in a systematic manner that facilitates their analysis and the understanding of the correlation problem. The method is size-consistent and its computational cost is not excessive and so medium-size and even larger molecules can be treated. The approach does have disadvantages. It is not variational, the energies can be more negative than the exact ones. At a given perturbation order p, there does not exist a well-defined wavefunction. This makes it impossible to define a molecular property in terms of an expectation value. Finally, sometimes it is possible to observe an erratic non monotonic convergence behaviour of the calculated MP energies [30, 31].

In Møller-Plesset theory the electronic Hamiltonian operator $\hat{H}$ is written as the sum of two parts

$$\hat{H} = \hat{H}_0 + \lambda \hat{V} \tag{1.42}$$

where $\hat{H}_0$ is the sum of the one-electron Hartree-Fock operators, $\hat{V}$ is a pertur-

bation operator and λ is a dimensionless parameter determining the strength of the perturbation. Increasing λ to a finite number, the new energy E and the new wavefunction Ψ associated with the perturbed Schrödinger equation are expanded as a Taylor series in terms of λ

$$E = \lambda^0 E_0 + \lambda^1 E_1 + \lambda^2 E_2 + ...\lambda^p E_p \tag{1.43}$$

$$\Psi = \lambda^0 \Psi_0 + \lambda^1 \Psi_1 + \lambda^2 \Psi_2 + ...\lambda^p \Psi_p \tag{1.44}$$

Truncation at first order gives MP1, which corresponds to the Hartree-Fock method. Truncation at second order gives MP2, which accounts for correlation effects

$$E_{\text{MP2}} = E_{\text{HF}} - \frac{1}{4} \sum_{ijab} \frac{(ij||ab)^2}{D_{ij}^{ab}} \tag{1.45}$$

where $\frac{1}{4}$ prevents double counting $(ij||ab)$ denotes

$$(ij||ab) = (ai|bj) - (aj|bi) \tag{1.46}$$

and

$$D_{ij}^{ab} = \varepsilon_a + \varepsilon_b - \varepsilon_i - \varepsilon_j \tag{1.47}$$

Formally MP2 scales as N^5, making it the most economical method for including correlation, after density functional theory.

1.5.2 Coupled Cluster theory

Møller-Plesset perturbation theory in principle adds all the types of corrections to the wavefunction up to a given order. In coupled cluster theory (CC) [32, 33] there is no limitation to the order [34], since all the infinite corrections are included. The formalism of this method is based on the representation of the wavefunction Ψ_{CC} in terms of the cluster operator $\hat{T}$ and the Hartree-Fock reference wavefunction Ψ_{HF}

$$\Psi_{\text{CC}} = \exp(\hat{T}) \cdot \Psi_{\text{HF}} \tag{1.48}$$

where

$$\exp(\hat{T}) = 1 + \hat{T} + \frac{1}{2}\hat{T}^2 + \frac{1}{6}\hat{T}^3 + ... = \sum_{k=0}^{\infty} \frac{1}{k!}\hat{T}^k \tag{1.49}$$

Acting with the operator $\hat{T}$ on the Hartree-Fock reference wavefunction, generates all the excited Slater determinants

$$\hat{T}_1\Psi_{\text{HF}} = \sum_{i}^{\text{occ}} \sum_{a}^{\text{vir}} t_i^a \Psi_i^a \tag{1.50}$$

$$\hat{T}_2\Psi_{\text{HF}} = \sum_{i<j}^{\text{occ}} \sum_{a<b}^{\text{vir}} t_{ij}^{ab} \Psi_{ij}^{ab} \tag{1.51}$$

where t are the expansion coefficients. Substituting Eq. (1.48) into the Schrödinger equation and integrating, we obtain the expression for the coupled-cluster energy for different excitations. Since the energy depends on the level of excitations, in order to obtain accurate results, it is necessary to include higher excitations, but from a computational point of view this is unfeasible for all but small molecular systems. The level of excitation is defined by the number of terms constituting the cluster operator. Including only $\hat{T}_1$ will provide results of the same degree of accuracy as Hartree-Fock. Hence, the lowest level of approximation required to include correlation effects is $\hat{T}_2$, which is then known as Coupled-Cluster-Doubles (CCD) whose computational cost is N^6.

A sub-category of coupled cluster methods is represented by CCSD(T) and CCSD(TQ) [35]. They include additional terms obtained from higher orders of perturbation theory. They are still computationally very demanding ($\sim N^7$ for CCSD(T)) although they are cheaper than conventional coupled-cluster methods at the same level of accuracy ($\sim N^8$) for CCSDT [36, 37].

For all the methods discussed so far, the single excitations do not provide any substantial contribution to the correlation energy when the Hartree-Fock orbitals are used. Brueckner theory [38, 39] is a variation of the coupled cluster method. Brueckner orbitals are optimized so that the contribution from the singles is exactly zero ($t_i^a = 0$). Hence, the lowest level of Brueckner theory includes only doubles excitations, giving the acronym BD.

In theory, this method should provide a higher accuracy than CCSD. However, in practice it provides comparable results with comparable computational costs. Similarly, BD(T) is essentially equivalent to CCSD(T) [40] and BD(TQ) to CCSD(TQ).

Chapter 2

Density functional theory

Since the rigorous development of density functional theory forty years ago, the method has become extremely useful for understanding molecular properties. It represents an alternative approach to the traditional wave function based methods which are described in terms of the many electron wavefunction $\Psi(\mathbf{r}_1....\mathbf{r}_N)$. The chief building blocks of traditional methods are single-electron orbitals $\varphi_i(\mathbf{r})$ and the many electron wavefunction built from them, in DFT instead the chief element is the electron density $\rho(\mathbf{r})$ and in the Kohn-Sham approach the single-particle orbitals $\varphi_i^{\mathrm{KS}}(\mathbf{r})$.

In this chapter, following a definition of the electron density, we discuss density functional theory, from the early work of Thomas, Fermi and Dirac to the celebrated Kohn-Sham approach. Particular attention is paid to the exchange-correlation potential. We also present an overview of the various approximations to the exchange-correlation energy, which we will apply in the later chapters.

2.1 The electron density

The central quantity in DFT is the electron density $\rho(\mathbf{r})$, a non-negative function, which vanishes at infinity and integrates to the total number of electrons N. It is represented as a multiple integral over the spin coordinates

of all the electrons and over all but one of the spatial coordinates

$$\rho(\mathbf{r}_1) = N \int ... \int |\Psi(\mathbf{x}_1....\mathbf{x}_N)|^2 ds_1 d\mathbf{x}_2 ... d\mathbf{x}_N \tag{2.1}$$

It represents the probability measure of finding any of the N electrons within the volume element $d\mathbf{r}_1$. The electron density also provides information about the nuclear charge Z of the nuclei due to the cusp condition [41], see Ref. [42].

2.2 The models of Thomas, Fermi and Dirac

The first attempt to use the electron density rather than the wavefunction as a central quantity was introduced by Thomas and Fermi in 1927 [43]-[46]. They considered a quantum statistical model for a non-interacting uniform electron gas (UEG). Since direct expressions in terms of the electron density for the nuclear-electron attraction and for the classical electron-electron repulsion contributions were known, Thomas and Fermi derived a corresponding definition of the kinetic energy in terms of the electron density

$$T_{\text{TF}}[\rho(\mathbf{r})] = \frac{3}{10}(3\pi^2)^{\frac{2}{3}} \int \rho^{\frac{5}{3}}(\mathbf{r}) d\mathbf{r} \tag{2.2}$$

The total energy functional is then the sum of the kinetic energy functional Eq.(2.2) and the classical terms

$$E_{\text{TF}}[\rho(\mathbf{r})] = \frac{3}{10}(3\pi^2)^{\frac{2}{3}} \int \rho^{\frac{5}{3}}(\mathbf{r}) d\mathbf{r} - Z \int \frac{\rho(\mathbf{r})}{r} d\mathbf{r} + \frac{1}{2} \int \int \frac{\rho(\mathbf{r})\rho(\mathbf{r}')}{|\mathbf{r} - \mathbf{r}'|} d\mathbf{r} d\mathbf{r}' \tag{2.3}$$

This is known as the Thomas-Fermi model (TF). In 1930, Dirac added an exchange contribution [47]

$$K_{\text{D}}[\rho(\mathbf{r})] = -\frac{3}{4}\left(\frac{3}{\pi}\right)^{\frac{1}{3}} \int \rho^{\frac{4}{3}}(\mathbf{r}) d\mathbf{r} \tag{2.4}$$

obtained by evaluating the exchange expression with plane-waves orbitals, which are appropriate for a UEG. The $\frac{4}{3}$ power is easily derived from scaling conditions. Suppose we write

$$K_{\text{D}}[\rho(\mathbf{r})] = \int \rho^n(\mathbf{r}) d\mathbf{r} \tag{2.5}$$

then for the scaled electron density

$$\rho_\lambda(\mathbf{r}) = \lambda^3 \rho(\lambda \mathbf{r}) \tag{2.6}$$

the exact exchange energy must satisfy

$$K[\rho_\lambda(\mathbf{r})] = \lambda K[\rho(\mathbf{r})] \tag{2.7}$$

Hence, for Eq.(2.5)

$$\int \lambda^{3n} \rho^n(\lambda \mathbf{r}) d\mathbf{r} = \lambda \int \rho^n(\mathbf{r}) d\mathbf{r} \tag{2.8}$$

Substituting $x' = \lambda x, y' = \lambda y, z' = \lambda z$, this becomes

$$\lambda^{3n} \int \rho^n(\mathbf{r}') \frac{d\mathbf{r}'}{\lambda^3} = \lambda \int \rho^n(\mathbf{r}) d\mathbf{r} \tag{2.9}$$

or

$$\lambda^{3n-3} \int \rho^n(\mathbf{r}') d\mathbf{r}' = \lambda \int \rho^n(\mathbf{r}) d\mathbf{r} \tag{2.10}$$

which requires n to equal $\frac{4}{3}$. Including Eq.(2.4) in the Thomas-Fermi model leads to the Thomas-Fermi-Dirac model (TFD) [48].

The importance of these models stems from the fact that the energy was completely expressed in terms of the electron density $\rho(\mathbf{r})$ and not from the accuracy of their predictions. The assumptions of a non-interacting UEG do not hold for atomic and molecular systems. Energy errors are typically 15-50%, but more seriously neither TF nor TFD predict molecular binding.

2.3 Hohenberg-Kohn theorems

In 1964 Hohenberg and Kohn [49] proved in their two theorems how the previous TF and TFD models could be considered as an approximation of an exact ground-state theory.

Quoting from the Hohenberg-Kohn paper, the first theorem states that *'The external potential v is determined within a trivial additive constant by the electron density $\rho(\mathbf{r})$'*. Since, in turn, $\rho(\mathbf{r})$ integrates to the number of the

electrons, it follows that $\rho(\mathbf{r})$ also determines the ground-state wavefunction Ψ and all the other properties of the molecule.

The proof of the theorem is based on a *reduction ad absurdum*. Consider two external potentials v_{ext} and v'_{ext} that differ by more than a constant, but give rise to the same electron density $\rho(\mathbf{r})$. The two Hamiltonians $\hat{H}$ and $\hat{H}'$ then differ only by the potential

$$\hat{H} = \hat{T} + V_{\text{ee}} + v_{\text{ext}} \tag{2.11}$$

$$\hat{H}' = \hat{T} + V_{\text{ee}} + v'_{\text{ext}} \tag{2.12}$$

where $\hat{T}$ and $\hat{V}_{ee}$ are the kinetic and electron-electron repulsion operators. The two Hamiltonians $\hat{H}$ and $\hat{H}'$ give two different energies and wavefunctions but their associated electron density is the same. Using Ψ' as a trial function for the $\hat{H}$ problem, applying the variational principle gives

$$E_0 < \langle \Psi' | \hat{H} | \Psi' \rangle = \langle \Psi' | \hat{H}' | \Psi' \rangle + \langle \Psi' | \hat{H} - H' | \Psi' \rangle = E'_0 + \int \rho(\mathbf{r})[v_{\text{ext}} - v'_{\text{ext}}] d\mathbf{r} \tag{2.13}$$

taking instead Ψ as a trial function for $\hat{H}'$ we have

$$E'_0 < \langle \Psi | \hat{H}' | \Psi \rangle = E_0 - \int \rho(\mathbf{r})[v_{\text{ext}} - v'_{\text{ext}}] d\mathbf{r} \tag{2.14}$$

Adding the two energy expressions above we obtain the contradiction

$$E_0 + E'_0 < E'_0 + E_0 \tag{2.15}$$

Hence, the electron density determines all the ground state properties of a molecular system, and the total energy of a system can be written in terms of the external potential as

$$E_{v_{\text{ext}}}[\rho] = \int \rho(\mathbf{r}) v_{\text{ext}}(\mathbf{r}) d\mathbf{r} + F_{\text{HK}}[\rho] \tag{2.16}$$

where $F_{\text{HK}}[\rho]$, the Hohenberg-Kohn functional, is a universal functional of the electron density, including the kinetic energy of the system, the classical Coulomb repulsion and all the remaining non-classical terms

$$F_{\text{HK}}[\rho] = T[\rho] + J[\rho] + \text{nonclassical terms.} \tag{2.17}$$

The second theorem is the variational principle in DFT. Its existence is necessary in order to ensure that the electron density used to predict the properties of interest is the exact one which minimizes the energy of the molecule. The theorem states that *'For a trial density* $\tilde{\rho}(\mathbf{r})$ *such that* $\tilde{\rho}(\mathbf{r}) \geq 0$ *and* $\int \tilde{\rho}(\mathbf{r})d\mathbf{r} = N$

$$E_0 \leq E_{v_{ext}}[\tilde{\rho}] \tag{2.18}$$

where $E_{v_{ext}}$ *is the energy functional above.'*

The proof is based on the wavefunction variational principle. Any trial density $\tilde{\rho}(\mathbf{r})$ defines its own Hamiltonian $\tilde{H}$ and its own wavefunction $\tilde{\Psi}$; taking it as a trial wavefunction for the real Hamiltonian $\hat{H}$ generated by the true external potential $v_{\text{ext}}(\mathbf{r})$ we obtain

$$\langle\tilde{\Psi}|\tilde{\hat{H}}|\tilde{\Psi}\rangle = \int \tilde{\rho}(\mathbf{r})v_{\text{ext}}d\mathbf{r} + F_{\text{HK}}[\tilde{\rho}] = E[\tilde{\rho}] \geq E_{v_{\text{ext}}}[\rho] = \langle\psi_0|\hat{H}|\psi_0\rangle \tag{2.19}$$

By imposing that $E_{v_{\text{ext}}}$ is differentiable, and introducing the Lagrange multipliers μ, to enforce the condition that the electron density integrates to the total number of electrons, the variational principle Eq.(2.18) requires that the Euler-Lagrange equation

$$\mu = \frac{\delta E_v[\rho]}{\delta\rho(\mathbf{r})} = v_{\text{ext}}(\mathbf{r}) + \frac{\delta F_{\text{HK}}[\rho]}{\delta\rho(\mathbf{r})} \tag{2.20}$$

must be satisfied.

2.4 The Kohn-Sham approach

In 1965, Kohn and Sham observed that most of the problems related with the Thomas-Fermi and Dirac models were connected with the poor description of the kinetic energy [50]. Hence, they developed a new approach, introducing an auxiliary reference system of N non-interacting electrons moving in an external potential v_{S} whose density equals the true density. The Hamiltonian $\hat{H}_{\text{S}}$ for this system is

$$\hat{H}_{\text{S}} = -\frac{1}{2}\sum_i^N \nabla_i^2 + \sum_i^N v_{\text{S}}(\mathbf{r}_i) \tag{2.21}$$

and its wavefunction Ψ_S is a single Slater determinant

$$\Psi_S(\mathbf{x}_1, \mathbf{x}_2, \cdots, \mathbf{x}_N) = \frac{1}{\sqrt{N!}} \begin{vmatrix} \varphi_1^{KS}(\mathbf{x}_1) & \varphi_2^{KS}(\mathbf{x}_1) & \cdots & \varphi_N^{KS}(\mathbf{x}_1) \\ \varphi_1^{KS}(\mathbf{x}_2) & \varphi_2^{KS}(\mathbf{x}_2) & \cdots & \varphi_N^{KS}(\mathbf{x}_2) \\ \vdots & \vdots & & \vdots \\ \varphi_1^{KS}(\mathbf{x}_N) & \varphi_2^{KS}(\mathbf{x}_N) & \cdots & \varphi_N^{KS}(\mathbf{x}_N) \end{vmatrix} \tag{2.22}$$

The Kohn-Sham orbitals φ_i^{KS} are obtained from the one-electron equations

$$\hat{F}_{KS}\varphi_i^{KS} = \left[-\frac{1}{2}\nabla_i^2 + \upsilon_s(\mathbf{r}_i)\right]\varphi_i^{KS} = \varepsilon_i\varphi_i^{KS} \tag{2.23}$$

The kinetic energy T_S of this non-interacting system is then

$$T_S[\rho] = \sum_i^N \langle\varphi_i^{KS}\left|-\frac{1}{2}\nabla_i{}^2\right|\varphi_i^{KS}\rangle \tag{2.24}$$

and its density is

$$\rho(\mathbf{r}) = \sum_i |(\varphi_i^{KS})(\mathbf{r})|^2 \tag{2.25}$$

In the Kohn-Sham approach, the Hohenberg-Kohn functional $F_{HK}[\rho]$ is rewritten as

$$F_{HK}[\rho] = T_S[\rho] + J[\rho] + E_{XC}[\rho] \tag{2.26}$$

where

$$E_{XC}[\rho] = (T[\rho] - T_S[\rho]) + (V_{ee}[\rho] - J[\rho]) \tag{2.27}$$

is the exchange-correlation energy term including the difference between the real kinetic energy and that of the non-interacting system, and all the non-classical contributions to the electron repulsion. The total energy of the system is then

$$E[\rho] = T_S[\rho] + \int \rho(\mathbf{r})\upsilon_{ext}(\mathbf{r})d\mathbf{r} + J[\rho] + E_{XC}[\rho] \tag{2.28}$$

By applying the second Hohenberg-Kohn theorem to Eq.(2.28), recalling that the the electron density that minimizes the total energy $E[\rho]$ is the ground-state electron density which satisfies the Euler equation Eq.(2.20), we obtain

$$\mu = \frac{\delta T_S[\rho]}{\delta\rho(\mathbf{r})} + \upsilon_{ext}(\mathbf{r}) + \frac{\delta J[\rho]}{\delta\rho(\mathbf{r})} + \frac{\delta E_{xc}[\rho]}{\delta\rho(\mathbf{r})} \tag{2.29}$$

or

$$\mu = v_{\text{eff}}(\mathbf{r}) + \frac{\delta T_{\text{S}}[\rho]}{\delta \rho(\mathbf{r})} \tag{2.30}$$

where $v_{\text{eff}}(\mathbf{r})$ is the effective Kohn-Sham potential

$$v_{\text{eff}}(\mathbf{r}) = v_{\text{ext}}(\mathbf{r}) + \int \frac{\rho(\mathbf{r}')}{|\mathbf{r} - \mathbf{r}'|} d\mathbf{r}' + v_{\text{XC}}(\mathbf{r}) \tag{2.31}$$

and

$$v_{\text{XC}}(\mathbf{r}) = \frac{\delta E_{\text{XC}}[\rho]}{\delta \rho(\mathbf{r})} \tag{2.32}$$

is the exchange-correlation potential. Eq.(2.30) is the same as is obtained in conventional DFT (Eq.(2.20)) when applied to a non-interacting system with potential $v_{\text{eff}}(\mathbf{r})$. Hence, it is possible to obtain the electron density that minimizes the energy of the real system by solving the N one-electron Kohn-Sham equations

$$\left[-\frac{1}{2}\nabla^2 + v_{\text{eff}}(\mathbf{r})\right] \varphi_i^{\text{KS}}(\mathbf{r}) = \varepsilon_i \varphi_i^{\text{KS}}(\mathbf{r}) \tag{2.33}$$

with

$$\rho(\mathbf{r}) = \sum_i |\varphi_i^{\text{KS}}(\mathbf{r})|^2 \tag{2.34}$$

The total energy expression Eq.(2.28) can equivalently be written as

$$E = \sum_i^N \varepsilon_i - \frac{1}{2} \int \frac{\rho(\mathbf{r})\rho(\mathbf{r}')}{|\mathbf{r} - \mathbf{r}'|} d\mathbf{r} d\mathbf{r}' + E_{\text{XC}}[\rho] - \int v_{\text{XC}}(\mathbf{r})\rho(\mathbf{r}) d\mathbf{r} \tag{2.35}$$

The Kohn-Sham and Hartree-Fock equations are very similar. However, there are key differences. The Kohn-Sham equations include a more general multiplicative potential, which fully incorporates the exchange-correlation interaction. Much of this thesis attempts to derive improved expressions for the only unknown term E_{XC}. The exact knowledge of it would provide, exactly, both the electron density and the energy of the system.

2.4.1 The unrestricted Kohn-Sham approach

By analogy with Hartree-Fock, in an unrestricted formalism, there are two spin-dependent Kohn-Sham effective potentials

$$v_{\text{eff}}^{\alpha}(\mathbf{r}) = v_{\text{ext}}(\mathbf{r}) + \int \frac{\rho(\mathbf{r}')}{|\mathbf{r} - \mathbf{r}'|} d\mathbf{r}' + \frac{\delta E_{\text{xc}}[\rho^{\alpha}, \rho^{\beta}]}{\delta \rho^{\alpha}(\mathbf{r})} \tag{2.36}$$

$$v_{\text{eff}}^{\beta}(\mathbf{r}) = v_{\text{ext}}(\mathbf{r}) + \int \frac{\rho(\mathbf{r}')}{|\mathbf{r} - \mathbf{r}'|} d\mathbf{r}' + \frac{\delta E_{\text{xc}}[\rho^{\alpha}, \rho^{\beta}]}{\delta \rho^{\beta}(\mathbf{r})} \tag{2.37}$$

2.4.2 Interpretation of the Kohn-Sham orbitals

Significant interest has been paid to the physical meaning of the Kohn-Sham orbitals. For a long time they were considered only a mathematical tool leading to the exact electron density, without any physical meaning [51]-[54]. However, this statement is not completely true. It has been shown that the eigenvalue of the highest occupied Kohn-Sham orbital $\varphi_{\text{HOMO}}^{\text{KS}}(\mathbf{r})$ is exactly equal to negative of the exact ionization energy [55, 56]

$$\varepsilon_{\text{HOMO}}^{\text{KS}} = -I \tag{2.38}$$

which contrast the approximate Hartree-Fock results in Eq. 1.19. This is a direct consequence of the long-range law for the electron density which states that its asymptotic behaviour is governed by the first ionization energy [57]

$$\rho(\mathbf{r}) \sim \exp[-2(2I)^{\frac{1}{2}} r] \tag{2.39}$$

Hence, if $\rho(\mathbf{r})$ is represented by a finite number of Kohn-Sham orbitals, its asymptotic behaviour is determined by the one-electron energy of the highest occupied orbital, that has to be equal minus the ionization energy. Note that, this is valid only if the Kohn-Sham orbitals are obtained from the exact asymptotically vanishing exchange-correlation potential.

By contrast, no precise interpretations have been defined for the remaining Kohn-Sham orbitals, both occupied or virtuals. To date, they have been used only as qualitative tools to interpret the excitation energies in DFT. Further insights in this direction are under development within time-dependent density functional theory [58].

2.4.3 The exchange-correlation potential

The exchange-correlation potential $v_{\text{XC}}(\mathbf{r})$ in Eq.(2.32) is the functional derivative of the exchange-correlation energy. Since the exact energy functional is

still unknown, the exact potential also remains unknown.

Nevertheless, in recent years, many investigations have been performed to describe the principal characteristics of the exchange-correlation potential, since it is central to DFT. By its definition, it is a multiplicative potential that introduces the effects of exchange and correlation within the Kohn-Sham approach. Moreover, it has been shown that its asymptotic behaviour plays an important role in the description of molecular properties such as polarizabilities and excitation energies to Rydberg states [59, 60].

2.4.3.1 The derivative discontinuity

In 1982, Perdew *et al.* [55] demonstrated that the exact exchange-correlation potential has a discontinuity when passing through an integer number of electrons. The potentials on the electron deficient and electron abundant sides of the integer are parallel but shifted from one another by some system dependent amount. In practical calculations, no continuum functionals can reproduce such a discontinuity; they can at best provide an average description [61]. Hence, as a consequence, an accurate continuum potential should not vanish asymptotically [55, 62, 63].

In 1998, Tozer and Handy [64] argued that in an unrestricted formalism, the best continuum potential must have the form

$$v_{\mathrm{XC}}(\mathbf{r}) = v^{0}_{\mathrm{XC}} + v_{\mathrm{XC}}(\infty) \tag{2.40}$$

where $v_{\mathrm{XC}}(\mathbf{r})$ is the potential which vanishes asymptotically and $v_{xc}(\infty)$ is the asymptotic potential. In asymptotic regions Eq.(2.40) behaves as

$$\lim_{r\to\infty} v_{\mathrm{XC}}(\mathbf{r}) = -\frac{1}{r} + v_{\mathrm{XC}}(\infty) \tag{2.41}$$

From the asymptotic form of the Kohn-Sham equations [56, 57, 65], it is then possible to obtain the generalized Koopmans' theorem

$$\varepsilon_{\mathrm{HOMO}} - v_{\mathrm{XC}}(\infty) = -I \tag{2.42}$$

where I is the lowest ionization energy and $\varepsilon_{\text{HOMO}}$ is the HOMO Kohn-Sham eigenvalues.

It is important to point out that rather than regarding the Koopman's theorem as a simple way to relate the highest occupied eigenvalue to the ionization potential, it represents instead a way to define the asymptotic potential for all the molecular systems

$$v_{\text{XC}}(\infty) = -I + \varepsilon_{\text{HOMO}} \tag{2.43}$$

which can be substituted in Eq.(2.41), to give

$$\lim_{r\to\infty} v_{\text{XC}}(\mathbf{r}) = -\frac{1}{r} + I + \varepsilon_{\text{HOMO}} \tag{2.44}$$

2.4.3.2 The Zhao-Morrison-Parr procedure

In recent years there has been much interest in obtaining near-exact exchange-correlation potentials from electron densities [66]-[71]. Our interest has focused on the Zhao, Morrison, Parr approach (ZMP) [72].

Within the Kohn-Sham framework, ZMP proposed to minimize the non-interacting kinetic energy $T_s[\rho]$, over all the one-electron determinants which yield the exact density ρ_0 [73]. Consequently, by imposing that the self-repulsion is zero

$$\int\int \frac{[\rho(\mathbf{r}) - \rho_0(\mathbf{r})][\rho(\mathbf{r}') - \rho_0(\mathbf{r}')]}{|\mathbf{r} - \mathbf{r}'|} d\mathbf{r}d\mathbf{r}' = 0 \tag{2.45}$$

they enforced the constraint that, during the entire minimization process, a density ρ equals the exact density ρ_0. Introducing Lagrange multipliers to enforce the orthonormality condition of the Kohn-Sham orbitals and λ for the constraint in Eq.(2.45), minimizing with respect to the form of the orbitals gives

$$\left[-\frac{1}{2}\nabla^2 + v_c^{\lambda}(\mathbf{r})\right] \psi_i^{\lambda}(\mathbf{r}) = \epsilon_i^{\lambda}\psi_i^{\lambda}(\mathbf{r}) \tag{2.46}$$

where

$$v_c{}^{\lambda}(\mathbf{r}) = \lambda \int \frac{\rho^{\lambda}(\mathbf{r}') - \rho_0(\mathbf{r}')}{|\mathbf{r}' - \mathbf{r}|} d\mathbf{r}' \tag{2.47}$$

with the superscript λ indicating a dependence on the value of λ. ZMP then introduced two more terms into the minimization. These did not affect the solution of the problem but gave the equation a more recognizable form

$$\left[-\frac{1}{2}\nabla^2 + v_{\text{ext}}(\mathbf{r}) + \left(1 - \frac{1}{2N}\right) v_{\text{J}}^{\lambda}(\mathbf{r}) + v_{\text{c}}^{\lambda}(\mathbf{r})\right] \psi_i^{\lambda}(\mathbf{r}) = \epsilon_i^{\lambda} \psi_i^{\lambda}(\mathbf{r}) \tag{2.48}$$

where

$$v_{\text{ext}}(\mathbf{r}) = -\sum_A \frac{Z_A}{|\mathbf{A} - \mathbf{r}|} \tag{2.49}$$

is the external potential and

$$v_{\text{J}}^{\lambda}(\mathbf{r}) = \int \frac{\rho^{\lambda}(\mathbf{r}')}{|\mathbf{r}' - \mathbf{r}|} d\mathbf{r}' \tag{2.50}$$

is the Coulomb potential. The constraint $(1 - \frac{1}{2N})$ is the Fermi Amaldi factor [74].

Through Eq. (2.48) they obtained the orbitals that minimize the non-interacting kinetic energy: the Kohn-Sham orbitals. Hence, Eq.(2.48) are the Kohn-Sham equations and the corresponding exchange correlation potential $v_{\text{XC}}(\mathbf{r})$ is rewritten as the sum of the Fermi-Amaldi contribution, which introduces the correct asymptotic $(-\frac{1}{r})$ behaviour to the exchange-correlation potential, and the constraint potential $v_{\text{c}}^{\lambda}(\mathbf{r})$

$$v_{\text{XC}}(\mathbf{r}) = \left(-\frac{1}{N} v_{\text{J}}^{\lambda}(\mathbf{r}) + v_{\text{c}}^{\lambda}(\mathbf{r})\right) \tag{2.51}$$

The last step of this process is the optimization of the parameter λ to the value for which the minimization returns the trial density $\rho^{\lambda}(\mathbf{r})$ equal to the exact density $\rho_0(\mathbf{r})$ [75]. By denoting the function to be minimized $F(\rho)$ and the constraint $G(\rho)$, then the Lagrange equations are $\nabla F + \lambda \nabla G = 0$ from which $\lambda = \nabla F / \nabla G$. The constraint G is quadratic in $\rho^{\lambda} - \rho_0$, so its gradient is linear in $\rho^{\lambda} - \rho_0$, hence $\nabla G = 0$ when the equations are satisfied. We can therefore deduce that the limit for $\lambda \to \infty$ must be taken to ensure that the minimization returns $\rho^{\lambda} = \rho_0$. In conclusion, the exact expression for the exchange-correlation potential is

$$v_{\text{XC}}(\mathbf{r}) = \lim_{\lambda \to \infty} \left(-\frac{1}{2N} v_{\text{j}}^{\lambda}(\mathbf{r}) + v_{\text{c}}^{\lambda}(\mathbf{r})\right) \tag{2.52}$$

The potential vanishes asymptotically and so it represents the exact potential on the electron deficient side of the integer.

2.4.4 The self-interaction problem

As mentioned in Chapter 1, self-interaction can be a problem in DFT. Considering the total Kohn-Sham energy expression Eq.(2.28) and applying it to a one-electron system, it is clear that the only relevant energetic contributions are the kinetic energy term and the nuclear-electron attraction. Hence, the classical repulsion term

$$J[\rho] = \frac{1}{2}\int\int \frac{\rho(\mathbf{r}_1)\rho(\mathbf{r}_2)}{r_{12}} d\mathbf{r}_1 d\mathbf{r}_2 \tag{2.53}$$

must be cancelled by $E_{xc}[\rho]$

$$E_{xc}[\rho(\mathbf{r})] = -J[\rho] \tag{2.54}$$

Conversely to Hartree-Fock theory, where for one-electron systems the exchange term does exactly cancel the Coulomb term, in density functional theory Eq.(2.54) is not satisfied with approximate functionals.

In 1981 Perdew and Zunger [76] proposed a self-interaction corrected procedure (SIC) to develop exchange-correlation functionals enforcing the condition in Eq.(2.54). This lead to complicated orbital dependent equations that, when applied to molecules, did not provide significant improvement over the regular Kohn-Sham equations [77]. Nowadays, the self-interaction problem is still under study since it is commonly believed to be the cause of the poor performance of DFT in representing the reaction barriers and the dissociation of radicals [78, 79]. We investigate this in Chapter 3.

2.5 Approximations for $E_{xc}[\rho]$

It is therefore vital is to find the best approximation for the exchange-correlation energy functional. Since the advent of DFT, many different approximations for $E_{xc}[\rho]$ have been developed. We now introduce the three

main families of exchange-correlation functionals that are used in practical calculations.

2.5.1 Local density approximation (LDA)

The local density approximation (LDA) locally applies expressions that are appropriate for a uniform electron gas. For this approximation the expressions for the exchange-correlation energy are known precisely or with a very high accuracy. The general expression for $E_{\mathrm{XC}}[\rho]$ can be cast in the following form

$$E_{\mathrm{XC}}^{\mathrm{LDA}}[\rho] = \int \rho(\mathbf{r})\varepsilon_{\mathrm{XC}}(\rho)d\mathbf{r} \tag{2.55}$$

where $\varepsilon_{\mathrm{XC}}$ represents the exchange-correlation energy per particle of a UEG of density ρ. $\varepsilon_{\mathrm{XC}}$ is then split into an exchange part and a correlation part

$$\varepsilon_{\mathrm{XC}} = \varepsilon_{\mathrm{X}} + \varepsilon_{\mathrm{C}} \tag{2.56}$$

where the exchange term [80]

$$\varepsilon_{\mathrm{X}}^{\mathrm{LDA}}(\rho) = -\frac{3}{4}\left(\frac{3}{\pi}\right)^{\frac{1}{3}} \rho^{\frac{1}{3}}(\mathbf{r}) \tag{2.57}$$

gives the Dirac expression

$$E_{\mathrm{X}}^{\mathrm{LDA}}[\rho] = -\frac{3}{4}\left(\frac{3}{\pi}\right)^{\frac{1}{3}} \int \rho^{\frac{4}{3}}(\mathbf{r})d\mathbf{r} \tag{2.58}$$

This case is valid when ρ_α and ρ_β are equal (closed-shell), however when $\rho_\alpha \neq \rho_\beta$, Eq.(2.58) is replaced by the local spin density approximation (LSDA) where the two spin densities are employed; the corresponding exchange energy is

$$E_{\mathrm{X}}^{\mathrm{LSDA}}[\rho] = -2^{\frac{1}{3}}\frac{3}{4}\left(\frac{3}{\pi}\right)^{\frac{1}{3}} \int \left[\rho_\alpha^{\frac{4}{3}} + \rho_\beta^{\frac{4}{3}}\right] d\mathbf{r} \tag{2.59}$$

From Eq.(2.58) and Eq.(2.59) it is clear that for closed shell molecules ($\rho_\alpha = \rho_\beta = \frac{\rho}{2}$) LDA and LSDA are exactly coincident.

The correlation contribution in LDA is equally important and many studies have been performed to develop the corresponding accurate correlation

energy contribution. Unfortunately, no explicit expressions are available for ε_{C}, however, thanks to the work of Ceperley and Alder [81] who performed a series of quantum Monte-Carlo calculations, accurate values for ε_{C} have been derived. Vosko, Wilk and Nusair (VWN) [82] later interpolated these values, providing an analytic form for ε_{C}, which is amongst the most widely used nowadays. A more recent description of the correlation energy was introduced by Perdew and Wang (PW) [83].

It is necessary to underline that the LDA approximation assumes a uniform electron density. For this reason, its applicability is not recommended for atoms and molecules where the electron density does not approach the UEG situation. Nevertheless solid-state physicists consider it satisfactory and for many years it has been used, due to the slowly varying density in solids when pseudopotentials are employed.

2.5.2 Generalized gradient approximation (GGA)

A more accurate approximation over LDA is represented by generalized gradient approximation (GGA) exchange-correlation functionals. The origin of this approximation is the idea of considering not only the electron density but also its gradient, in order to represent properly the real inhomogeneity. The first study in this direction considered the LDA approximation as the first term of a Taylor expansion in which the second term, involving the second-order gradient of the electron density, would have represented the required correction to improve the molecular predictions. This attempt, which is known as the gradient expansion approximation (GEA) [84]-[87], did not bring any improvement; it provided even worse results than LDA. At the beginning of the 1980's Perdew [88] proposed to include only the gradient of the electron density removing any higher order, generating the so-called GGA functionals. The general expression for a GGA is written

$$E_{\mathrm{XC}}^{\mathrm{GGA}}[\rho_\alpha, \rho_\beta] = \int f(\rho_\alpha, \rho_\beta, \nabla\rho_\alpha, \nabla\rho_\beta) d\mathbf{r} \tag{2.60}$$

which can be split into exchange and correlation contributions as

$$E_{\mathrm{XC}}^{\mathrm{GGA}} = E_{\mathrm{X}}^{\mathrm{GGA}} + E_{\mathrm{C}}^{\mathrm{GGA}} \tag{2.61}$$

Focusing our attention on the exchange functional we can rewrite it as

$$E_{\mathrm{X}}^{\mathrm{GGA}} = E_{\mathrm{X}}^{\mathrm{LDA}} - \sum_{\sigma} \int f(s_\sigma) \rho_\sigma^{\frac{4}{3}}(\mathbf{r}) d\mathbf{r} \tag{2.62}$$

where s_σ is the reduced density gradient

$$s_\sigma(\mathbf{r}) = \frac{|\nabla \rho_\sigma(\mathbf{r})|}{\rho_\sigma^{\frac{4}{3}}(\mathbf{r})} \tag{2.63}$$

a dimensionless parameter describing the local inhomogeneity. Eq.(2.62) ensures the scaling condition, Eq.(2.7) is satisfied.

Many studies have been carried out in order to develop the best GGA exchange functional and two main approaches have been followed. The first one, known as semi-empirical, was suggested by Becke in 1988 [89], who introduced a general procedure in order to derive the parameters of the functionals by fitting to known thermochemical values. The first functional derived following this method is the so called B88

$$f^{\mathrm{B88}} = \frac{\beta s_\sigma^2}{1 + 6\beta s_\sigma \sinh^{-1} s_\sigma} \tag{2.64}$$

where the parameter β, was derived via a least-squares fit to the exactly known exchange energies of the rare gas atoms He through Rn. In the second approach, leading to the first-principles functionals, the integrand f is expanded as a rational function of the electron density and of its gradient without the introduction of any semi-empirical terms. This category includes the widely used PW91 functional [90, 91]

$$f^{\mathrm{PW91}} = \varepsilon_{\mathrm{X}}^{\mathrm{LDA}} \frac{1 + s_\sigma a_1 \sinh^{-1}(s_\sigma a_2) + (a_3 + a_4 e^{-b s_\sigma^2}) s_\sigma^2}{1 + s_\sigma a_1 \sinh^{-1}(s_\sigma a_2) + a_5 s_\sigma^2} \tag{2.65}$$

where $a_1 ... a_5$ are suitable parameters and the Perdew Burke and Ernzerhof (PBE) functional [92].

An even more complicated task is to derive the corresponding GGA correlation functionals. In many cases, very sophisticated mathematical expressions are necessary. Among the most widely used correlation functionals, we mention the counterpart of the exchange P86 [93] which involves a semi-empirical parameter determined by a fitting of the correlation energy of the neon atom. A few years later, Lee, Yang and Parr [94] derived the correlation functional LYP, involving only one parameter obtained with the definition of the correlation energy of the helium atom, from a detailed study by Colle and Salvetti [95].

It is important to point out that the correlation functionals, due to their functional expansion or the fitting procedure used to derive them, include only short-range correlation effects (dynamic correlation). Long-range effects (left-right or non-dynamical correlation) are not taken into account. Recently, Handy and Cohen [96] highlighted that left-right correlation effects are already included in local exchange functionals.

Once expressions for $E_{\mathrm{X}}^{\mathrm{GGA}}$ and $E_{\mathrm{C}}^{\mathrm{GGA}}$ have been obtained and their performances have been assessed, it is possible to combine them according to Eq.(2.61) to create a complete GGA exchange-correlation functional. In principle, any exchange functional could be combined with any correlation one. So far, however, only a few combinations are in common use and among them we mention BLYP, BP86 and BPW91.

We note that it is possible to determine GGA functionals where the exchange and the correlation part are derived together, simultaneously. Among these functionals, one of the most successful is HCTH-93 [97] which has been built through a re-parameterisation of the B97 GGA component [98] (that we will introduce in Section 3.1) with expansion parameters derived by fitting to thermochemical data, molecular geometries and exchange-correlation potentials. We will describe in detail its derivation in Chapter 3. Further re-formulations of HCTH-93 using larger sets of fitting data led to the development of HCTH-120 [99], HCTH-147 [99], and HCTH-407 [100].

Finally, most recently, the so called meta-GGA functionals [101] were proposed where, besides the local density and its gradient, the laplacian or the kinetic energy density also enters the equations. To date, these functionals have not been widely used as their performance is no better than other approximations.

2.5.2.1 The enhancement factor

In order to describe the gradient dependence in GGA functionals, we introduce the exchange-correlation enhancement factor $f'_{\rm XC}(r_s, s)$ [102]. In general, in the spin-unpolarized case where $(\rho_\alpha = \rho_\beta = \frac{\rho}{2})$, the expression for a GGA functional can be written as

$$E_{\rm XC}^{\rm GGA} = -\int \frac{3}{4\pi}(3\pi^2\rho)^{\frac{1}{3}}\rho(\mathbf{r})f'_{\rm XC}(r_s, s)d\mathbf{r} \tag{2.66}$$

where $f'_{\rm XC}(r_s, s)$ is the enhancement factor. This is a function of the Wigner-Seitz radius r_s

$$r_s = \left(\frac{3}{4\pi\rho}\right)^{\frac{1}{3}} \tag{2.67}$$

and of the reduced density gradient s

$$s(\mathbf{r}) = \frac{|\nabla\rho(\mathbf{r})|}{\rho^{\frac{4}{3}}(\mathbf{r})} \tag{2.68}$$

The enhancement factor must satisfy a range of exact conditions:

1. In the case of a slowly varying electron density, which corresponds to very small values of s

$$f'_{\rm XC}(r_s, s = 0) = f_{\rm XC}^{\rm LSDA}(r_s) \tag{2.69}$$

2. From the following fundamental scaling condition

$$E_{\rm XC}[\rho_\lambda] > \lambda E_{\rm XC}[\rho] \text{ for } (\lambda > 1) \tag{2.70}$$

it follows that [103, 104]

$$f'_{\rm XC}(r'_s, s) > f'_{\rm XC}(r_s, s) \text{ for } (r'_s > r_s) \tag{2.71}$$

3. In the high density regions, i.e. for small values of r_s, if $f'_{\mathrm{XC}} = f'_{\mathrm{X}} + f'_{\mathrm{C}}$

$$\lim_{r_s \to 0} f'_{\mathrm{XC}}(r_s, s) = f'_{\mathrm{X}}(s) \tag{2.72}$$

4. At large values of s

$$\lim_{s \to \infty} f'_{\mathrm{C}}(r_s, s) \to 0 \tag{2.73}$$

5. Finally, f'_{XC} must satisfy the Lieb-Oxford bound [105], which originally was equal to 2.27 and recently was redefined to be 2.2143 [106]

$$f'_{\mathrm{XC}}(r_s, s) \leq 2.2143 \tag{2.74}$$

2.5.3 Hybrid functionals

A third approximation are the so-called hybrid functionals. The exchange-correlation functional $E_{\mathrm{XC}}[\rho]$ is represented as a combination of GGA components for exchange and correlation, with the introduction of an amount of exact Hartree-Fock exchange. Since their first appearance, hybrid functionals obtained a positive feedback among computational chemists due to their reduced errors compared to GGAs.

The most natural approach would be to use the exact Hartree-Fock exchange and rely on approximate functionals only for the correlation contribution. If applied to atoms, this method delivers promising results, however when applied to molecules, it is inappropriate. In 1993, Becke proposed a different approach, known as the half-and-half (HH) approximation [107], combining 50% of exact exchange and a density functional exchange-correlation energy

$$E_{\mathrm{XC}}^{\mathrm{HH}} = \frac{1}{2} E_{\mathrm{X}}^{\mathrm{LSDA}} + \frac{1}{2} E_{\mathrm{X}}^{\mathrm{HF}} + E_{\mathrm{C}} \tag{2.75}$$

Following this, Becke developed the following functional [108].

$$E_{\mathrm{XC}} = (1 - a) E_{\mathrm{X}}^{\mathrm{LSDA}} + a E_{\mathrm{X}}^{\mathrm{HF}} + b E_{\mathrm{X}}^{\mathrm{B88}} + E_{\mathrm{C}}^{\mathrm{LSDA}} + c E_{\mathrm{C}}^{\mathrm{PW91}} \tag{2.76}$$

This is considered the cornerstone among hybrid functionals and its three parameters *a, b, c* weighting the different contributions, are determined through a fit to experimental data. In 1994 Stevens *et al.* [109] replaced the PW91 correlation contribution with LYP, generating the well known B3LYP functional where $a = 0.20$, $b = 0.72$ and $c = 0.81$.

In 1997 Becke proposed a more general expansion [110]

$$E_{\mathrm{XC}}^{\mathrm{B97}} = E_{\mathrm{X}}^{\alpha\alpha} + E_{\mathrm{X}}^{\beta\beta} + E_{\mathrm{C}}^{\alpha\alpha} + E_{\mathrm{C}}^{\beta\beta} + E_{\mathrm{C}}^{\alpha\beta} + c_{\mathrm{X}}^{\mathrm{HF}} E_{\mathrm{X}}^{\mathrm{HF}} \tag{2.77}$$

with all terms, except the exact exchange energy, being a polynomial expansion involving the electron density and its gradient. These expansions were truncated at second order, to avoid over-parameterized functionals. The ten expansion coefficients were determined by a least-squares fit to energetic data. The results obtained with this functional were very successful and there have been further attempts to re-parameterize it. In 1998 Hamprecht *et al* [97] derived the B97-1 hybrid functional and more recently Tozer *et al* [111] proposed B97-2. Further re-parameterization of B97 is still in progress, as will be discussed in Chapter 6. Important aspects regarding the quality of experimental data and the amount of exact exchange to include in the functional still need to be addressed.

Amongst hybrid approximations, there are also parameter-free functionals (which corresponds to the first principle category among GGA). Among the most successful ones we mention PBE0 [112, 113] which has been determined by Barone and Adamo, connecting the GGA functional PBE with a predefined 25% of exact exchange.

$$E_{\mathrm{XC}}^{\mathrm{PBE0}} = 0.25 E_{\mathrm{X}}^{\mathrm{HF}} + 0.75 E_{\mathrm{X}}^{\mathrm{PBE}} + E_{\mathrm{C}}^{\mathrm{PBE}} \tag{2.78}$$

Chapter 3

New GGA exchange-correlation functionals

The development of new approximations to the exchange-correlation energy functional is of vital importance. In this chapter we investigate a completely new approach, developing functionals solely from *ab initio* electron densities. A range of functionals are determined by emphasizing different regions of space. Functional quality is assessed by considering a wide range of atomic and molecular properties. Attempts are made to further improve functional performance.

3.1 The HCTH-93 functional

We commence with a discussion of the HCTH-93 functional, since our new functional will use the same mathematical form. The general expression for the HCTH-93 [97] functional is written in terms of the GGA component of the B97 functional [98], developed by Becke. It is written as the sum of an exchange and a correlation term where the exchange part is

$$E_{\mathrm{X}} = \sum_{\sigma} \int e_{\mathrm{X}\sigma}^{\mathrm{LSDA}}(\rho_{\sigma}) g_{\mathrm{X}\sigma}(s_{\sigma}^{2}) d\mathbf{r} \tag{3.1}$$

The $e_{\mathrm{X}\sigma}^{\mathrm{LSDA}}(\rho_\sigma)$ term represents the σ-spin exchange energy density of a uniform electron gas with spin density equal to its local value ρ_σ and is written as

$$e_{\mathrm{X}\sigma}^{\mathrm{LSDA}}(\rho_\sigma) = -\frac{3}{2}(\frac{3}{4\pi})^{\frac{1}{3}}\rho_\sigma^{\frac{4}{3}}. \tag{3.2}$$

$g_{\mathrm{X}\sigma}$ is the gradient factor correcting the LSDA underestimation of the exchange energies for inhomogeneous systems. It depends on s_σ which is the reduced spin-density gradient (See Eq.(2.68)) and is defined as

$$g_{\mathrm{X}\sigma} = \sum_{i=0}^{m} c_{\mathrm{X}\sigma} u_{\mathrm{X}\sigma}^i \tag{3.3}$$

where

$$u_{\mathrm{X}\sigma} = 0.004 s_\sigma^2 (1 + 0.004 s_\sigma^2)^{-1}. \tag{3.4}$$

The corresponding correlation part is separated into two contributions, one for parallel spins $E_{\mathrm{C}\alpha\alpha}^{\mathrm{GGA}}$ and one for opposite spins $E_{\mathrm{C}\alpha\beta}^{\mathrm{GGA}}$,

$$E_{\mathrm{C}} = \sum_{\sigma} E_{\mathrm{C}\sigma\sigma}^{\mathrm{GGA}} + E_{\mathrm{C}\alpha\beta}^{\mathrm{GGA}} \tag{3.5}$$

In a similar manner as in Eq.(3.1), the parallel-spin contribution is written as

$$E_{\mathrm{C}\sigma\sigma} = \sum_{\sigma} \int e_{\mathrm{C}\sigma\sigma}^{\mathrm{LSDA}}(\rho_\sigma) g_{\mathrm{C}\sigma\sigma}(s_\sigma^2) d\mathbf{r} \tag{3.6}$$

where the gradient correction term is written

$$g_{\mathrm{C}\sigma\sigma} = \sum_{i=0}^{m} c_{\mathrm{C}\sigma\sigma} u_{\mathrm{C}\sigma\sigma}^i \tag{3.7}$$

with

$$u_{\mathrm{C}\sigma\sigma} = 0.2 s_\sigma^2 (1 + 0.2 s_\sigma^2)^{-1}. \tag{3.8}$$

and the opposite-spin contribution is written

$$E_{\mathrm{C}\alpha\beta} = \int e_{\mathrm{C}\alpha\beta}^{\mathrm{LSDA}}(\rho_\alpha, \rho_\beta) g_{\mathrm{C}\alpha\beta}(s_{\mathrm{avg}}^2) d\mathbf{r} \tag{3.9}$$

where the corresponding gradient correction is

$$g_{\mathrm{C}\alpha\beta} = \sum_{i=0}^{m} c_{\mathrm{C}\alpha\beta} u_{\mathrm{C}\alpha\beta}^i \tag{3.10}$$

with

$$u_{C\alpha\beta} = 0.006 s^2_{avg}(1 + 0.006 s^2_{avg})^{-1} \tag{3.11}$$

and s^2_{avg} the average of the squared reduced density gradient for spin α and spin β

$$s^2_{avg} = \frac{1}{2}(s^2_\alpha + s^2_\beta). \tag{3.12}$$

In both Eq.(3.6) and Eq.(3.9), $e^{LSDA}_{C\sigma\sigma}$ and $e^{LSDA}_{C\alpha\beta}$ are uniform electron gas correlation energy densities per unit volume, derived from the total LSDA correlation energy density, using the following procedure [114]

$$e^{LSDA}_{C\alpha\beta}(\rho_\alpha, \rho_\beta) = e^{LSDA}_{C}(\rho_\alpha, \rho_\beta) - e^{LSDA}_{C}(\rho_\alpha, 0) - e^{LSDA}_{C}(\rho_\beta, 0) \tag{3.13}$$

$$e^{LSDA}_{C\sigma\sigma}(\rho_\sigma) = e^{LSDA}_{C}(\rho_\sigma, 0) \tag{3.14}$$

where e^{LSDA}_{C} has been derived from the parameterization of Perdew and Wang [83].

The parameters defining HCTH-93 were determined as follows. A set of 93 atoms and molecules from the first two rows of the periodic table were chosen. These systems, defining the training set (T), are listed in Table 3.1. The quantity Ω, defined as

$$\Omega = w_E \Omega_E + w_G \Omega_G + w_V \Omega_V \tag{3.15}$$

where w_E, w_G and w_V are energy, gradient and potential weights, was then minimized in order to ensure that the functional provided:

1) accurate total energies (E) for for first-row atoms and cations A_1 and A_1^+; accurate ionization potentials (IP) for selected second-row atoms A_2 and accurate atomization energies (AE) for systems M through

$$\Omega_E = \sum_{A_1}^{18}[E^{A_1,A_1^+}_{XC} - E^{A_1,A_1^+}_{fit}]^2 + \sum_{A_2}^{7}[IP^{A_2}_{XC} - IP^{A_2}_{fit}]^2 + \sum_{M}^{61}[AE^{M}_{XC} - AE^{M}_{fit}]^2 \tag{3.16}$$

2) accurate nuclear gradients (G) for molecules M (i.e. zero if the calculations are performed at equilibrium geometries), through

$$\Omega_G = \sum_{M}\sum_{I}^{N_{M-1}} \left| \frac{\partial E^{M}_{XC}}{\partial R_I} - \frac{\partial E^{M}_{fit}}{\partial R_I} \right| \tag{3.17}$$

3) accurate exchange correlation potentials for all the 93 systems M, A_1, A_1^+, A_2 and A_2^+ (indicated with T) through

$$\Omega_V = \sum_T \sum_\sigma^{\alpha,\beta} \int d\mathbf{r}[v_{ZMP}^{T\sigma} + k_{T\sigma} - v_{fit}^{T\sigma}(\mathbf{r})]^2 \rho_{T\sigma}^{\frac{2}{3}}(\mathbf{r}). \tag{3.18}$$

Initial values were chosen for $k_{T\sigma}$, which represents the unknown shift between the near-exact ZMP potential and the exact continuum σ potential for system T. Ω was then minimized with respect to the expansion coefficients $\{c_i\}$

$$\left.\frac{\partial\Omega}{\partial c_i}\right|_{k_{T\sigma}} = 0, \tag{3.19}$$

to obtain a set of least-squares equations for the new coefficients. The new coefficients were then used to determine a new set of shifts

$$\left.\frac{\partial\Omega}{\partial k_{T\sigma}}\right|_{c_i} = 0. \tag{3.20}$$

and the procedure was iterated to self-consistency.

3.2 A new fitting approach

The introduction of the exchange-correlation potentials in the fitting procedure of HCTH-93 corrected some deficient results obtained with functionals derived only by fitting to thermochemical data, where only integrated quantities were taken in consideration [97]. Following this consideration, we choose to consider a completely new approach to functional development, fitting solely to the exchange-correlation potentials. There are several reasons for this choice:

(a) By fitting only to potentials the emphasis will be shifted toward quantities related to the energy derivatives, such as molecular structures and NMR shielding constants. These are some of the most important theoretical predictions.

(b) Even though not directly included in our fitting procedure, energetic information will still be taken into account since the total exchange-correlation

Table 3.1: Specification of the systems (T) in the training-set used to generate HCTH-93

1. M: H_2, LiH, BeH, CH, $CH_2(^1A)$, $CH_2(^3B)$, CH_3, CH_4, NH, NH_2, NH_3, OH, H_2O, HF, Li_2, LiF, C_2H_2, C_2H_4, C_2H_6, CN, HCN, CO, HCO, H_2CO, CH_3OH, N_2, N_2H_4, O_2, H_2O_2, F_2, CO_2, $SiH_2(^1A)$, $SiH_2(^3B)$, SiH_3, SiH_4, PH_2, PH_3, HCl, Na_2, Si_2, P_2, S_2, Cl_2, NaCl, SiO, CS, SO, ClO, ClF, CH_3Cl, CH_3SH, HOCl, SO_2, HF^+, HCl^+, CO^+, N_2^+, O_2^+, P_2^+, S_2^+, Cl_2^+ {61}

2. A_1: H, He, Li, Be, B, C, N, O, F, Ne {10}

3. A_1^+: Li^+, Be^+, B^+, C^+, N^+, O^+, F^+, Ne^+ {8}

4. A_2: Na, Mg, Al, Si, P, S, Cl {7}

5. A_2^+: Na^+, Mg^+, Al^+, Si^+, P^+, S^+, Cl^+ {7}

[1]The number enclosed in the brackets indicate the number of molecules for each subset

energy can be written as a path integral over an appropriate function of the exchange-correlation potential [116]. Furthermore, differences on the potential energy surface (such as atomization energies and reaction barriers) can be written as a path integral over the nuclear derivative, which is itself determined by the potential.

(c) The exchange-correlation potential is a scalar field, so emphasizing different spatial regions of the field will give different functionals. This will provide information about the spatial dependence of molecular properties.

(d) Removing the thermochemical and gradient aspects of the fit will significantly reduce the empiricism. The only experimental data will be the structures used in the determination of the *ab initio* densities. They could be eliminated by using theoretically optimized geometries.

(e) It has been shown that the asymptotic contribution to the electronic energy is not insignificant [117]. Conventional functionals such as HCTH-93 fail to describe this energy because their potentials vanish asymptotically. If the experimental thermochemistry were to be reproduced, then the asymptotic energy contribution would be incorrectly accounted in the core/valence regions. Removing the thermochemical aspect of the fit will eliminate this inconsistency.

We note that several authors have emphasized exchange-correlation potentials in their studies [64],[118]-[120]. However, these studies have generally focused on determining model exchange-correlation potentials, rather than exchange-correlation functionals. The absence of an associated functional can lead to a breakdown in translational invariance because the potential is not necessarily a functional derivative [117]. By concentrating on new functionals rather than potentials, we do not encounter these problems.

3.2.1 Functional development

We use the same mathematical form as for HCTH-93 involving 15 expansion coefficients $\{c_i\}$. We also use the same training set of 93 molecules used to determine HCTH-93 although this time we will fit only to their exchange-correlation potentials, determined using the ZMP [72] procedure described in Chapter 2, with Brueckner doubles (closed-shell) and MP2 (open-shell) electron densities with the TZ2P basis set [121]. Optimum coefficients were therefore determined by setting

$$\Omega = \Omega_{\mathrm{V}} = \sum_{\mathrm{T}}^{\mathrm{Mols}} \sum_{\sigma}^{\alpha,\beta} \int d\mathbf{r} \left[v_{\mathrm{ZMP}}^{\mathrm{T}\sigma}(\mathbf{r}) + k_{\mathrm{T}\sigma} - v_{\mathrm{fit}}^{\mathrm{T}\sigma} \right]^2 W_{\mathrm{T}\sigma}(\mathbf{r}) \qquad (3.21)$$

where $W_{\mathrm{T}\sigma}(\mathbf{r})$ is a spatial weighting function, and minimizing Ω with respect to the coefficients and to the shifts as in Eq.(3.19) and Eq.(3.20). This generates a functional whose potential for each of the systems T is maximally parallel (shifted by $k_{\mathrm{T}\sigma}$) to the ZMP potential of that system. A related approach was previously investigated in Ref. [122], although a much less flexible functional form was used and the fitting data set was much more restricted. Moreover, the spatial weighting functions were not varied and most importantly, the discontinuity in the potential (hence, the shifts k_σ) was not accounted for.

If the potential of the fitted functional could exactly reproduce the near-exact ZMP potential then Ω would be zero for any weighting function $W_{\mathrm{T}\sigma}(\mathbf{r})$. In the original HCTH-93 development $W_{\mathrm{T}\sigma}(\mathbf{r})$ was chosen to be

$$W_{\mathrm{T}\sigma}(\mathbf{r}) = \rho_{\mathrm{T}\sigma}^{p}(\mathbf{r}) \qquad (3.22)$$

where p was fixed to $\frac{2}{3}$. In the present study, we again use the same form for $W_{\mathrm{T}\sigma}(\mathbf{r})$, but we emphasize different regions of space using the following range for p

$$p = \frac{i}{6} \qquad (3.23)$$

where $i = 0...7$. Regions close to the nuclei are emphasized with large values of p and regions far away are emphasized with small values. As in previous

studies [63, 123], the converged shifts $k_{T\sigma}$ are positive, of the order of several electron volts. This reflects the dominant role of the Dirac local exchange term (with prefactors close to the unity) in our new functionals, which approximately averages over the discontinuity in the potential in nonasymptotic regions, and so is shifted from the asymptotically vanishing ZMP potential. The resulting functionals therefore give highest-occupied molecular orbital (HOMO) eigenvalues that lie significantly above $-I$, as they should. All the expansion coefficients defining the functionals developed in this chapter are presented in Appendix A.

3.3 Functional assessment

The eight functionals were implemented in the CADPAC [124] program and were used to determine molecular structures, thermochemistry, polarizabilities and shielding constants for a range of molecules defined in Tables 3.1 and 3.2. Mean and mean absolute errors are presented in Table 3.3. All the calculations were performed using the TZ2P basis-set [121], unless otherwise stated.

3.3.1 Molecular structures

We determined the optimized molecular structures for the systems S defined in Table 3.2. This is a subset of the molecules M in Table 3.1, where the experimental structures are well known. $p = 0$ gives errors comparable with HCTH-93 and bond angles that are a slight improvement. Increasing the value of p to $\frac{1}{6}$ and $\frac{2}{6}$ led to a significant improvement in the bond lengths, with mean absolute errors of 0.007 Å and 0.006 Å, respectively. Further increasing p reduces the accuracy.

Table 3.2: Specification of the systems studied in this work

1. S: H_2, LiH, BeH, CH, $CH_2(^1A)$, $CH_2(^3B)$, CH_3, CH_4, NH, NH_2, NH_3, OH, H_2O, HF, Li_2, LiF, C_2H_2, C_2H_4, CN, HCN, CO, HCO, H_2CO, N_2, O_2, H_2O_2, F_2, CO_2, HCl, Na_2, Si_2, P_2, S_2, Cl_2, NaCl, SiO, CS, SO, ClO, ClF {40}

2. P: HF, H_2O, N_2, CO, F_2, NH_3, CO_2, CH_4, C_2H_4, PH_3, H_2S, SO_2, HCl, Cl_2 {14}

3. SC: HF, H_2O, CO, N_2, F_2, O_3, H_2S, SO_2, PN, trans-N_2F_2 {10}

4. Radicals: BH^+, NH^+, OH^+, BeF, BN, BO, C_2^+, CF, NF, NO, OF, F_2^+, Al_2, SiCl, NS, PO {16}

5. Others: FOOF, FNO_2, O_3, FO_2, $Cr(CO)_6$, $Ni(CO)_4$, $[Co(CN)_6]^{3-}$, N_2, H_2CO, C_6H_6 {10}

[2]The number enclosed in the brackets indicate the number of molecules for each subset

Table 3.3: Error assessments for self-consistent molecular structures (Å and degrees), thermochemistry (kcal/mol), isotropic polarisabilities (a.u.), and isotropic nuclear shielding constants (ppm and %) for systems defined in Table 1, as a function of the power p in Eq.(3.21).

		p							
	HCTH 93	0	1/6	2/6	3/6	4/6	5/6	6/6	7/6
				Molecular structures of systems S					
Mean r	0.012	0.007	0.001	0.003	0.013	0.028	0.046	0.055	0.051
Mean abs. r	0.013	0.013	0.007	0.006	0.013	0.028	0.046	0.055	0.051
Mean θ	−0.5	−0.3	−0.2	−0.4	−0.6	−0.8	−0.9	−0.9	−1.0
Mean abs. θ	0.7	0.4	0.4	0.5	0.8	0.9	1.1	1.1	1.2
				Combined thermochemistry of systems M, A_1, A_1^+, and A_2					
Mean abs.	3.3	44.6	13.3	20.8	29.3	72.8	104.7	123.1	132.7
				Polarisabilities of systems P					
Mean	0.32	0.39	0.20	0.16	0.49	1.26	2.09	2.69	2.55
Mean abs.	0.36	0.62	0.27	0.24	0.50	1.26	2.09	2.69	2.55
				Shielding constants of systems SC					
Mean	−57.0	−67.0	−72.3	−68.1	−61.4	−55.4	−50.7	−46.0	−41.6
Mean abs.	57.0	67.0	72.3	68.1	61.4	55.4	50.7	46.0	43.1
Mean abs. %	56.9	85.1	90.0	80.1	65.0	51.7	39.9	29.9	27.0

3.3.2 Thermochemistry

We calculated total atomic energies of the systems A_1, A_1^+, ionization energies of A_2 and atomization energies of M in Table 3.1 at near-experimental geometries [115]. The values in Table 3.3 combine all the 86 energies, and so we present only the mean absolute errors. For $p = 0$ we obtained a large error of 44.6 kcal/mol. This error reduces significantly as p is increased to $\frac{1}{6}$ and $\frac{2}{6}$ although it stays higher than with HCTH-93. A further increase of p leads to a steady degradation in the thermochemistry. This degradation is not due to the divergence in the potential of the new functionals at the nuclei [125]; the same trend is observed when the divergent density gradient terms are removed from the functionals.

3.3.3 Polarizabilities

We calculated static isotropic polarizabilities of the system P presented in Table 3.2 using the Sadlej basis set [126] at near-experimental geometries [115, 64]. The behaviour of the polarizabilities is the same as that of the structures and thermochemistry. There is an improvement in moving from $p = 0$ to $p = \frac{1}{6} - \frac{2}{6}$ and a further increase in p reduces the accuracy. Zero-point vibrational corrections (ZPVC's) [127] are not included in our calculations. Hence, accurate non-corrected theoretical predictions should underestimate the experimental values.

3.3.4 Shielding constants

We have determined LORG-DFT-NMR isotropic shielding constants of the systems SC in Table 3.2 using the Huzinaga (IGLO IV) basis set [128] at near-experimental geometries [129, 130]. Due to the large variation in the absolute shieldings, we also present mean absolute percentage errors. The dependence on p is now very different. The mean absolute error increases from $p = 0$ to $p = \frac{1}{6}$, although further increasing p leads to an improvement

in the shieldings. At $p = \frac{7}{6}$ the mean absolute error is 43.1 ppm compared to 57.0 ppm for HCTH-93. This improvement is particularly marked when we consider the mean absolute percentage error (27.0 % compared to 56.9 %). If the value of p increases beyond $\frac{7}{6}$ then the errors increase again.

Structures, thermochemistry and polarizabilities are therefore optimal when the weighting is $p = \frac{1}{6} - \frac{2}{6}$. We therefore determined an intermediate functional with $p = \frac{1}{4}$. This functional provides structures and polarizabilities as accurate as those for $p = \frac{1}{6}$ and $p = \frac{2}{6}$, but additionally improves the thermochemistry results, with a mean absolute error of 10.1 kcal/mol. This functional will hereafter be denoted $\frac{1}{4}$.

3.4 Detailed assessment of $\frac{1}{4}$ functional

A detailed assessment of the performance of $\frac{1}{4}$ is now presented. All the results are compared with HCTH-93 and the high quality hybrid functional B97-1 [97].

3.4.1 Molecular structures

In Table 3.4 we present optimized structures of molecules S in Table 3.2 Whereas HCTH-93 overestimates the bond lengths with a mean and a mean absolute error of 0.012 Å and 0.013 Å respectively, the $\frac{1}{4}$ functional shortens them and the corresponding mean and mean absolute errors are reduced to just 0.001 Å and 0.006 Å. The bond angles are also an improvement. The $\frac{1}{4}$ bond lengths are also an improvement over B97-1, whose errors are 0.005 Å and 0.008 Å. The performance of $\frac{1}{4}$ for the challenging Li_2 molecule is a notable improvement over the other functionals. This improved behaviour is a consequence of the fact that the functional is designed to yield accurate exchange-correlation potentials at the experimental geometries; the quality of the nuclear derivative (hence, the structures) is completely governed by

the quality of the exchange-correlation potential.

We then performed an assessment of $\frac{1}{4}$ for molecules that are not contained in the training set. In Table 3.5, we consider the bond lengths of 16 radicals with the TZ2P basis-set. Once more, HCTH-93 overestimates the bond lengths with mean and mean absolute errors of 0.012 Å and 0.012 Å respectively . The corresponding errors for $\frac{1}{4}$ are 0.002 Å and 0.008 Å once again a notable improvement also over B97-1.

In Table 3.6, we present the molecular structures for FOOF, FNO_2, O_3, FO_2, $Cr(CO)_6$ and $Ni(CO)_4$, which are demanding tests for computational methods. For the first row atoms, we used the TZ2P basis set and for the transition metals the (14s13p6d)/[8s7p4d] contraction, obtained by augmenting the basis set of Watchers [135].

HCTH-93 significantly overestimates the F-O and F-N bonds in FOOF and FNO_2. This overestimation is considerably reduced by $\frac{1}{4}$ although the other bond lengths become marginally less accurate. The $\frac{1}{4}$ bond angles are as accurate as HCTH-93. For the O_3 molecule, where the HCTH bond lengths are already too short, $\frac{1}{4}$ further shortens them. In FO_2, with HCTH-93 the F-O bond is reasonably accurate, although it shortens too much with $\frac{1}{4}$. For the bond angles, the results achieved with $\frac{1}{4}$ are an improvement over HCTH-93. It is important to point out that where $\frac{1}{4}$ has been unsuccessful, B97-1 is also problematic. Finally, for the transition metals complexes $Cr(CO)_6$ and $Ni(CO)_4$, the C-O bond length improves from HCTH-93 to $\frac{1}{4}$, although the metal-carbon bond shortens too much.

Table 3.4: Optimised geometries (in Å and degrees) for molecules S using 1/4, HCTH-93, and B97-1, with the TZ2P basis set

Molecule	Expt[1]	1/4	HCTH-93	B97-1
H_2	0.741	0.744	0.742	0.739
LiH	1.596	1.590	1.615	1.595
BeH	1.343	1.342	1.360	1.348
CH	1.120	1.127	1.133	1.127
$CH_2(^3B)$	1.078	1.077	1.081	1.080
	136.0	135.0	135.2	135.1
$CH_2(^1A)$	1.110	1.114	1.119	1.113
	101.9	100.9	100.6	101.4
CH_3	1.080	1.078	1.081	1.080
CH_4	1.086	1.087	1.090	1.090
NH	1.036	1.042	1.045	1.042
NH_2	1.024	1.027	1.030	1.028
	103.3	102.6	102.2	102.8
NH_3	1.012	1.012	1.014	1.014
	106.7	106.5	105.8	106.5
OH	0.970	0.976	0.976	0.973
H_2O	0.957	0.961	0.961	0.960
	104.5	104.5	104.1	104.7
HF	0.917	0.923	0.921	0.920
Li_2	2.673	2.696	2.772	2.729
LiF	1.564	1.571	1.594	1.575
C_2H_2	1.203	1.199	1.204	1.199
	1.063	1.064	1.066	1.064
C_2H_4	1.331	1.322	1.330	1.328
	1.081	1.083	1.086	1.084
	121.4	121.7	121.8	121.7
CN	1.172	1.163	1.170	1.165
HCN	1.065	1.069	1.071	1.068
	1.153	1.150	1.154	1.149
CO	1.128	1.128	1.133	1.128

Cont

Table 3.4: continued.

Molecule	Expt[1]	1/4	HCTH-93	B97-1
HCO	1.173	1.174	1.179	1.175
	1.123	1.124	1.128	1.125
	124.2	124.3	123.8	123.9
H_2CO	1.203	1.199	1.203	1.201
	1.102	1.109	1.113	1.108
	121.9	122.1	122.2	122.0
N_2	1.098	1.096	1.099	1.095
O_2	1.207	1.206	1.211	1.208
H_2O_2	1.456	1.443	1.455	1.447
	0.966	0.968	0.967	0.965
	100.5	100.3	100.1	100.5
F_2	1.412	1.400	1.407	1.396
CO_2	1.160	1.162	1.166	1.162
HCl	1.275	1.279	1.280	1.284
Na_2	3.079	3.023	3.169	3.073
Si_2	2.246	2.255	2.278	2.273
P_2	1.893	1.891	1.900	1.894
S_2	1.889	1.900	1.912	1.919
Cl_2	1.988	2.000	2.014	2.023
NaCl	2.361	2.357	2.397	2.373
SiO	1.510	1.516	1.522	1.513
CS	1.535	1.536	1.544	1.538
SO	1.481	1.494	1.502	1.494
ClO	1.570	1.573	1.583	1.591
ClF	1.628	1.641	1.650	1.647
Mean r		0.001	0.012	0.005
Mean abs. r		0.006	0.013	0.008
Mean θ		−0.3	−0.5	−0.2
Mean abs. θ		0.4	0.7	0.3

[1] Ref [115]

Table 3.5: Optimised bond lengths (in Å) for diatomic radicals, using 1/4, HCTH-93, and B97-1, with the TZ2P basis set

		Expt[1]	1/4	HCTH-93	B97-1
BH^+	$^2\Sigma^+$	1.215	1.205	1.218	1.210
NH^+	$^2\Pi$	1.070	1.084	1.084	1.078
OH^+	$^3\Sigma^-$	1.029	1.042	1.040	1.035
BeF	$^2\Sigma^+$	1.361	1.371	1.382	1.373
BN	$^3\Pi$	1.329[2]	1.317	1.333	1.324
BO	$^2\Sigma^+$	1.205	1.202	1.211	1.204
C_2^+	$^2\Pi_u$	1.301	1.311	1.322	1.325
CF	$^2\Pi$	1.272	1.276	1.285	1.277
NF	$^3\Sigma^-$	1.317	1.317	1.323	1.320
NO	$^2\Pi$	1.151	1.148	1.152	1.149
OF	$^2\Pi$	1.354[3]	1.346	1.352	1.348
F_2^+	$^2\Pi_g$	1.305[4]	1.305	1.309	1.294
Al_2	$^3\Sigma_g^-$	2.466	2.451	2.494	2.514
SiCl	$^2\Pi$	2.058	2.076	2.091	2.088
NS	$^2\Pi$	1.494	1.496	1.503	1.496
PO	$^2\Pi$	1.476	1.485	1.491	1.482
Mean			0.002	0.012	0.007
Mean abs.			0.008	0.012	0.011

[1]Ref. [131] unless otherwise stated

[2]Ref. [132]

[3]Ref. [133]

[4]Ref. [134]

Table 3.6: Optimised structures (in Å and degrees) of FOOF, FNO_2, O_3, FO_2, $Cr(CO)_6$ and $Ni(CO)_4$, using 1/4, HCTH-93, and B97-1. See text for basis set details.

	Expt	1/4	HCTH-93	B97-1
		FOOF		
r_{FO}	1.575[1]	1.593	1.614	1.513
r_{OO}	1.217[1]	1.183	1.184	1.236
θ_{FOO}	109.5[1]	111.3	111.8	109.1
τ	87.5[1]	89.1	89.7	87.9
		FNO_2		
r_{FN}	1.467[2]	1.502	1.518	1.470
r_{NO}	1.180[2]	1.172	1.175	1.179
θ_{ONO}	136.0[2]	136.8	136.8	135.8
		O_3		
r_{OO}	1.272[3]	1.257	1.263	1.256
θ_{OOO}	116.8[3]	118.3	118.4	118.1

Table 3.6: continued.

	Expt	1/4	HCTH-93	B97-1
		FO_2		
r_{FO}	1.649[4]	1.630	1.654	1.603
r_{OO}	1.200[4]	1.185	1.188	1.194
θ_{FOO}	111.2[4]	112.1	112.5	111.2
		$Cr(CO)_6$		
r_{CrC}	1.914 ± 0.002[5], 1.916 ± 0.002[6]	1.886	1.907	1.921
r_{CO}	1.140 ± 0.002[5], 1.140 ± 0.003[6]	1.144	1.148	1.141
		$Ni(CO)_4$		
r_{NiC}	1.838 ± 0.002[7], 1.817 ± 0.002[8]	1.812	1.838	1.844
r_{CO}	1.141 ± 0.002[7], 1.127 ± 0.003[8]	1.140	1.144	1.137

[1]Ref. [136]
[2]Ref. [137]
[3]Ref. [138]
[4]Ref. [139]
[5]Ref. [140]
[6]Ref. [141]
[7]Ref. [142]
[8]Ref. [143]

3.4.2 $\frac{1}{4}$ thermochemistry

The mean and mean absolute errors for atomization energies of molecules M in Table 3.1 are -0.6 and 7.0 kcal/mol with $\frac{1}{4}$, compared with values of 0.9 and 3.2 kcal/mol for HCTH-93. $\frac{1}{4}$ therefore provides a good average description although individual errors are larger than those obtained with HCTH-93. However, since the $\frac{1}{4}$ functional was built without including any explicit thermochemical information, the results achieved are very encouraging, since they are comparable with those obtained with the first-principles PBE GGA functional [113].

The performance of $\frac{1}{4}$ for total atomic energies and ionization energies is much less accurate. Total energies are significantly underestimated with mean and mean absolute errors of -16.9 and 18.0 kcal/mol, compared to -0.9 and 4.2 kcal/mol for HCTH-93. Ionization energies are overestimated with mean and mean absolute errors of 16.3 and 16.3 kcal/mol compared with 0.1 and 1.6 kcal/mol for HCTH-93.

A reason for the poor performance of the $\frac{1}{4}$ functional for total energies can be found in the work of van Leeuwen and Baerends [116], where they investigated the relationship between the exchange-correlation energy and potential. They demonstrated that a knowledge of the exchange-correlation potential for a given density is not sufficient to calculate the total exchange-correlation energy at that density. It is instead necessary to know the potential along a path in density space, connecting the system in question to one where the density is infinitely diffuse. Such a path is poorly represented by our fitting data. We also note that by fitting to shifted exchange-correlation potentials, the total energies from $\frac{1}{4}$ are only defined to within any functional whose potential is a constant [122].

In order to understand the atomization energy errors we considered the following analysis. The atomization energy is defined as the integral of the nuclear derivative along a path connecting the molecule to its constituent

atoms

$$\Delta E = \int_{R_{\text{exp}}}^{\infty} \frac{\partial E}{\partial X} dX \tag{3.24}$$

By construction the $\frac{1}{4}$ functional yields accurate nuclear derivatives close to equilibrium geometries, however they are not constrained to be accurate as the molecule dissociates. Figure 3.1 and Figure 3.2 shows the electronic energy and the nuclear gradient curve for the CH molecule, calculated with the HCTH-93 and $\frac{1}{4}$ functionals.

We observe good agreement between the nuclear gradient curves around the equilibrium geometry, however in the region between 2.5 and 5.0 Bohr, the $\frac{1}{4}$ nuclear gradient curve lies above HCTH-93. This inaccuracy is reflected in Figure 3.2 where we plot the cumulative atomization energy contribution

$$\Delta E = \int_{R_{\text{exp}}}^{R} \frac{\partial E}{\partial X} dX. \tag{3.25}$$

We believe that a reason for such an inaccuracy is due to the fact that the $\frac{1}{4}$ functional has been built only by fitting to potentials at experimental geometries. Hence, the nuclear gradient is no longer accurate when the molecule dissociates.

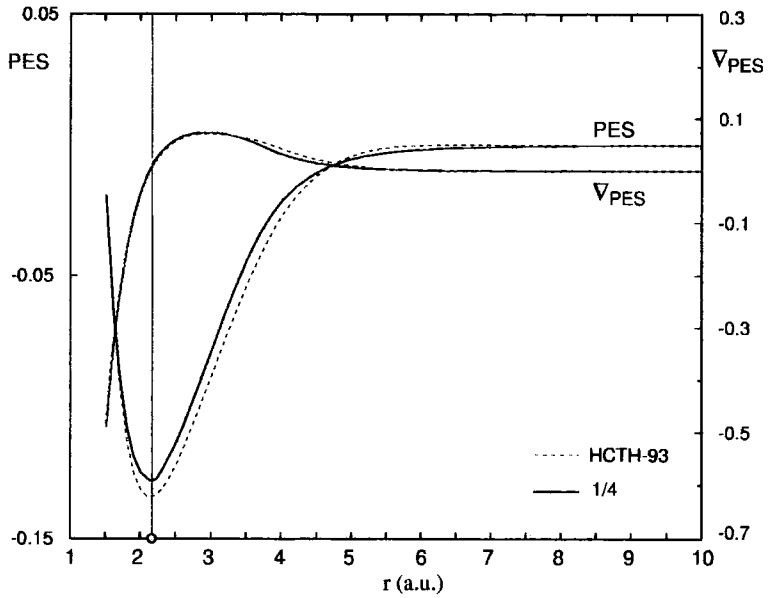

Figure 3.1: Comparison between the potential energy surface and its gradient for CH

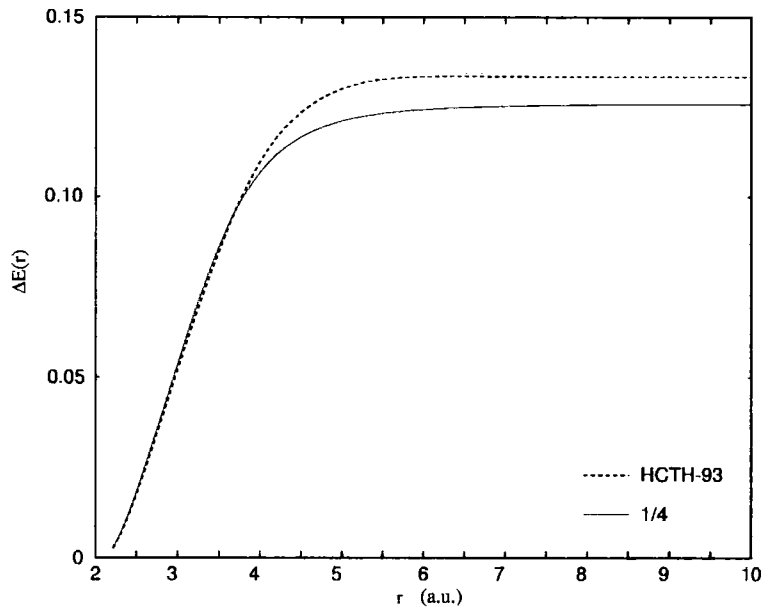

Figure 3.2: Comparison between the atomization energy contribution for CH calculated as the integral of the nuclear derivative

3.4.3 $\frac{1}{4}$ polarizabilities and excitation energies

In Table 3.7, we present the static isotropic polarizabilities of the systems P in Table 3.2, calculated using the Sadlej basis set [126] at near experimental geometries. As mentioned before, zero-point vibrational corrections would increase the calculated polarizabilities; Russell *et al* [127] have calculated corrections of 0.10, 0.29, 0.57, 0.90, 0.83, 0.40 and 0.15 a.u. for HF, H_2O, NH_3, CH_4, PH_3, H_2S and HCl respectively at the MP2 level of theory. In this thesis, where no zero-point corrections are introduced, accurate functionals should always give values that underestimate experimental values.

Conventional functionals such as LDA [146] and BLYP [89, 94] overestimate the polarizabilities of these systems. Mean and mean absolute errors are 0.83 and 0.83 a.u. for LDA [64] and 0.90, 0.90 a.u. for BLYP [64]. The results reflect overdiffuse electron densities caused by the poor representation of the asymptotic behavior of the exchange-correlation potential [64]. HCTH-93 already reduces this overestimation. However, $\frac{1}{4}$, having been built by fitting only to exchange-correlation potentials in relatively diffuse regions, has a further improved accurate asymptotic behaviour, reducing even more the mean and mean absolute errors to 0.15 and 0.24 a.u. respectively. The B97-1 (hybrid) functional provides the most accurate polarizabilities with errors of 0.09 and 0.22 a.u. respectively. This can be explained by the presence of a fraction of exact orbital exchange [147], which introduces Hartree-Fock character; Hartree-Fock tends to underestimate polarizabilities [148].

To assess the frequency dependence of the polarizability we present in Table 3.9 the vertical excitation energies for N_2, H_2CO and C_6H_6 at experimental geometries (CC=1.392 Å and CH=1.086 Å for C_6H_6. For N_2 and H_2CO see Table 3.4). For N_2 and H_2CO we used the Sadlej basis set [126] augmented with additional diffuse functions and for C_6H_6 we used the TZ2P basis-set augmented with a diffuse double-zeta *s-p-d* set at the center of the ring plane, with exponents 0.01 and 0.04. All the excitations in C_6H_6 are

from the HOMO π orbital e_{1g}.

Rydberg excitation energies depend on regions relatively far away from the molecule, so they are particularly sensitive to the asymptotic part of the exchange-correlation potential [150]. The HCTH-93 Rydberg excitation energies are in significant error reflecting the incorrect asymptotic form. By emphasizing the potential at relatively large distance, $\frac{1}{4}$ gives much improved Rydberg excitations. These values are particularly good for C_6H_6, where they are also an improvement over B97-1. Analogous improvements have also been observed for CO and C_2H_4 molecules.

Valence excitations from $\frac{1}{4}$ are not an improvement over HCTH-93. Indeed several of them are slightly smaller, hence less accurate with $\frac{1}{4}$. This suggests that the improved polarizabilities obtained with $\frac{1}{4}$ are associated with a better description of the higher lying virtual orbitals rather than the valence ones.

Although the $\frac{1}{4}$ potential is an improvement over HCTH-93, at large distances it still does not exhibit the correct form. This is evident for N_2 and H_2CO where the Rydberg errors remain unacceptably large. One way to improve these results would be to asymptotically correct the potential [64]. However, we did not consider this possibility since it relies on the accurate calculation of the ionization energies.

Table 3.7: Static isotropic polarisabilities (in atomic units) using 1/4, HCTH-93, and B97-1, with the Sadlej basis set.

	Expt[1]	1/4	HCTH-93	B97-1
HF	5.60	5.96	6.02	5.75
H_2O	9.64	10.11	10.25	9.81
N_2	11.74	11.83	11.94	11.84
CO	13.08[2]	13.19	13.33	13.05
F_2	8.38	8.63	8.69	8.62
NH_3	14.56	14.82	15.08	14.54
CO_2	17.51	17.31	17.42	17.17
CH_4	17.27	16.98	17.08	16.86
C_2H_4	27.70	27.56	27.96	27.92
PH_3	30.93	31.08	31.30	30.99
H_2S	24.71	24.91	25.18	24.99
SO_2	25.61	25.72	25.95	25.50
HCl	17.39	17.69	17.84	17.73
Cl_2	30.35	30.71	30.89	30.91
Mean		0.15	0.32	0.09
Mean abs.		0.24	0.36	0.22

[1]Ref. [144] unless otherwise stated

[2]Ref. [145]

Table 3.8: Singlet vertical excitation energies (in eV) for N_2, H_2CO, and C_6H_6 using 1/4, HCTH-93, and B97-1. See text for basis set details.

State	Transition	Expt[1]	1/4	HCTH-93	B97-1
		N_2			
$^1\Pi_u$	$\pi_u \rightarrow 3s\sigma_g$	13.24	12.15	11.48	12.15
$^1\Sigma_u^+$	$\sigma_g \rightarrow 3p\sigma_u$	12.98	11.20	10.48	11.71
$^1\Pi_u$	$\sigma_g \rightarrow 3p\pi_u$	12.90	11.23	10.49	11.69
$^1\Sigma_g^+$	$\sigma_g \rightarrow 3s\sigma_g$	12.20	10.85	10.19	11.35
$^1\Delta_u$	$\pi_u \rightarrow \pi_g$	10.27	10.16	10.08	9.79
$^1\Sigma_u^-$	$\pi_u \rightarrow \pi_g$	9.92	9.70	9.73	9.34
$^1\Pi_g$	$\sigma_g \rightarrow \pi_g$	9.31	9.12	9.15	9.29
Mean			−0.86	−1.25	−0.75
Mean abs.			0.86	1.25	0.75
		H_2CO			
$^1A_2$	$n \rightarrow 3db_1$	9.22	7.81	7.11	8.06
$^1A_2$	$n \rightarrow 3pb_1$	8.38	7.19	6.54	7.49
$^1B_1$	$\sigma \rightarrow \pi^*$	8.68	8.93	8.98	9.08
$^1B_2$	$n \rightarrow 3pa_1$	8.12	6.96	6.38	7.30
$^1A_1$	$n \rightarrow 3pb_2$	7.97	6.92	6.33	7.30
$^1B_2$	$n \rightarrow 3sa_1$	7.09	6.14	5.69	6.58
$^1A_2$	$n \rightarrow \pi^*$	3.94	3.84	3.92	3.95
Mean			−0.80	−1.21	−0.52
Mean abs.			0.87	1.29	0.64

[1]Ref. [149]
[2]CASPT2 values

Table 3.9: Singlet vertical excitation energies (in eV) for C_6H_6 using 1/4, HCTH-93, and B97-1. See text for basis set details.

State	Transition	Expt[1]	1/4	HCTH-93	B97-1
		C_6H_6			
3^1E_{1g}	$\pi \rightarrow 3d_{z^2}$	7.57[2]	7.38	6.72	7.21
1^1A_{2g}	$\pi \rightarrow 3d_{zx}, 3d_{zy}$	7.81	7.60	6.84	7.38
1^1E_{2g}	$\pi \rightarrow 3d_{zx}, 3d_{zy}$	7.81	7.58	6.83	7.36
2^1A_{1g}	$\pi \rightarrow 3d_{zx}, 3d_{zy}$	7.81?	7.59	6.84	7.36
2^1E_{1g}	$\pi \rightarrow 3d_{x^2-y^2}, 3d_{xy}$	7.535	7.31	6.65	7.19
1^1B_{2g}	$\pi \rightarrow 3d_{x^2-y^2}, 3d_{xy}$	7.460	7.32	6.66	7.19
1^1B_{1g}	$\pi \rightarrow 3d_{x^2-y^2}, 3d_{xy}$	7.460	7.30	6.65	7.19
2^1E_{1u}	$\pi \rightarrow 3p\pi$	7.41	7.18	6.40	6.88
1^1A_{1u}	$\pi \rightarrow 3p_x, 3p_y$	6.99[2]	6.77	6.17	6.75
1^1E_{2u}	$\pi \rightarrow 3p_x, 3p_y$	6.953	6.75	6.16	6.70
1^1A_{2u}	$\pi \rightarrow 3p_x, 3p_y$	6.932	6.75	6.17	6.67
1^1E_{1g}	$\pi \rightarrow 3s$	6.334	6.13	5.69	6.17
1^1E_{1u}	$\pi \rightarrow \pi^*$	6.94	6.92	6.99	7.13
1^1B_{1u}	$\pi \rightarrow \pi^*$	6.20	6.04	6.01	6.13
1^1B_{2u}	$\pi \rightarrow \pi^*$	4.90	5.27	5.28	5.46
Mean			−0.16	−0.69	−0.24
Mean abs.			0.19	0.73	0.32

[1]Ref. [149]

[2]CASPT2 values

3.4.4 $\frac{1}{4}$ and $\frac{7}{6}$ shielding constants

It has been shown [151, 152] that for highly correlated molecules containing nuclei from the first and the second rows of the periodic table, GGA shielding constants are more accurate than those from hybrid functionals. Although MP2 accuracy can be achieved [153], existing functionals cannot compete with more sophisticated wavefunction based methods.

Wilson *et al* [129] have presented a pragmatic new approach to improve DFT shielding constants. Kohn-Sham orbitals and eigenvalues calculated using a small amount of exact exchange (0.04) are used in an uncoupled formalism to determine the shieldings. In the context of the B97 functional, this method is denoted $\mathrm{B97}^{0.04}_{\mathrm{GGA}}$. The success of this inconsistent method, together with the poor performance of conventional functionals, highlights the difference between shielding constants and other chemical properties. The results in Table 3.3 also demonstrate this.

As a final assessment, in Table 3.10 we present the $\frac{1}{4}$ and $\frac{7}{6}$ shielding constants for the systems SC (in Table 3.2) determined using the Huzinaga (IGLO IV) basis set [128] at near experimental geometries. We compare the results with HCTH-93, B97-1, $\mathrm{B97}^{0.04}_{\mathrm{GGA}}$, high-level *ab initio* studies, and experimental values. Whereas $\frac{1}{4}$ shielding constants are very poor, $\frac{7}{6}$ is a notable improvement over HCTH-93 for most systems. This is a significant result since HCTH-93 has previously been shown [129] to offer an improvement over conventional hybrid and GGA functionals for these molecules.

To understand these shielding results, we considered the calculation of the paramagnetic shielding contributions $\sigma^{A\alpha\beta}_{\mathrm{para}}$. The mathematical expression for this quantity for nucleus A can be written as

$$\sigma^{A\alpha\beta}_{\mathrm{para}} = \sum_{bj} C^{A\alpha\beta}_{bj} \tag{3.26}$$

where $C^{A\alpha\beta}_{bj}$ is the contribution from the occupied-virtual molecular orbital excitation $j \rightarrow b$. An analysis of the quantity $C^{A\alpha\beta}_{bj}$ provides important insights into the behaviour of exchange-correlation functionals [155, 156].

Table 3.10: Isotropic shielding constants (in ppm) using 1/4, 7/6, HCTH-93, and B97-1, with the Huzinaga (IGLO IV) basis set.

		Expt[1]	Best *ab initio*[1]	$B97^{0.04}_{GGA}$	1/4	7/6	HCTH-93	B97-1
HF	F	419.7 ± 6	418.6	416.4	413.1	412.6	411.5	412.3
H_2O	O	357.6 ± 17.2	337.9	333.6	329.4	332.3	327.5	328.3
CO	C	2.8 ± 0.9	5.6	5.3	−15.7	1.8	−7.6	−13.9
	O	−36.7 ± 17.2	−52.9	−49.9	−74.9	−66.3	−67.0	−81.0
N_2	N	−59.6 ± 1.5	−58.1	−57.7	−84.4	−68.9	−76.6	−87.7
F_2	F	−192.8	−186.5	−194.2	−278.4	−262.9	−269.6	−241.5
$O_3(O'OO')$	O′	−1290	−1208.2	−1174.3	−1526.4	−1428.9	−1477.0	−1723.6
	O	−724	−754.6	−736.4	−900.0	−846.7	−872.5	−1135.8
H_2S	S	752 ± 12	754.6	739.1	718.7	763.5	720.1	716.8
SO_2	S	−126 ± 12	−134.2	−129.2	−214.0	−156.2	−185.6	−228.7
	O	−205 ± 17	−170.4	−213.4	−270.6	−263.4	−262.5	−280.4
PN	P	53	86	60.3	−34.0	23.9	−1.0	−30.0
	N	−349	−341	−332.0	−389.4	−363.4	−375.2	−415.8
trans-N_2F_2	N	−181.7	−165.5	−202.1	−246.5	−217.4	−235.1	−255.8
	F	95.1	103.7	67.4	24.5	31.5	31.6	47.6
Mean			8.0	1.2	−70.9	−41.6	−57.0	−100.3
Mean abs.			18.1	18.1	70.9	43.1	57.0	100.3
Mean abs.%			18.2	14.3	86.3	27.0	56.9	85.3

[1]Refs. [129, 130]

By contrast, diamagnetic terms are almost invariant to functional type, since they involve occupied orbitals only.

In Table 3.11 we consider the $C_{bj}^{A\alpha\beta}$ for the $\frac{7}{6}$ and $\frac{1}{4}$ functionals, for ^{13}C and ^{17}O nuclei in the CO and H_2O molecules. Since there are many occupied-virtual molecular orbital excitations (a total of 749 and 460 in CO and H_2O respectively), the analysis is limited to include only the dominant contributions ($|C_{bj}^{A\alpha\beta}| > 10$ ppm) involving excitations to the lowest-unoccupied molecular orbitals (LUMO), and excitations from the HOMO.

For comparison we also present the HCTH-93, B97-1, and $B97_{GGA}^{0.04}$ values. Single origin rather than LORG shielding constants are presented because the former conveniently partitions the total shieldings into diamagnetic and paramagnetic terms (due to the large basis-sets employed in this study, the total shieldings obtained from both methods are almost the same). HCTH-93 shielding constants are too low, i.e. too deshielded. Table 3.11 indicates that the improved performance of $B97_{GGA}^{0.04}$ arises because its dominant contributions to the paramagnetic shielding are less deshielded than those of HCTH-93. Interestingly, for the first three tabulated excitations in CO and the first four in H_2O, the $\frac{7}{6}$ contributions in Table 3.11 also exhibit a significant reduction in deshielding compared to HCTH-93. The orbitals involved in these excitations are low-lying and compact, correlating qualitatively with the regions emphasized in the $\frac{7}{6}$ development. For the remaining tabulated excitations, it is the $\frac{1}{4}$ functional that generally provides a reduction in deshielding (values that are often close to those of $B97_{GGA}^{0.04}$). These excitations involve more diffuse orbitals, which correlate better with the regions emphasized in the $\frac{1}{4}$ development. This reduction in deshielding is consistent with the increased excitation energies to the higher states, discussed in Section 3.4.3. In summary, for a given excitation, a general reduction in deshielding is exhibited by the functional which better emphasizes the region of space appropriate for that particular excitation. (We have also observed this general trend for the other dominant excitations that do not involve HOMO and LUMO).

Unfortunately, neither $\frac{7}{6}$ nor $\frac{1}{4}$ reproduces the general trend of $B97^{0.04}_{GGA}$ for all the excitations. $\frac{7}{6}$ and $\frac{1}{4}$ tend to give values that are too deshielded relative to $B97^{0.04}_{GGA}$ for the higher and lower excitations, respectively, which corresponds to the spatial regions that are not well emphasized in their respective fits. Given that the dominant contributions to the shielding are from excitations involving low-lying orbitals, $\frac{7}{6}$ is the more accurate of the two functionals.

This analysis raises an interesting suggestion. Since $\frac{7}{6}$ and $\frac{1}{4}$ can independently reduce the shieldings of the different classes of excitations, a more flexible functional that allow us to emphasize both regions of space simultaneously is necessary. We investigate this possibility in Section 3.6.

In view of the growing number of DFT studies involving the computation of metal shieldings in transition metal complexes, we conclude by considering the performance of the $\frac{1}{4}$ and $\frac{7}{6}$ functionals on the ^{59}Co shielding in the $[Co(CN)_6]^{3-}$ complex. We choose this complex because an experimental shielding value (-5400 ppm) has been determined. The $\frac{1}{4}$ and $\frac{7}{6}$ shieldings are almost identical (-3500 and -3497 ppm, respectively) and are inferior to HCTH-93 (-3610 ppm). The B97-1 value of -5277 ppm reinforces the fact that for the metal-shieldings in transition metal complexes, hybrid functionals generally provide a dramatic improvement over GGA functionals.

Table 3.11: Dominant paramagnetic shielding contributions $C_{bj}^{A\alpha\beta}$ (in ppm) involving the HOMO and LUMO for CO and H_2O.

j	b	$\alpha\beta$	7/6	1/4	HCTH-93	B97-1	$B97_{GGA}^{0.04}$
				$A = {}^{13}C$ in CO[a]			
3	8	xx	−11.1	−15.2	−13.8	−13.4	−13.3
4	8	xx	−40.8	−52.2	−48.0	−45.2	−45.6
7	8	xx	−252.2	−294.9	−285.7	−263.4	−258.9
7	12	xx	−53.2	−28.9	−31.2	−43.4	−28.2
7	21	xx	−23.0	−15.7	−17.8	−17.8	−16.1
				$A = {}^{17}O$ in H_2O[b]			
3	6	yy	−25.4	−31.2	−29.9	−25.8	−28.9
5	6	xx	−41.8	−47.8	−46.9	−40.4	−44.0
5	7	zz	−5.6	−37.4	−30.6	−28.6	−30.5
5	8	xx	15.0	13.4	12.9	11.1	13.1
5	10	zz	−26.7	−21.3	−24.9	−20.9	−21.5
5	13	xx	−29.0	−19.1	−23.0	−20.5	−19.3
5	14	zz	−7.4	−25.0	−23.8	−17.4	−21.2
5	16	zz	−71.8	−37.5	−44.5	−51.5	−42.1
5	18	zz	11.1	9.2	9.9	8.9	9.2
5	26	zz	−10.8	−10.4	−10.4	−10.7	−10.1

[a] Internuclear axis in z direction

[b] Molecule in xz plane with z component along C_{2v} axis

3.5 The exchange-correlation potential

To help understand the results in Section 3.3 it is informative to investigate the behaviour of the exchange-correlation potentials associated with each functional. We considered the Neon atom, comparing with the near-exact ZMP potential, shifted by the appropriate amount for each functional.

Figure 3.3 examines the potentials close to the nucleus, between 0 and 2 a.u. In moving from $p = 0$ to $p = \frac{7}{6}$, the agreement improves. This is as expected, since increasing p emphasizes regions closer to the nucleus. In particular, by increasing p the description of the inter-shell peak improves. Keal and Tozer [157] have demonstrated that an accurate description of the inter-shell peak is important for accurate shieldings. Hence, this explains our observation in Table 3.3 that shieldings improve notably from $p = 0$ to $p = \frac{7}{6}$.

Figure 3.4 considers the region from 2 and 6 a.u. As expected, optimal agreement is now obtained with smaller values of p. This explains the high-quality Rydberg excitations from $\frac{1}{4}$. Furthermore, given that the best quality structures are obtained with smaller p, this suggests that the long-range potential is also important for structural predictions.

Finally in Figure 4.8, we plot the $\frac{1}{4}$ exchange-correlation potential compared with the near-exact shifted ZMP one. We observe a very good agreement in the long range part of the plot and a poor representation of the core-region which is consistent with the molecular properties predicted with $\frac{1}{4}$.

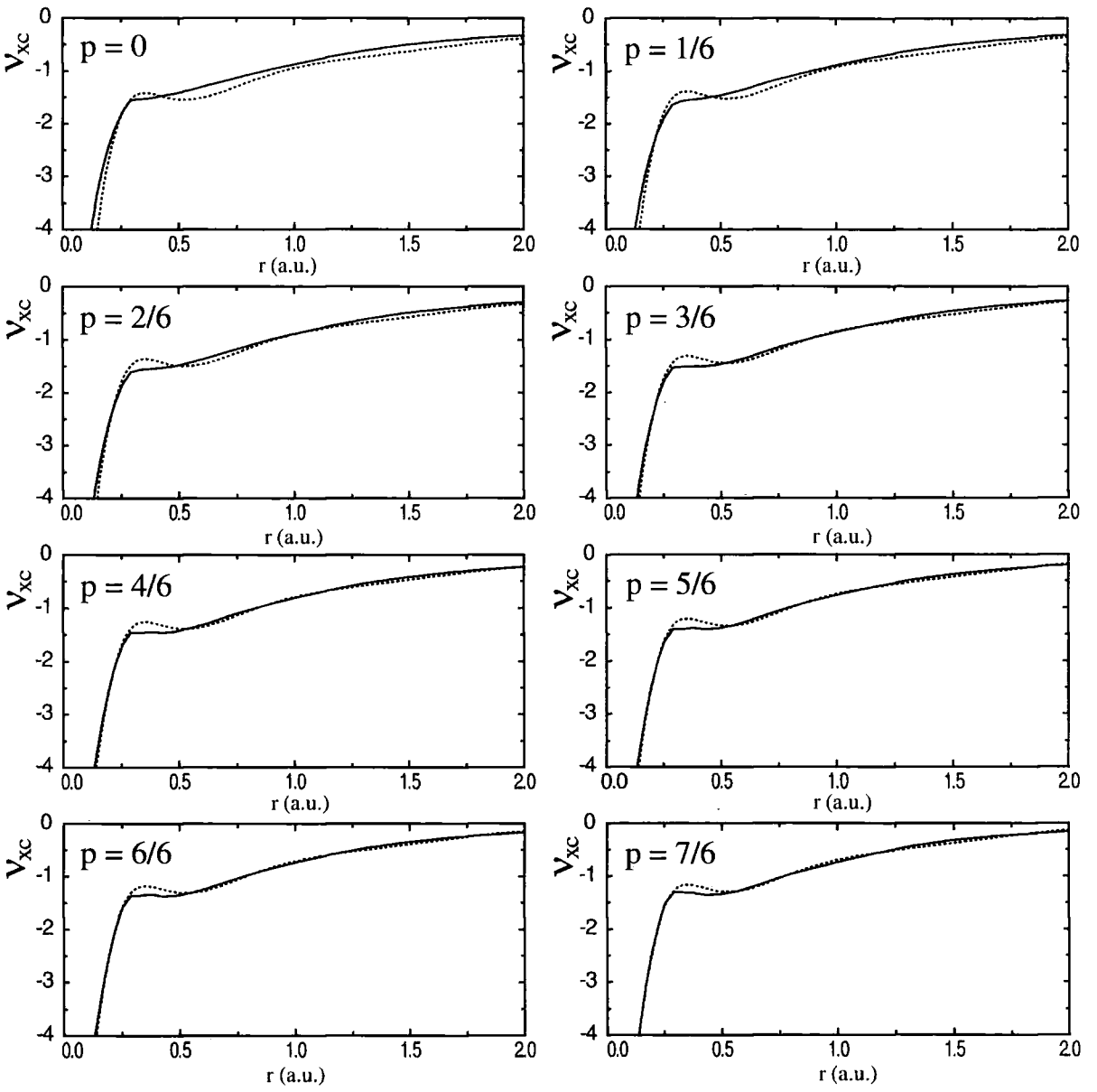

Figure 3.3: Comparison between the description of the core regions for the Ne atom by all the functionals developed for values of p=0...$\frac{7}{6}$ compared to the ZMP+k potential

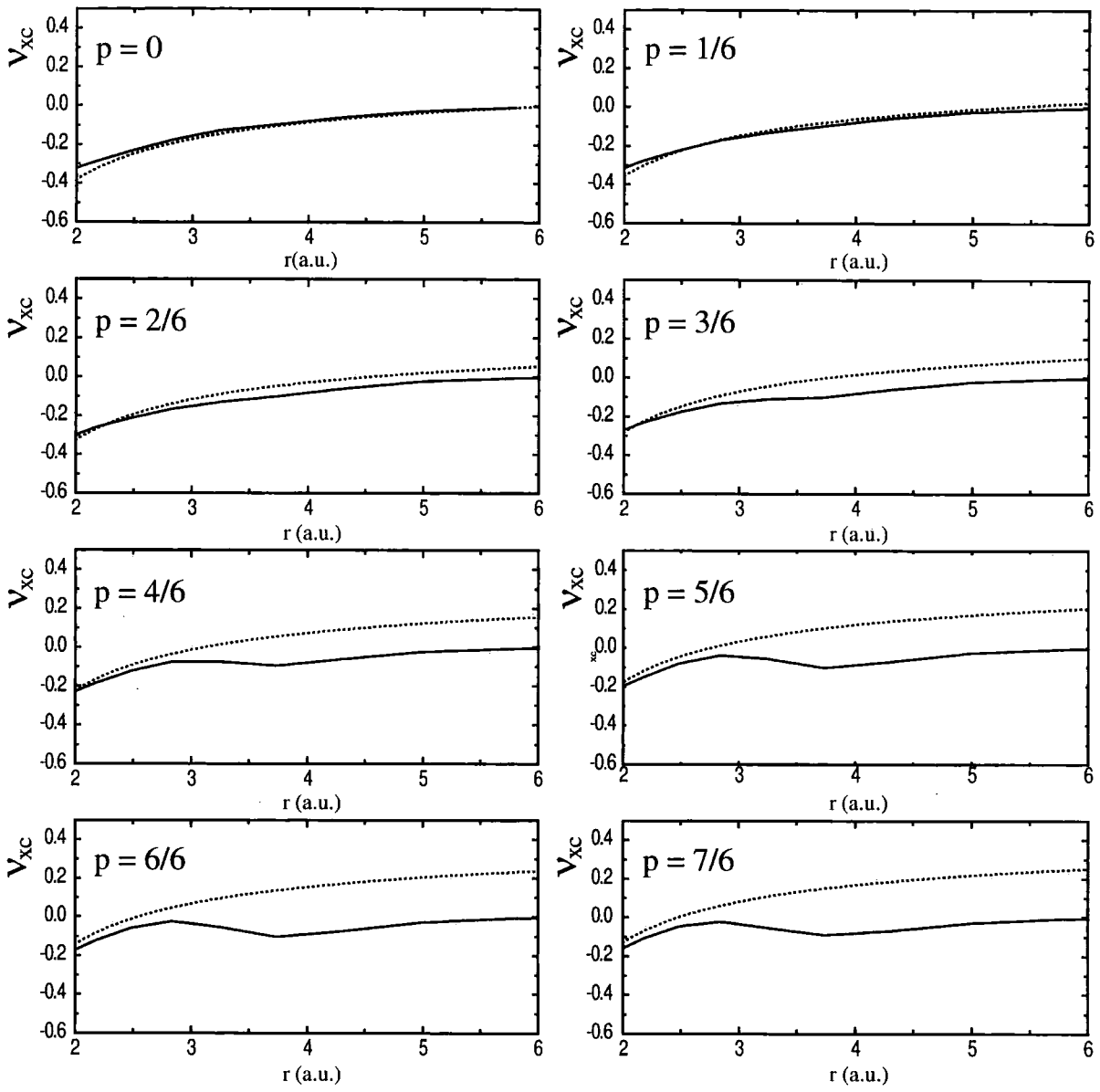

Figure 3.4: Comparison between the description of the long-range regions for the Ne atom by all the functionals developed for values of p=0...$\frac{7}{6}$ compared to the ZMP+k potential

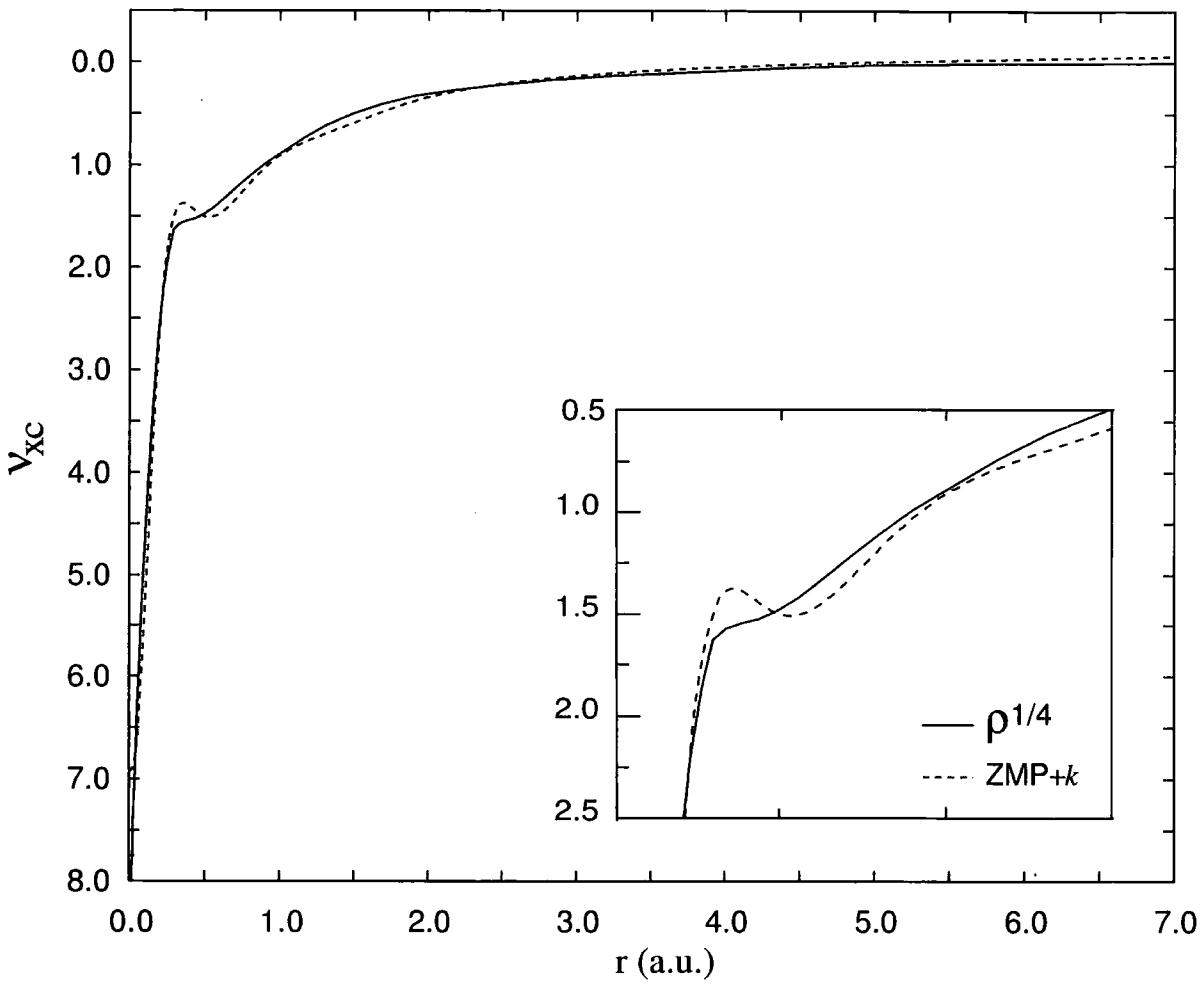

Figure 3.5: Comparison between the $\frac{1}{4}$ and the ZMP+k potentials for the Ne atom

3.6 Improving functional performance

We investigated several approaches for improving functional performance. All the coefficients for the more significant functionals are presented in Appendix A.

3.6.1 Changing the functional form

We considered the introduction of additional expansion terms in the functional. To prevent the number of parameters becoming excessively large, we initially considered whether all 15 terms in the original $\frac{1}{4}$ functional form were important. In Figure 3.6 we plot the trend of the minimized values of Ω as a function of the number of expansion coefficients composing the $p = \frac{1}{4}$ functional. We observe that the most significant jump occurs between 3 and

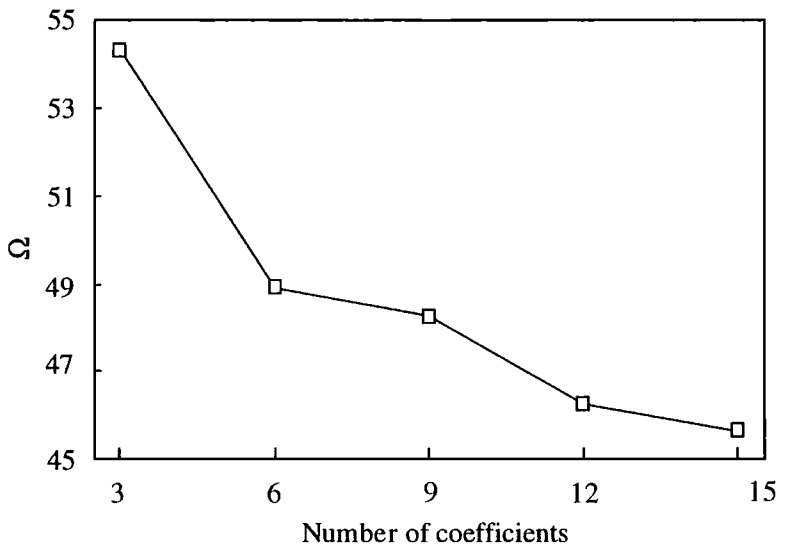

Figure 3.6: Minimized values of Ω_V plotted as a function of the number of coefficients composing the functional.

6 coefficients. We therefore assessed the performance of the $p = \frac{1}{4}$ functional with only 6 expansion coefficients. In moving from 15 to 6 solutions, the new $p = \frac{1}{4}$ functional overestimates the bond lengths, with MAE errors degrading

from 0.006 Å to 0.014 Å. The same trend is observed for the thermochemistry, where the combined MAE degrades from 10.1 kcal/mol to 14.9 kcal/mol.

It is therefore clear that reducing the number of terms leads to a significant reduction in accuracy; the 6 term functional is a poor starting point for further functional expansion. We therefore considered adding new terms directly to the original 15 terms. We considered the general term

$$F_{\text{extra}} = \rho^a \left(\frac{0.004|\nabla\rho|^2}{\rho^{\frac{8}{3}} + 0.004|\nabla\rho|^2} \right)^b \tag{3.27}$$

where a and b are new coefficients to determine. The new functional form is then

$$E_{\text{xc}}^{\text{GGA}} = \sum_i c_i \int f_i(\rho_\sigma, |\nabla\rho_\sigma|) d\mathbf{r} + F_{\text{extra}} \tag{3.28}$$

After coding the new term in the CADPAC package, we performed extensive tests to check our implementation. We confirmed that our code was variational by checking agreement between the analytic dipole and the finite difference dipole determined from energies in the presence of an electric field (Hellmann-Feynman). We also confirmed the agreement between analytic and numerical polarizabilities.

We performed extensive investigations into values of a and b, together with the number of extra terms. Our best functional involved the addition of the 6 terms

$$\begin{gathered} \rho^{\frac{14}{12}} u^1 \\ \rho^{\frac{14}{12}} u^2 \\ \rho^{\frac{14}{12}} u^3 \\ \rho^{\frac{18}{12}} u^1 \\ \rho^{\frac{18}{12}} u^2 \\ \rho^{\frac{18}{12}} u^3 \end{gathered} \tag{3.29}$$

using $p = 0$. It provided MAE for the bond lengths of 0.007 Å. At the same time also the MAE for the shielding constants improved significantly, decreasing to 31.3 ppm, compared with the 35 ppm of HCTH-93. Shieldings are presented in Table 3.12 However, very poor results for polarizabilities and thermochemistry were observed. It is interesting to point out that, by

Table 3.12: Isotropic shielding constants (in ppm) using HCTH-93, 1/4, and the best 21-solutions functional, with the TZ2P basis set.

			Best			
		Expt[1]	*ab initio*[1]	HCTH-93	1/4	21 solns
HF	H	419.7	418.6	411.5	412.2	415
H_2O	O	357.6	337.9	327.6	328.5	331.9
CH_4	C	198.4	198.9	189.3	188.8	192.4
CO	C	2.8	5.6	−7.5	−12.9	−8.3
	O	−36.7	−52.9	−66.8	−73.1	−66.2
N_2	N	−59.6	−58.1	−76.9	−82.2	−75.2
F_2	F	−192.8	−186.5	−269.9	−276.6	−251.2
O'OO'	O'	−1290	−1208.2	−1438.2	−1470.9	−1404.2
	O	−724	−754.6	−859.4	−883.4	−841.7
PN	P	53	86	−7.6	−27.8	−18.2
	N	−349	−341	−378.5	−391.8	−377.3
H_2S	S	752	754.6	720.1	715.5	727.6
NH_3	N	273.3	270.7	259.8	260.3	264
HCN	C	82.1	86.3	75.7	72.1	75.8
	N	−20.4	−13.6	−33.4	−41.3	−32.9
C_2H_2	C	117.2	121.8	112.2	108.4	112.2
H_2CO	C	−4.4	4.7	−17.7	−24.8	−20.7
	O	−375	−383.1	−406.7	−431.6	−414.6
CO_2	C	58.8	63.5	57.5	53.7	57.7
	O	243.4	236.4	215.3	213.5	217.5
HCl	Cl	952	962.3	949.4	947.6	956.4
SO_2	S	−126	−134.2	−183.9	−203.8	−182.4
	O	−205	−170.4	−260.6	−267.9	−253.1
PH_3	P	599.9	594	576.6	570.4	581.4
Mean abs.			12.9	35	43.5	31.3

[1]Refs. [129] and [130]

contrast with the assessment presented in Section 3.5, increasing the value of p beyond $p = 0$ lead to very poor geometries.

3.6.2 Changing the weighting factor

Next we investigated whether improved performance could be obtained by varying the weighting factor $W_{T\sigma}(\mathbf{r})$ in Eq.(3.21). In particular, we wished to investigate whether improved shielding constants could be obtained. It is known [158] that the HOMO-LUMO contribution to the shielding can be particularly important. We therefore considered a weighting factor that emphasized the regions of space where the HOMO and LUMO orbitals are significant. Results are presented in Table 3.13.

Using the original 15 expansion coefficients, we investigated different expressions for $W_{M\sigma}(\mathbf{r})$ starting with

$$W_{M\sigma}(\mathbf{r}) = \varphi^2_{\text{HOMO}}(\mathbf{r}) + \varphi^2_{\text{LUMO}}(\mathbf{r}) \tag{3.30}$$

The corresponding mean absolute error for shieldings decreased to 40.9 ppm compared to 43.5 ppm predicted by $\frac{1}{4}$, but still is not an improvement over the original HCTH-93. We then considered

$$W_{M\sigma}(\mathbf{r}) = \rho(\mathbf{r}) + \varphi^2_{\text{LUMO}}(\mathbf{r}) \tag{3.31}$$

which reduced the error to 31.7 ppm, which is not only an improvement over $\frac{1}{4}$ but also over HCTH-93. Finally, we studied the possibility of removing one of the core-orbitals, so that the corresponding exchange-correlation potential could have a larger degree of freedom to represent the inter-shell peak

$$W_{M\sigma}(\mathbf{r}) = \rho(\mathbf{r}) - \varphi^2_{1s}(\mathbf{r}) \tag{3.32}$$

This final attempt was particularly successful, reducing the MAE to 26.6 ppm. These are the most accurate results obtained in this chapter. The removal of other core orbitals did not introduce any further improvement. It is important to point out that the predictions of all the other molecular

Table 3.13: Isotropic shielding constants (in ppm) using HCTH-93, 1/4, and the best 21-solutions functional, with the TZ2P basis set.

		Expt[1]	Best *ab initio*[1]	HCTH-93	1/4	$(\varphi_H^2 + \varphi_L^2)$	$(\rho + \varphi_L^2)$	$(\rho - \varphi_{1s}^2)$
HF	H	419.7	418.6	411.5	412.2	411.4	411.5	410.3
H_2O	O	357.6	337.9	327.6	328.5	327.3	329.4	329.5
CH_4	C	198.4	198.9	189.3	188.8	188.5	191.3	191.1
CO	C	2.8	5.6	−7.5	−12.9	−11.8	−3	1.8
	O	−36.7	−52.9	−66.8	−73.1	−70.9	−66.1	−64.5
N_2	N	−59.6	−58.1	−76.9	−82.2	−81.1	−73.4	−68.4
F_2	F	−192.8	−186.5	−269.9	−276.6	−276.1	−271.5	−260.1
O'OO'	O'	−1290	−1208.2	−1438.2	−1470.9	−1463.8	−1422.6	−1387.8
	O	−724	−754.6	−859.4	−883.4	−873.6	−853.6	−846.5
PN	P	53	86	−7.6	−27.8	−22.7	−7.1	21.3
	N	−349	−341	−378.5	−391.8	−387.1	−374.3	−372.3
H_2S	S	752	754.6	720.1	715.5	716.6	738.4	742.4
NH_3	N	273.3	270.7	259.8	260.3	259.2	262.6	263.2
HCN	C	82.1	86.3	75.7	72.1	73.2	78	80.4
	N	−20.4	−13.6	−33.4	−41.3	−37.9	−32.2	−30.7
C_2H_2	C	117.2	121.8	112.2	108.4	110.1	113.5	114.4
H_2CO	C	−4.4	4.7	−17.7	−24.8	−21.8	−15.9	−12.8
	O	−375	−383.1	−406.7	−431.6	−419.3	−420.2	−425.1
CO_2	C	58.8	63.5	57.5	53.7	55.1	58.2	58.7
	O	243.4	236.4	215.3	213.5	213.4	219	223.1
HCl	Cl	952	962.3	949.4	947.6	947.9	959.9	962.1
SO_2	S	−126	−134.2	−183.9	−203.8	−195.9	−170.5	−158.5
	O	−205	−170.4	−260.6	−267.9	−266	−261.9	−258.1
PH_3	P	599.9	594	576.6	570.4	571.5	592.9	596.1
Mean abs.			12.9	35	43.5	40.9	31.7	26.6

[1]Refs. [129] and [130]

properties were rather poor with these functionals. They can be viewed as being designed especially for shielding calculations.

Chapter 4

Applications of the $\frac{1}{4}$ functional

Chapter 3 demonstrated that the $\frac{1}{4}$ functional provides very high quality molecular structures for molecules resembling those in the fitting data. In this chapter we investigate $\frac{1}{4}$ structural predictions for a much wider range of molecules; harmonic frequencies are also considered.

First, we investigate a benchmark of sulfur containing molecules that have been considered a challenge for GGA functionals. We then develop a completely new benchmark of molecules, drawn uniformly from the first three rows of the periodic table. Results are discussed in terms of the enhancement factor.

4.1 Sulfur compounds

Several studies have been performed to assess the performance of DFT functionals for benchmarks of sulfur containing compounds [159, 160]. This is due to the fact that, in general, GGAs overestimate the bond lengths of these systems, especially when sulfur is bonded to electronegative elements such as F and Cl. One solution to this overestimation is to apply hybrid functionals, which are known to shorten the bond lengths.

Nevertheless, it is also important to assess the performance of GGAs for these systems in order to understand to what extent they can provide

satisfactory approximations. Altmann and Handy [161] have shown that the HCTH-93 [97] functional improves the bond lengths and the vibrational frequencies of such molecules, with respect to the widely used BLYP [89, 94] functional, however some molecules remain particularly problematic. We now investigate whether our $\frac{1}{4}$ functional can further reduce the inaccuracies in the molecular predictions.

4.1.1 Computational details

We considered the benchmark of 20 small sulfur containing molecules investigated by Altmann and Handy [161]. Molecular structures were determined using the cc-pVTZ basis set of Dunning [162, 163], in order to be consistent with this earlier study. Vibrational frequencies were calculated using a two-point finite difference of first derivatives. To reduce numerical integration errors, extensive integration grids were used. The $\frac{1}{4}$ results are compared with those of HCTH-93 and MP2. We have confirmed that our HCTH-93 results are in excellent agreement with those of Altmann and Handy.

4.1.2 Molecular geometries

Tables 4.1 and 4.2 present the HCTH-93, $\frac{1}{4}$, MP2 and experimental bond lengths and bond angles for the benchmark of sulphur compunds. All the molecules have been classified according to the nature of the bond. The errors Δ_n (where n= HCTH-93, $\frac{1}{4}$ and MP2) are the differences between the calculated and experimental values. The largest sulfur-halogen errors are highlighted in bold.

In general, the results show that HCTH-93 tends to overestimate bond lengths, particularly for F_2SO, F_2S, Cl_2S and Cl_2S_2 molecules. It has been argued [161] that the reason for this lack of accuracy is that molecules containing sulfur-halogen bonds were not included into the training set used to develop HCTH-93. However, our $\frac{1}{4}$ functional, which has been determined

using the same training set as HCTH-93, reduced these errors and in general shortens all the bond lengths compared to HCTH-93. In moving from HCTH-93 to $\frac{1}{4}$ the error in the S-F bond for F_2SO decreases from 0.045 to 0.034 Å and in F_2S it decreases from 0.030 to 0.022 Å. The same trend is observed for the S-Cl bond length error in Cl_2S, which decreased from 0.021 Å to 0.005 Å and in Cl_2S_2 which decreased from 0.053 Å to 0.032 Å. It is also important to point out that for CL_2S $\frac{1}{4}$ gives improved geometries also compared to MP2. Finally, we note that the S-O bonds that are overestimated by HCTH-93 are also shortened by $\frac{1}{4}$, which achieves an accuracy comparable to MP2.

Figure 4.1 plots values of Δ_n for the three different methods. It is clear that $\frac{1}{4}$ lowers the errors of HCTH-93, and for many systems approaches the accuracy of MP2. These observations are also reflected by the magnitude of the corresponding mean absolute errors (for the bond lengths in Table 4.1 the errors are 0.010, 0.011 and 0.016 Å for MP2, $\frac{1}{4}$ and HCTH-93 respectively. Unlike bond lengths, HCTH-93 and $\frac{1}{4}$ predict almost identical bond angles and their differences from the experimental values are within one degree. The only exceptions are SSCl and ClSCl, where their values reduce from 2.8 to 2.3 deg and from 2.4 to 1.9 deg respectively, for HCTH-93 and $\frac{1}{4}$.

We have therefore demonstrated that the inclusion of sulphur-halogen compounds in the training set used to develop a GGA exchange correlation functional is not necessary to improve the performance of the functional. Improvements can instead be achieved by introducing appropriate physics by fitting solely to exchange-correlation potentials, as in the $\frac{1}{4}$ development.

4.1.3 Vibrational frequencies

Table 4.3 shows the harmonic vibrational frequencies and their errors from experiment for the benchmark molecules using HCTH-93, $\frac{1}{4}$ and MP2. Since

Table 4.1: Experimental bond lengths in Å and errors (difference between calculated and expt) with the triple-ζ cc-pVTZ basis set.

	Mol	HCTH-93	$\Delta_{\text{HCTH-93}}$	1/4	$\Delta_{1/4}$	MP2	Δ_{MP2}	r_{exp}	ref
S-H	H_2S	1.346	0.010	1.343	0.007	1.335	−0.001	1.336	[165]
	HSOH	1.358		1.355		1.342			
	H_2S_2	1.353	0.011	1.351	0.009	1.339	−0.003	1.342	[166]
	HSF	1.354		1.351		1.339			
	CLS2H	1.358		1.356		1.343			
S-O	F_2SO	1.439	0.026	1.435	0.022	1.433	0.020	1.413	[167]
	SO_3	1.445	0.025	1.441	0.021	1.442	0.022	1.420	[168]
	HSOH	1.682		1.670		1.676			
	FSOH	1.636		1.625		1.625			
	FSOF	1.477		1.474		1.449			
S-C	CS_2	1.559	0.006	1.552	−0.001	1.562	0.009	1.553	[169]
	H_2CS	1.611	0.000	1.603	−0.008	1.614	0.003	1.611	[170]
	OCS	1.565	0.004	1.557	−0.004	1.566	0.005	1.561	[171]
	C_2H_6S	1.812	0.010	1.793	−0.009	1.806	0.004	1.802	[172]
S-F	F_2SO	1.630	**0.045**	1.619	**0.034**	1.602	0.017	1.585	[167]
	F_2S	1.617	**0.030**	1.609	**0.022**	1.601	0.014	1.587	[173]
	FSOH	1.645		1.636		1.627			
	FSOF	1.618		1.610		1.595			
	HSF	1.639		1.631		1.628			
	F_2S_2	1.670		1.661		1.641			
S-Cl	Cl_2S	2.036	**0.021**	2.020	**0.005**	2.024	0.009	2.015	[174]
	Cl_2S_2	2.110	**0.053**	2.089	**0.032**	2.063	0.006	2.057	[174]
	ClS_2H	2.089		2.071		2.058			
S-S	H_2S_2	2.066	0.011	2.049	−0.006	2.065	0.010	2.055	[166]
	F_2S_2	1.902		1.889		1.906			
	Cl_2S_2	1.939	0.008	1.929	−0.002	1.964	**0.033**	1.931	[174]
	ClS_2H	2.015		2.000		2.023			
S-N	H_3NS	1.830		1.812		1.826			
S-P	H_3PS	1.938		1.928		1.938			
O-H	HSOH	0.964		0.965		0.963			
	FSOH	0.968		0.968		0.966			
C-H	H_2CS	1.093	0.000	1.090	−0.003	1.086	−0.007	1.093	[170]
	C_2H_6S	1.093	0.002	1.091	0.000	1.087	−0.004	1.091	[172]
C-O	OCS	1.164	0.007	1.160	0.003	1.168	0.011	1.157	[171]
F-O	FSOF	1.777		1.748		1.841			

Table 4.2: Experimental bond angles in degrees and errors (difference between calculated and expt) with the triple-ζ cc-pVTZ basis set.

	Mol	HCTH-93	$\Delta_{\text{HCTH-93}}$	1/4	$\Delta_{1/4}$	MP2	Δ_{MP2}	r_{exp}	ref
HSH	H_2S	92.0	0.2	92.8	0.6	92.2	0.0	92.2	[165]
FSH	HSF	96.2		96.1		96.1			
FSF	F_2SO	93.7	0.9	93.4	0.6	92.7	−0.1	92.8	[167]
	F_2S	99.7	1.6	99.3	1.2	98.7	0.6	98.1	[173]
HSO	HSOH	98.9		98.6		98.4			
SOH	HSOH	105.9		106.5		105.8			
	FSOH	108.1		109.6		107.8			
FSO	FSOH	102.2		101.9		101.3			
	F_2SO	106.6	−0.2	106.4	−0.4	106.7	−0.1	106.8	[?]
	FSOF	108.6		108.3		109.6			
SOF	FSOF	111.5		111.0		107.2			
SSH	H_2S_2	98.7	0.8	98.7	0.8	97.8	−0.1	97.9	[166]
	ClS_2H	100.0		100.0		98.5			
SSCl	Cl_2S_2	111.0	**2.8**	110.5	**2.3**	107.1	−1.1	108.2	[174]
	Cl_2S_2H	108.0		107.6		105.3			
SSF	F_2S_2	109.8		109.6		108.0			
HCS	C_2H_6S	106.6	0.0	107.1	0.5	107.5	0.8	106.6	[172]
	C_2H_6S	111.5	0.7	111.4	0.6	110.8	0.0	110.8	[175]
CSC	C_2H_6S	99.2	0.3	99.8	0.9	96.9	−2.0	98.9	[172]
ClSCl	Cl_2S	105.1	**2.4**	104.6	**1.9**	102.7	0.0	102.7	[174]
SCH	H_2CS	122.3	0.7	122.2	0.6	121.8	0.2	121.6	[170]
SNH	H_3NS	110.9		110.9		110.5			
HNH	H_3NS	108.1		108.0		108.4			
SPH	H_3PS	118.1		118.2		117.7			
HPH	H_3PS	99.6		99.6		100.2			

the range of the vibrational frequencies is very large, Δ_n is instead a percentage error

$$\Delta_n = \frac{(\omega_{\text{calc}} - \omega_{\text{exp}})}{\omega_{\text{exp}}} \cdot 100 \tag{4.1}$$

For molecules without halogen atoms, both HCTH-93 and $\frac{1}{4}$ perform well. For halogen-containing molecules, the HCTH-93 accuracy degrades whereas $\frac{1}{4}$ generally performs better. Figure 4.2 is a histogram of the absolute values of the averaged percentage errors in Table 4.3 for each of the compounds except H_3PS, HSF and HSOH, due to the difficulty in assigning their fundamentals. The figure reflects our analysis, showing that on average, relative to MP2, HCTH-93 and $\frac{1}{4}$ have a similar trend for molecules without halogens, whereas $\frac{1}{4}$ is more successful for halogen-containing compounds. In particular, the calculated mean absolute errors for the molecules in Figure 4.2 are 2.8, 1.9 and 2.1% for HCTH-93, $\frac{1}{4}$ and MP2 respectively.

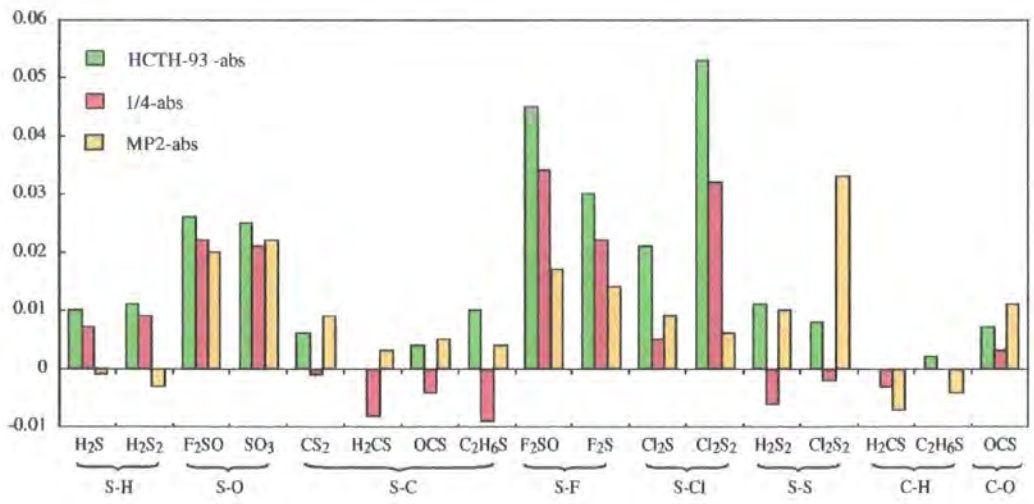

Figure 4.1: Bond length differences: (HCTH-93 minus expt.), ($\frac{1}{4}$ minus expt.) and (MP2 minus expt.) for the different type of bonds.

Table 4.3: Experimental harmonic vibrational frequencies in cm^{-1} and percentage difference errors Δ (see text for details) with the cc-pVTZ basis set.

Mol	HCTH-93	$\Delta_{\text{HCTH-93}}$	1/4	$\Delta_{1/4}$	MP2	Δ_{MP2}	ω_{exp}	Ref.
H_2S								
A_1	2670	−2	2693	−1	2780	2	2727	[164]
	1181	0	1174	−1	1211	2	1183	[164]
B_2	2688	−2	2711	−1	2799	2	2739	[164]
OCS								
$\sum^+$	2098	2	2123	3	2100	2	2062	[164]
	874	2	892	4	890	4	859	[164]
Π	513	−1	519	0	523	1	520	[164]
	513	−1	519	0	523	1	520	[164]
CS_2								
$\sum_u$	1565	2	1594	4	1625	6	1533	[164]
$\sum_g$	667	1	681	4	676	3	658	[164]
Π_u	394	−1	400	1	402	1	397	[164]
	394	−1	400	1	402	1	397	[164]
C_2H_6S								
A_1	3098	−1	3132	0	3186	2	3136	[176]
	2994	−2	3024	−1	3070	0	3064	[176]
	1457	1	1434	−1	1503	4	1447	[176]
	1339	0	1331	0	1372	3	1337	[176]
	1031	0	1032	0	1057	3	1030	[176]
	680	−2	760	9	726	4	695	[176]
	275	−2	263	−6	264	−6	280	[176]
B_1	3098	−1	3129	0	3187	2	3137	[176]
	2997	−2	3016	−1	3076	1	3058	[176]
	1452	1	1426	−1	1495	4	1442	[176]
	1313	0	1306	−1	1347	2	1315	[176]
	900	0	894	−1.0	922	2	903	[176]
	725	−2	708	−5	779	5	742	[176]

Cont

Table 4.3: continued.

Mol	HCTH-93	$\Delta_{\text{HCTH-93}}$	1/4	$\Delta_{1/4}$	MP2	Δ_{MP2}	ω_{exp}	Ref
A_2	3084	−1	3104	0	3171	2	3109	[176]
	1438	1	1450	2	1479	3	1427	[25]
	945	0	933	−1	964	2	946	[176]
	176	0	188	7	181	3	175	[176]
B_2	3075	−1	3093	−1	3162	2	3109	[176]
	1449	1	1443	0	1488	3	1439	[176]
	976	0	971	0	999	3	973	[176]
	225	23	183	0	193	6	183	[176]
F_2SO								
A'	1303	−2	1319	−1	1365	2	1333	[177]
	756	−6	776	−4	810	0	808	[177]
	485	−9	490	−8	520	−2	530	[177]
	331		336		368			[177]
A''	695	−6	717	−3	749	1	740	[177]
	367	−6	368	−6	386	−1	390	[177]
Cl_2S								
A_1	506	−2	509	−2	544	5	518	[178]
	198	−5	200	−4	209	1	208	[178]
B_2	490	−7	522	−1	541	3	526	[178]
Cl_2S_2								
A	571	5	587	8	548	0	546	[178]
	417	−11	437	−6	493	6	466	[178]
	205	2	207	3	208	3	202	[178]
	97	5	97	5	95	3	92	[178]
B	401	−12	421	−8	482	6	457	[178]
	229	−5	233	−3	245	2	240	[178]
F_2S_2								
A	674	−6	695	−3	745	4	717	[179]
	628	2	656	7	621	1	615	[179]
	285	−11	287	−10	294	−8	320	[179]
	176	−4	178	−3	187	2	183	[179]

Cont

Table 4.3: continued.

Mol	HCTH-93	$\Delta_{\text{HCTH-93}}$	1/4	$\Delta_{1/4}$	MP2	Δ_{MP2}	ω_{exp}	Ref.
B	637	−7	647	−5	711	4	681	[179]
	303	1	306	2	325	8	301	[179]
H_2S_2								
A	2582	−2	2613	0	2733	4	2621	[178]
	881	0	880	0	906	3	882	[178]
	503	−1	521	2	537	6	509	[178]
	446		452		442			
B	2586	−3	2618	−2	2735	3	2669	[178]
	883	2	879	1	903	4	868	[178]
SO_3								
A_1	1024	−4	1042	−2	1049	−2	1065	[180]
	465	−7	470	−6	485	−3	498	[180]
E	1352	−3	1375	−1	1409	1	1391	[180]
	1352	−3	1375	−1	1409	1	1391	[180]
	499	−6	500	−6	514	−3	530	[180]
	499	−6	500	−6	514	−3	530	[180]
CH_2S								
A_1	3012		3039		3113			
	1462		1458		1504			
	1079		1099		1100			
B_1	999		999		1024			
B_2	3093		3123		3209			
	987		985		1014			
F_2S								
A_1	806	−4	825	−2	856	2	839	[181]
	329	−8	332	−7	351	−2	357	[181]
B_2	782	−4	802	−1	832	2	813	[181]

Cont

Table 4.3: continued.

Mol	HCTH-93	$\Delta_{\text{HCTH-93}}$	1/4	$\Delta_{1/4}$	MP2	Δ_{MP2}	ω_{exp}	Ref.
H_3NS								
A'	3477		3482		3588			
	3388		3399		3469			
	1634		1617		1665			
	1314		1303		1338			
	839		835		858			
	608		634		656			
A''	3477		3482		3588			
	1634		1617		1665			
	839		835		858			
H_3PS								
A'	2342	−1	2368	0	2499	6	2359	[182]
	2321		2347		2488			
	1100	−11	1095	−12	1155	−7	1240	[182]
	1075		1072		1147			
	701		700		741			
	670	−22	685	−20	693	−19	858	[182]
A''	2321	−2	2347	−1	2488	5	2371	[182]
	1075	−6	1072	−6	1148	0	1143	[182]
	701	−37	700	−37	741	−34	1114	[182]
HSF								
	2603	−1	2627	0	2748	5	2628	[183]
	994	−3	995	−3	1043	2	1023	[184]
	769	−2	788	0	811	3	788	[184]

Cont

Table 4.3: continued.

Mol	HCTH-93	$\Delta_{\text{HCTH-93}}$	1/4	$\Delta_{1/4}$	MP2	Δ_{MP2}	ω_{exp}	Ref.
HSOH								
	3755	7	3766	7	3830	9	3525	[185]
	2556		2582		2712			
	1196	2	1185	1	1219	4	1177	[185]
	990		995		1035			
	750	−2	773	1	788	3	763	[185]
	485	9	489	10	485	9	445	[185]
FSOH								
	3692		3698		3787			
	1194		1180		1219			
	843		838		867			
	738		757		793			
	573		582		574			
	327		334		351			
FSOF								
	1118		1127		1369			
	761		777		813			
	431		450		519			
	397		406		421			
	289		298		241			
	158		163		138			
ClSSH								
	2545		2567		2707			
	879		880		906			
	517		535		540			
	436		455		504			
	427		429		406			
	198		200		208			

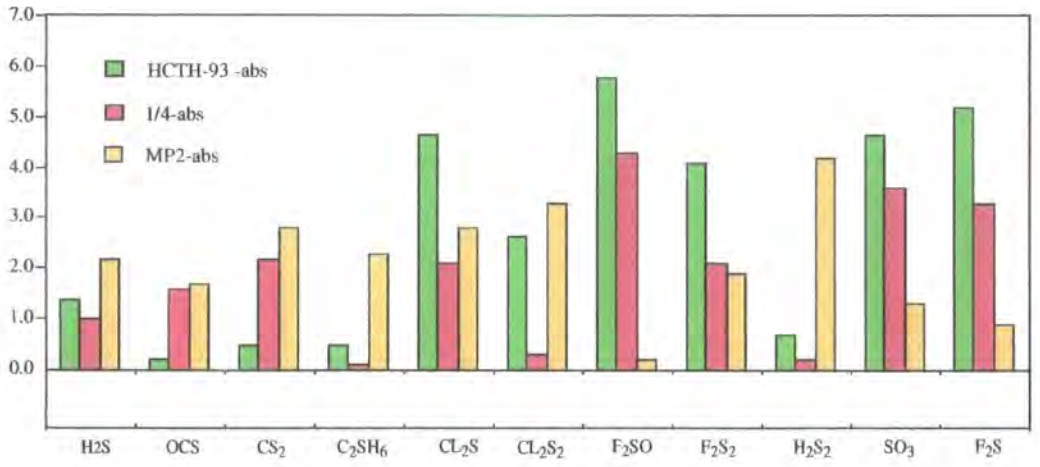

Figure 4.2: Mean absolute percentage frequency differences for MP2, HCTH-93 and $\frac{1}{4}$

4.1.4 Molecular polarizabilities

We finally investigate the performance of HCTH-93 and $\frac{1}{4}$ functionals for predicting isotropic polarizabilities. The reason of this assessment is that in Ref. [160], Altmann *et al.* calculated the polarizabilities for this benchmark of molecules to investigate how the performance of hybrid functionals depended on the choice of the basis-set. Even though our aim in this work is to compare the performance of GGA functionals rather than basis-sets, we consider the calculation of polarizabilities an interesting test to perform.

We therefore calculated the isotropic polarizabilities at near-experimental geometries using the extensive Sadlej basis set [126], comparing with HCTH-93 and experimental values (where available). Recall that an accurate functional should give polarizabilities below experiment. In Table 4.4 we observe that for all the systems in the benchmark, $\frac{1}{4}$ lowers the HCTH-93 values, which is consistent with the results presented in Chapter 3.

Table 4.4: Isotropic polarizabilities in a.u. for HCTH-93 and $\frac{1}{4}$ with the Sadlej basis set. Experimental values are also shown where available.

Mol	HCTH-93	1/4	α_{exp}	Ref
H_2S	25.18	24.91	24.71	[186, 187]
OCS	33.23	31.71	33.72	[186, 187]
CS_2	54.71	54.26	55.28	[186, 187]
CH_2S	34.74	34.24		
Cl_2S	52.24	51.99		
F_2S	24.53	24.30		
C_2H_6S	78.50	76.49	50.95	[188]
SO_3	30.55	30.32		
H_3NS	40.30	39.34		
H_3PS	43.27	42.57		
HSF	27.17	26.87		
H_2S_2	45.08	44.72		
SOF_2	28.60	28.45		
F_2S_2	46.13	45.52		
Cl_2S_2	79.32	79.05		
HSOH	32.00	31.58		
FSOH	29.44	29.17		
FSOF	36.89	36.67		
ClSSH	60.48	60.16		

4.2 Diatomic molecules

We now present a systematic study of the performance of the $\frac{1}{4}$ functional, compared to several recently developed functionals, for the prediction of bond lengths and harmonic vibrational frequencies of ground state diatomic molecules. The reason for choosing diatomic molecules is that it allows molecules to be drawn evenly from rows of the periodic table: many recently developed functionals have been parameterized by constraining them to be accurate for molecules high in the periodic table, often containing many hydrogen atoms. The performance of such functionals for molecules outside the training set is not well documented. We consider 45 molecules containing atoms Li-Br (no hydrogen), which provide a stringent test of functional quality. The DFT results are compared with MP2 and reference experimental data.

4.2.1 The exchange-correlation functionals

We choose seven different functionals. They are the GGAs HCTH-93, HCTH-407 [100], $\frac{1}{4}$, PBE [92], and the hybrids B3LYP [109], B97-2 [111] and PBE0 [112].

4.2.2 Choice of diatomic molecules

To choose the molecules consisting our benchmark we used as a criterion that they should be drawn evenly from rows of the periodic table. Hence, we considered three full rows: Li-Ne, Na-Ar and K-Kr neglecting Sc-Zn in the latter since this block is absent in the first two. This leaves the groups 1 [Li,Na,K]; 2 [Be,Mg,Ca]; 13 [B,Al,Ga]; 14 [C,Si,Ge]; 15 [N,P,As]; 16 [O,S,Se] and 17 [F,Cl,Br]. Combining one group with itself generates six diatomics, e.g. group 1 gives Li_2, LiNa, LiK, Na_2, NaK, K_2. Combining two different groups generates nine diatomics, e.g., groups 1 and 17 give LiF, LiCl, LiBr, NaF, NaCl, NaBr, KF, KCl, KBr. We then used Ref. [131] to find groups or

pairs of groups where experimental bond lengths r_e and harmonic frequencies ω_e were known for all possible singlet ground state combinations. Neglecting rare-gas dimers due to the difficulty of describing dispersion in DFT, the following combinations were obtained: (1-1), (15-15), (17-17), (1,17), (13,17) and (14,16). These molecules are summarized in Figure 4.3. For

1		13	14	15	16	17
Li	...	B	C	N	O	F
Na	...	Al	Si	P	S	Cl
K	...	Ga	Ge	As	Se	Br

1-1	Li_2	LiNa	LiK	Na_2	NaK	K_2			
15-15	N_2	NP	NAs	P_2	PAs	As_2			
17-17	F_2	FCl	FBr	Cl_2	ClBr	Br_2			
1-17	LiF	LiCl	LiBr	NaF	NaCl	NaBr	KF	KCl	KBr
13-17	BF	BCl	BBr	AlF	AlCl	AlBr	GaF	GaCl	GaBr
14-16	CO	CS	Cse	SiO	SiS	SiSe	GeO	GeS	GeSe

Figure 4.3: Specification of the molecules comprising the benchmark under study

LiNa, LiK, and NaK the values in ref. [131] were uncertain; by searching the literature [189]-[191], we found more accurate values for these systems. We also found a more accurate value for the bond length of K_2 [192]. The only other values with uncertainties in Ref. [131] are the bond lengths of PAs, Cl_2, BCl, and BBr. For the last three we found more recent experimental values that agree within 0.001 Å with the values of [131], hence we regard them as acceptable for this work.

4.3 Computational details

We performed all calculations using the extensive 6-311+G(2df) basis set, which corresponds to 5s4p2d1f for [Li-Ne], 7s6p2d1f for [Na-Ar] and 9s8p4d1f for [K-Kr]. Since $\frac{1}{4}$, HCTH-93 and B97-2 [111] were determined using the TZ2P basis set, it would have been appropriate to use this basis-set for this assessment. However, TZ2P is not available for third row atoms. We have confirmed that for molecules where the TZ2P basis set is available, average bond length errors change little in moving from TZ2P to 6-311+G(2df). In order to minimize the influence of the numerical integration errors in the Kohn-Sham calculations, extensive numerical integration grids were introduced. DFT harmonic vibrational frequencies were determined using a two point finite-difference of analytic first derivatives. MP2 frequencies were calculated analytically.

4.4 Results and discussions

4.4.1 Bond lengths

In Table 4.5 we present the experimental bond lengths and the errors for the seven functionals and MP2. We quote the differences between our calculated and experimental values to this precision so that the calculated values can be deduced (calculated=experiment+error).

The alkali metal dimers, combination (1-1), are very difficult molecules, leading to very large errors (particularly for HCTH-93 HCTH-407 and B97-2). Therefore we present mean errors d, mean absolute errors $|d|$ and mean absolute percentage errors $|d|\%$ compared to experiment, both omitting and including the (1-1) combination.

By considering the errors when the (1-1) combination is omitted, similar variations across the theoretical methods are observed for d, $|d|$ and $|d|\%$. HCTH-93 bond lengths are too long with a mean absolute error of 0.022 Å

Table 4.5: Experimental bond lengths in Å and errors (calculated minus experiment, in $\times 10^{-3}$Å) with the 6-311+G(2df) basis set.

Mol.	Expt.[1]	HCTH 93	HCTH 407	1/4	PBE	B3LYP	B97-2	PBE0	MP2
(1-1)									
Li_2	2.673	88	75	14	58	33	73	56	9
LiNa	2.885[2]	100	86	−7	36	9	70	37	28
LiK	3.319[3]	136	120	9	57	42	94	63	18
Na_2	3.079	108	96	−32	11	−21	65	16	26
NaK	3.497[4]	150	141	−13	37	11	94	47	−1
K_2	3.924[5]	205	208	14	72	47	132	84	−35
(15-15)									
N_2	1.098	1	−1	−3	5	−7	−8	−8	13
NP	1.491	3	1	−3	10	−7	−10	−11	27
NAs	1.618	0	−2	−7	8	−7	−15	−16	42
P_2	1.893	7	4	−2	16	1	−8	−8	29
PAs	1.999	7	2	−4	16	2	−10	−11	24
As_2	2.103	6	2	−7	14	1	−13	−16	18
(17-17)									
F_2	1.412	−15	−18	−22	−1	−17	−35	−38	−17
FCl	1.628	17	12	7	31	20	0	−2	8
FBr	1.759	20	17	10	32	19	1	−3	1
Cl_2	1.988	13	3	0	27	32	2	1	4
ClBr	2.136	17	10	2	27	32	3	−1	−3
Br_2	2.281	25	21	8	32	38	9	3	0
(1-17)									
LiF	1.564	26	23	5	17	6	11	4	13
LiCl	2.021	19	13	−9	6	3	8	−2	2
LiBr	2.170	27	21	−5	12	9	15	3	3
NaF	1.926	48	45	17	32	18	23	13	26
NaCl	2.361	43	35	2	18	16	22	6	15
NaBr	2.502	52	45	5	22	21	30	11	22
KF	2.171	19	18	−17	3	12	6	−3	26
KCl	2.667	29	23	−21	0	20	11	−2	14
KBr	2.821	42	39	−13	8	29	22	5	25

Cont.

Table 4.5: continued.

Mol.	Expt.[1]	HCTH 93	HCTH 407	1/4	PBE	B3LYP	B97-2	PBE0	MP2
(13-17)									
BF	1.263	10	8	0	11	0	1	−3	0
BCl	1.716	19	14	−1	18	8	9	4	−6
BBr	1.888	24	20	1	22	18	14	7	−13
AlF	1.654	35	32	24	37	24	19	16	18
AlCl	2.130	36	33	19	36	34	22	18	10
AlBr	2.295	48	46	26	44	45	32	26	21
GaF	1.774	40	38	26	41	30	21	16	13
GaCl	2.202	39	35	14	32	38	20	12	−1
GaBr	2.352	50	46	20	39	48	30	19	0
(14-16)									
CO	1.128	5	3	0	9	−3	−4	−5	6
CS	1.535	8	6	0	13	−1	−3	−4	0
CSe	1.676	9	6	−1	15	2	−3	−5	−4
SiO	1.510	13	11	7	20	4	0	−1	16
SiS	1.929	18	14	8	26	13	4	4	12
SiSe	2.058	22	19	10	29	17	7	5	8
GeO	1.625	12	10	5	20	5	−3	−5	17
GeS	2.012	18	12	6	25	16	2	1	5
GeSe	2.135	24	19	9	29	20	6	3	0
Omitting (1-1) alkali metal dimers:									
d		21	18	3	21	14	6	1	10
$\|d\|$		22	19	9	21	16	12	8	12
$\|d\|$%		1.1	0.9	0.5	1.1	0.8	0.6	0.5	0.7
All molecules:									
d		36	31	2	24	15	17	7	10
$\|d\|$		37	32	10	24	18	22	14	13
$\|d\|$%		1.5	1.3	0.5	1.1	0.8	0.9	0.6	0.7

(1.1 %); in moving to HCTH-407 the error is reduced to 0.019 Å (0.9 %). It is important to point out that for the 93 molecules used to develop HCTH-93, its mean absolute error was just 0.013 Å. The larger error in this study shows how the performance of the functional degrades when applied to molecules outside the training set. Boese and Handy [100] have already observed such behaviour for non-hydrogen containing molecules.

Bond lengths for the $\frac{1}{4}$ functional are considerably more accurate, with a mean and mean absolute errors of just 0.003 Å and 0.009 Å. These values are consistent with those presented in Chapter 3, where we demonstrated the high quality molecular structures from $\frac{1}{4}$.

PBE instead overestimates the bond lengths with a mean absolute error of 0.021 Å which is in between the mean absolute errors of HCTH-93 and HCTH-407; this reflects its rigorous theoretical derivation using exact conditions.

The widely used B3LYP hybrid functional gives a mean absolute error of 0.016 Å. This error is reduced to 0.012 Å for the recently developed B97-2, which is comparable to MP2. Finally, PBE0, which contains only one parameter, is the most accurate hybrid functional. It gives an error of 0.008 Å which is comparable with $\frac{1}{4}$.

We have investigated the reasons for such a good performance of PBE0. At first, we thought it was due to the 0.25 exact exchange, since the other hybrid functionals have just 0.20 and 0.21 exchange; but this was not the case. We reduced the amount of exact exchange in the PBE0 functional to 0.21 (increasing the GGA exchange expansion parameter to 0.79) but the mean absolute error remained at 0.008 Å.

We then performed a more general assessment, including the alkali metal dimers. In this case HCTH-93 and HCTH-407 become particularly poor with mean absolute errors of 0.037 Å and 0.032 Å respectively. PBE performs better with a mean absolute error of 0.024 Å. The performance of B97-2 degrades, becoming less accurate than B3LYP, whereas PBE0, with its

error of 0.014 Å is comparable to MP2. However, the best overall results are again obtained with $\frac{1}{4}$, which has a mean absolute error of only 0.010 Å. This functional performs particularly well for the challenging (1-1) molecules.

It is often assumed that DFT functionals provide accuracy comparable with MP2. In this study, when all the 45 molecules are considered, only $\frac{1}{4}$ (GGA) and PBE0 (hybrid) are competitive with MP2. We also observe that no degradation in the accuracy of the predictions is observed in moving down the periodic table, for the recently developed parameterized functionals. It is clear that within a given group combination, the largest percentage errors can be associated with molecules involving intermediate atomic number atoms. This is in spite of the fact that the atoms K, Ga, Ge, As, Se and Br are not in the molecules comprising the training set. This provides some justification for parameterising functionals by fitting to molecules high in the periodic table.

4.4.2 Harmonic vibrational frequencies

In Table 4.6 we present the experimental harmonic vibrational frequencies, together with the errors for the seven functionals under study. Since the range of vibrational frequencies is much larger (92-2359 cm^{-1}) than the range of bond lengths (1.098-3.924 Å), it is important to also present mean absolute percentage errors ($|d|\%$).

Considering the mean absolute errors, we observe a similar quality in the performances of HCTH-93, HCTH-407, B97-2, PBE and MP2. PBE and B3LYP give more accurate results, however the most accurate predictions are obtained by $\frac{1}{4}$, which gives a mean absolute error of only 14 cm^{-1}.

Considering the mean absolute percentage errors, HCTH-93 and HCTH-407 are poor and PBE0 is much more accurate. B97-2, B3LYP and PBE0 are comparable to, or better than, PBE. However, once again, $\frac{1}{4}$ performs particularly well, with a mean absolute percentage error of just 2.0%. In

Table 4.6: Experimental harmonic frequencies and errors (calculated minus expt) in cm^{-1} with the 6-311+G(2df) basis set.

Mol.	Expt.[1]	HCTH 93	HCTH 407	1/4	PBE	B3LYP	B97-2	PBE0	MP2
(1-1)									
Li_2	351	−25	−20	−3	−19	−10	−15	−11	30
LiNa	257	−21	−16	0	−10	−4	−10	−4	−3
LiK	212[2]	−21	−18	−3	−11	−9	−9	−6	3
Na_2	159	−12	−10	2	−3	1	−4	1	2
NaK	124	−12	−11	0	−4	−2	−4	0	5
K_2	92	−10	−10	0	−3	−3	−3	−1	6
(15-15)									
N_2	2359	16	31	43	−14	84	107	117	−155
NP	1337	15	19	35	1	65	80	91	−138
NAs	1069	31	36	50	20	70	91	102	−159
P_2	781	5	15	19	−4	23	42	47	−57
PAs	604	9	16	21	4	23	41	46	−30
As_2	430	6	9	17	5	18	31	36	−16
(17-17)									
F_2	917	89	90	115	81	132	166	184	99
FCl	786	−23	−16	−1	−31	−9	23	34	14
FBr	671	−29	−27	−9	−30	−8	13	24	13
Cl_2	560	−17	−12	−1	−18	−17	10	21	24
ClBr	444	−17	−15	−2	−14	−13	7	17	21
Br_2	325	−15	−15	−4	−11	−10	3	11	13
(1-17)									
LiF	910	−56	−51	−18	−35	−9	−24	−6	−9
LiCl	643	−27	−18	1	−10	−5	−10	3	5
LiBr	563	−24	−21	−2	−11	−7	−11	0	5
NaF	536	−46	−43	−17	−26	−10	−19	−6	−9
NaCl	366	−27	−21	−7	−12	−8	−12	−4	0
NaBr	302	−26	−24	−8	−13	−10	−15	−6	−4
KF	428	−37	−36	−9	−16	−12	−15	−6	−17
KCl	281	−27	−25	−5	−10	−11	−13	−5	−8
KBr	213	−11	−11	1	−1	−1	−2	3	3

Cont.

Table 4.6: continued.

Mol.	Expt.[1]	HCTH 93	HCTH 407	1/4	PBE	B3LYP	B97-2	PBE0	MP2
(13-17)									
BF	1402	−53	−47	−13	−49	1	−6	13	18
BCl	839	−40	−36	−10	−36	−22	−17	−5	24
BBr	684	−32	−28	−6	−27	−21	−14	−3	25
AlF	802	−66	−62	−46	−62	−37	−32	−23	−18
AlCl	481	−31	−31	−18	−27	−26	−15	−10	2
AlBr	378	−27	−28	−16	−21	−23	−15	−9	−5
GaF	622	−55	−53	−34	−46	−31	−23	−13	−6
GaCl	365	−24	−24	−9	−15	−18	−9	−1	14
GaBr	263	−16	−16	−3	−7	−11	−4	2	13
(14-16)									
CO	2170	−23	−17	7	−43	41	53	68	−36
CS	1285	−15	−5	10	−27	18	35	43	23
CSe	1035	−5	4	18	−14	22	41	50	46
SiO	1242	−37	−36	−17	−48	10	22	31	−42
SiS	750	−23	−19	−9	−29	−8	7	13	−1
SiSe	580	−19	−17	−7	−21	−6	6	13	8
GeO	986	−19	−17	−1	−27	17	35	45	−29
GeS	576	−16	−12	−3	−19	−5	11	16	15
GeSe	409	−18	−16	−8	−18	−8	2	7	12
All molecules:									
d		−18	−15	1	−16	3	12	20	−7
$\|d\|$		26	25	14	21	20	25	26	26
$\|d\|$%		5.1	4.7	2.0	3.4	3.0	3.5	3.1	3.4

[1]Ref. [131], unless otherwise stated

[2]Ref. [190]

general, the GGA functionals tend to underestimate vibrational frequencies, whereas hybrid functionals overestimate them.

4.4.3 Discussion

The results of this study are summarized in Figure 4.4 and Figure 4.5. The uniform high quality performance of $\frac{1}{4}$ is clear. It is important to point out that the PBE0 hybrid functional is also impressive; it involves only one parameter whereas all the others functionals have a larger number. However, its accuracy is due to the inclusion of a fraction of exact orbital exchange. By contrast, $\frac{1}{4}$ is a GGA, without exact exchange. Hence, it is particularly attractive for use in electronic structure codes that eliminate the 4-centre integrals by fitting the Coulomb term. Further investigations have also shown that it can be applied to study solid state systems with encouraging results. The improved structural prediction from $\frac{1}{4}$ are achieved at a cost, however, as energy predictions (particularly total energies) and NMR shielding constants are less accurate than HCTH-93. A pragmatic way to circumvent this problem would be to combine the $\frac{1}{4}$ functional with a second functional. The former could be used to determine the geometry and the latter could be used to determine quantities at that geometry.

4.5 Exchange-correlation enhancement factors

It is important to understand why $\frac{1}{4}$ is so successful. To investigate this we considered the enhancement factor introduced in Chapter 2. Recall that the general expression for a GGA functional is

$$E_{\mathrm{xc}}[\rho] = -\int \frac{3}{4}(3\pi^2)^{\frac{1}{3}}\rho^{\frac{4}{3}}(\mathbf{r})f'_{\mathrm{xc}}(r_s, s)d\mathbf{r} \tag{4.2}$$

where the enhancement factor $f'_{\mathrm{xc}}(r_s, s)$ is a function of the reduced density gradient s and of the Wigner-Seitz radius r_s. As explained in Chapter 2, the enhancement factor must satisfy a range of exact conditions. In particular, by

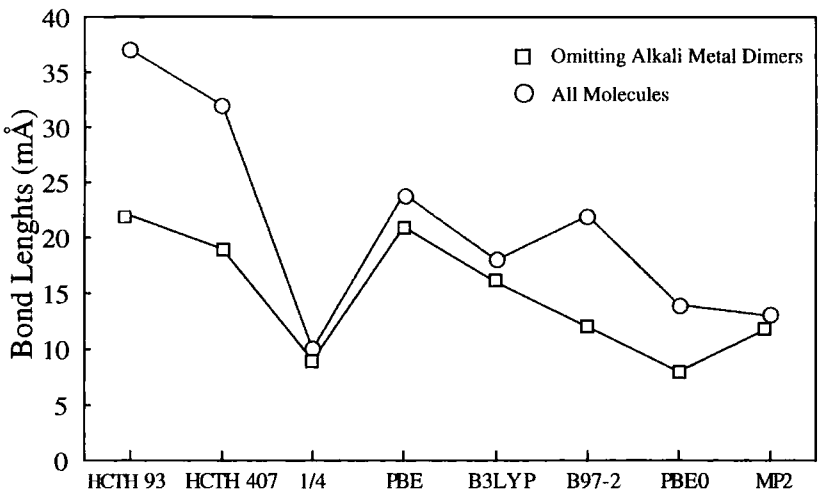

Figure 4.4: Trends of the average bond length accuracy for the seven methods studied in this work, with and without the inclusion of the alkali-metal dimers.

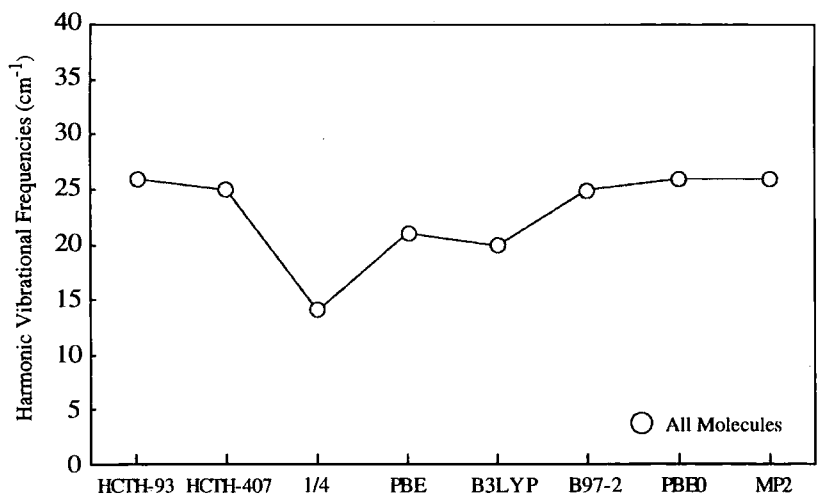

Figure 4.5: Trends of the average harmonic vibrational frequencies accuracy for the seven methods studied in this work.

considering the variation of the exchange-correlation energy under uniform density scaling, it can be shown [62] that

$$f'_{xc}(r'_s, s) > f'_{xc}(r_s, s); \qquad (r'_s > r_s) \tag{4.3}$$

hence, curves associated with different r_s values should not cross. In Figures 4.6-4.9, we present the enhancement factors of HCTH-93, HCTH-407, $\frac{1}{4}$ and PBE. See Ref. [62] for the enhancement factor plots of other functionals. It is clear that HCTH-93 and HCTH-407 have a similar structure. Neither satisfy Eq.(4.3); the crossing is particularly pronounced in HCTH-407. However, in very low density regions it is more similar to the (correct) PBE than HCTH-93. The $\frac{1}{4}$ functional has a completely different enhancement factor, and this is consistent with its completely different behaviour in this chapter. For different values of r_s, the curves are approximately parallel, hence it satisfies Eq.(4.3). We are extremely encouraged that this can be achieved using a parameterized functional. However, it fails to satisfy the other conditions such as the modified Lieb-Oxford bound [105, 106].

The reason for the non-crossing behaviour of $\frac{1}{4}$ derives from the fitting procedure used to develop it. Functionals in Chapter 3 emphasizing regions close to the nuclei give enhancement factors that cross whereas functionals that emphasize regions further out give enhancement factors that do not cross. In Chapter 5 we use this observation to develop new exchange-correlation functionals.

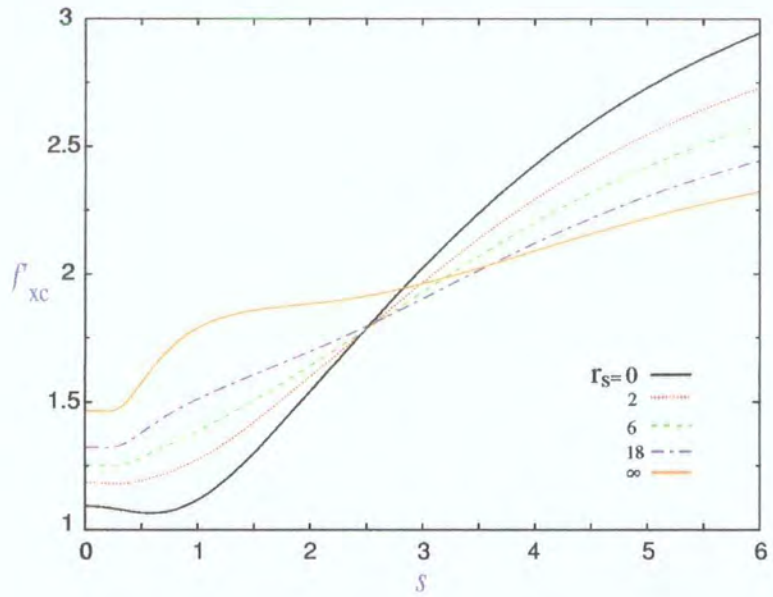

Figure 4.6: Exchange-correlation enhancement factor $f'_{\mathrm{XC}}(r_s, s)$ for HCTH-93 plotted as a function of s.

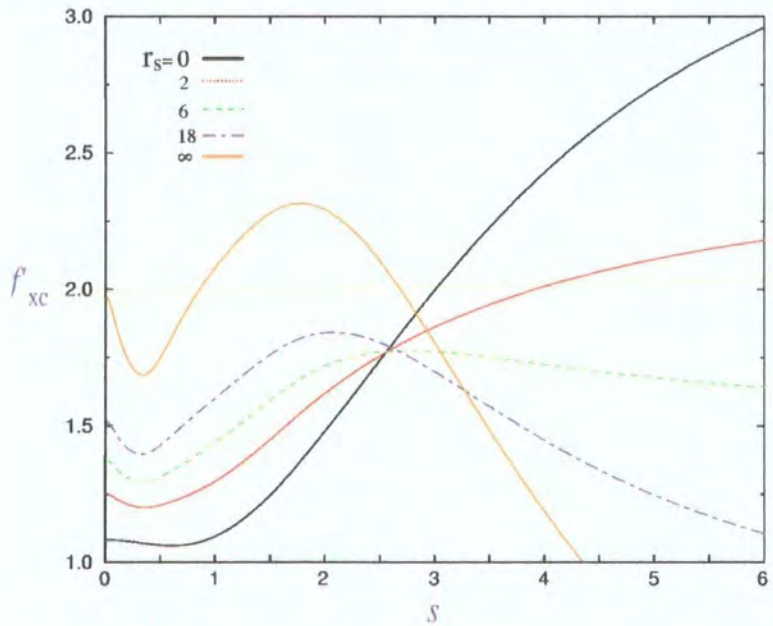

Figure 4.7: Exchange-correlation enhancement factor $f'_{\mathrm{XC}}(r_s, s)$ for HCTH-407 plotted as a function of s.

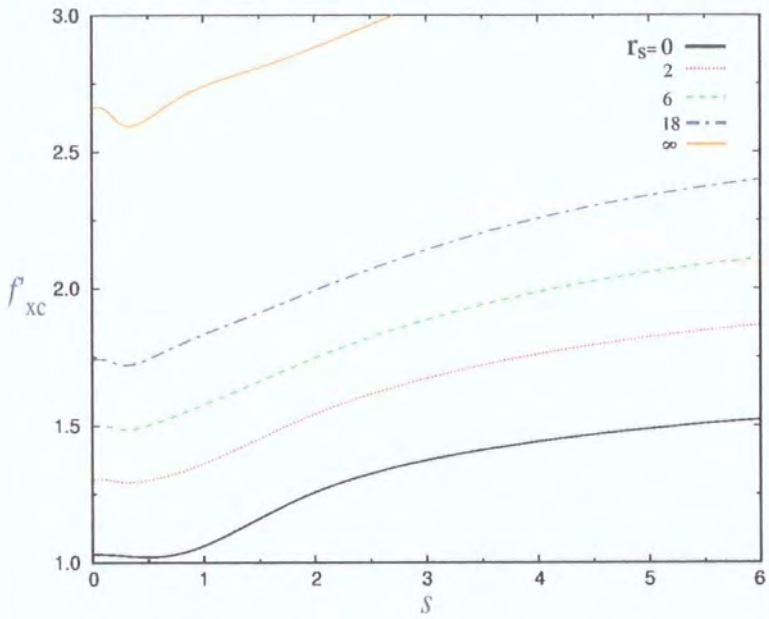

Figure 4.8: Exchange-correlation enhancement factor $f'_{\mathrm{XC}}(r_s, s)$ for $\frac{1}{4}$ plotted as a function of s.

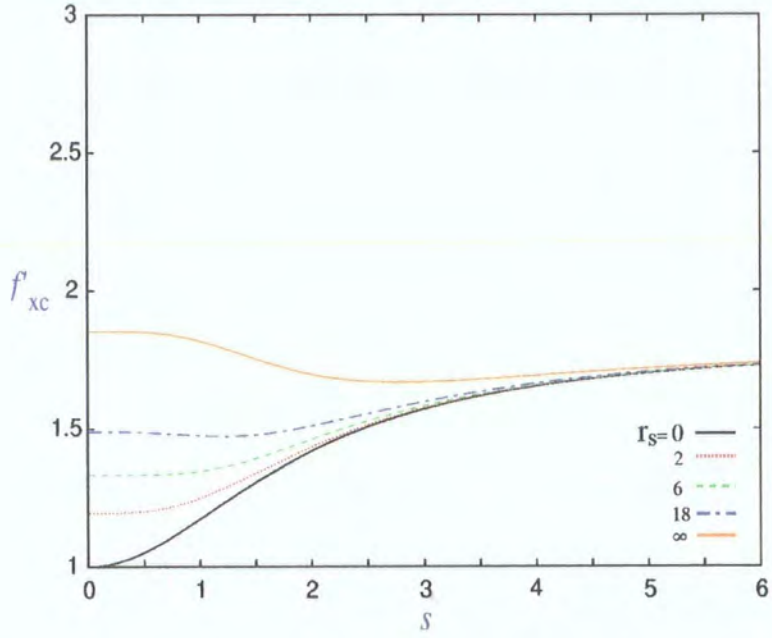

Figure 4.9: Exchange-correlation enhancement factor $f'_{\mathrm{XC}}(r_s, s)$ for PBE plotted as a function of s.

Chapter 5

GGAs from enhancement factors

In this chapter we demonstrate that for the functionals developed in Chapter 3 the enhancement factor varies smoothly as a function of the weighting factor. We use this observation to develop, for the first time, parameterized functionals that satisfy the uniform density scaling condition (i.e. non-crossing enhancement factor) and the Lieb-Oxord bound. Molecular structures, thermochemistry, polarizabilities and NMR shielding constants are assessed. The potential energy surface of the Helium dimer is also investigated since this is known to be sensitive to the shape of the enhancement factor.

5.1 Variation of the enhancement factor

Perdew *et al.* [62] have demonstrated that in practical calculations, extremely small values of r_s and s ($r_s \leq 1$ and $s \leq 1$) correspond to high density (core) regions, whereas $1 \leq r_s \leq 6$ and $s \leq 2$ emphasize valence regions. In this study we wish to develop new GGA functionals that satisfy exact conditions over a wide region of space, $0 \leq r_s \leq \infty$ and $0 \leq s \leq \infty$.

Figure 5.1 presents the enhancement factors of the eight functionals de-

veloped in Chapter 3 which were obtained through the minimization of

$$\Omega = \sum_{\mathrm{T}} \sum_{\sigma}^{\alpha,\beta} \int d\mathbf{r} [v_{\mathrm{ZMP}}^{\mathrm{T}\sigma}(\mathbf{r}) + k_{\mathrm{T}\sigma} - v_{\mathrm{fit}}^{\mathrm{T}\sigma}(\mathbf{r})]^2 \rho_{\sigma}^{p}(\mathbf{r}) \tag{5.1}$$

As p increases from 0 to $\frac{7}{6}$, the enhancement factors vary smoothly. From $p = \frac{4}{6}$, the order of the curves inverts, meaning that the highest curve corresponds to $r_s = 0$, whereas the lowest corresponds to $r_s = \infty$. This smooth variation is important as it indicates that, by choosing p appropriately, exact conditions can be satisfied. In particular, we can ensure that we satisfy:

1. The uniform density scaling

$$f'_{\mathrm{XC}}(r'_s, s) > f'_{\mathrm{XC}}(r_s, s) \quad \text{for} \quad (r'_s > r_s) \tag{5.2}$$

and

2. The modified Lieb-Oxford bound

$$f'_{\mathrm{XC}}(r_s, s) \leq 2.2143 \tag{5.3}$$

To the best of our knowledge, this is the first time that these exact conditions have been enforced in highly parameterized exchange-correlation functionals. In addition to these conditions, we also investigate

3. The uniform electron gas condition (UEG)

$$f'_{\mathrm{XC}}(r_s, s = 0) = f_{\mathrm{XC}}^{\mathrm{LSDA}}(r_s). \tag{5.4}$$

5.1.1 Enforcing the uniform electron gas condition

For our standard functional form the uniform electron gas condition is satisfied if the first three expansion coefficients are set equal to unity

$$c_1 = c_2 = c_3 = 1. \tag{5.5}$$

The minimization of Eq. (5.1) then requires

$$\frac{\partial \Omega}{\partial c_4} = \frac{\partial \Omega}{\partial c_5} = \frac{\partial \Omega}{\partial c_6} = ... = \frac{\partial \Omega}{\partial c_{15}} = 0 \tag{5.6}$$

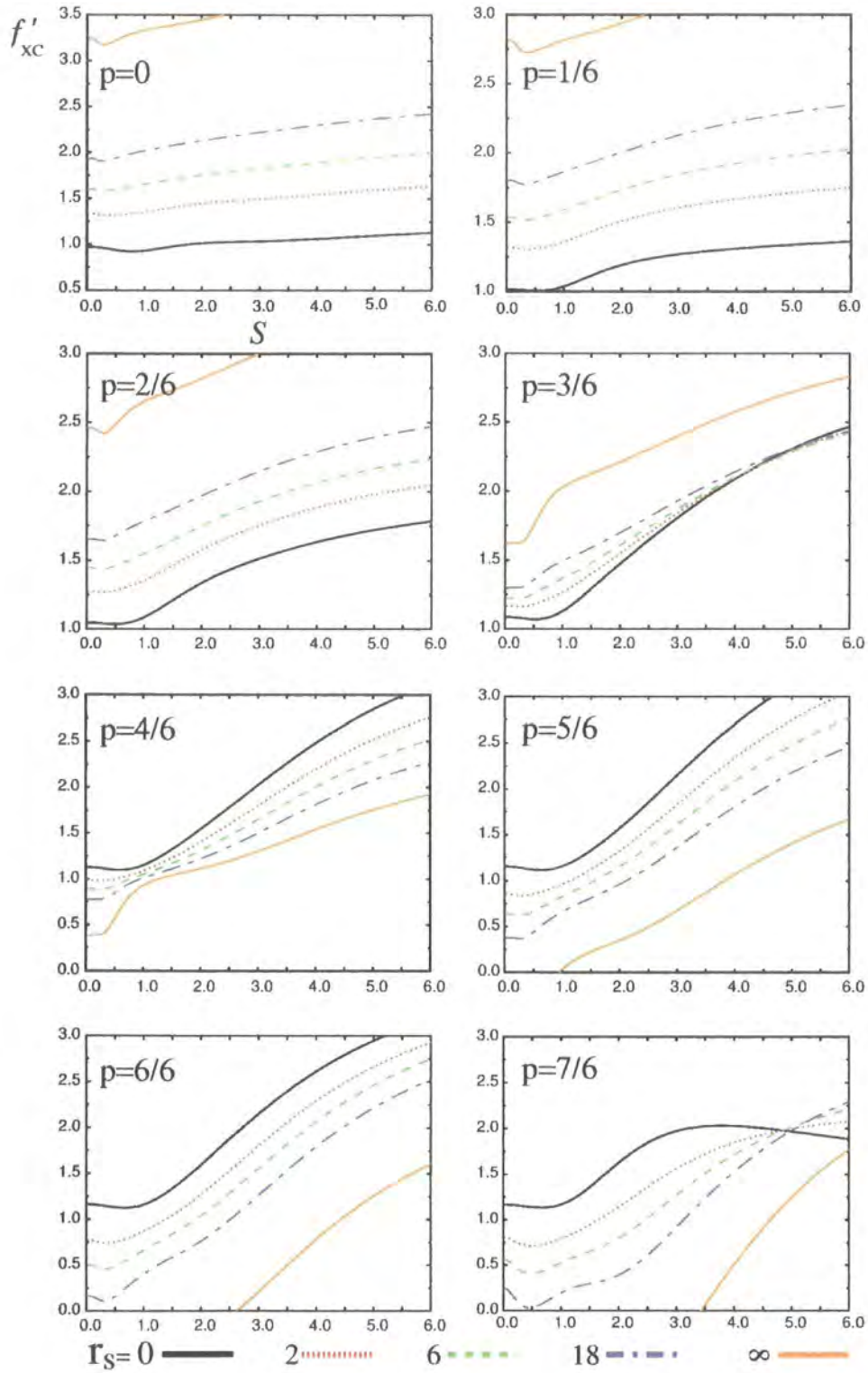

Figure 5.1: Exchange-correlation enhancement factors $f'_{\mathrm{XC}}(r_s, s)$ for $p = \frac{i}{6}$ with $i = 0...7$ plotted as a function of s for different values of the Wigner-Seitz radius r_s.

and the original least-squares expression

$$\sum_{j=1}^{15} A_{ij}C_j = B_i \tag{5.7}$$

reduces to

$$\sum_{j=1}^{3} A_{ij} + \sum_{j=4}^{15} A_{ij}C_j = B_i \tag{5.8}$$

or

$$\sum_{j=4}^{15} A_{ij}C_j = B_i - \sum_{j=1}^{3} A_{ij}. \tag{5.9}$$

We then define

$$X_i = B_i - \sum_{j=1}^{3} A_{ij} \tag{5.10}$$

and the new least-squares equation to solve in order to get the remaining 12 coefficients c_j under the UEG condition is

$$\sum_{j=4}^{15} A_{ij}c_j = X_i \tag{5.11}$$

Figure 5.2 presents minimized values of Ω (Eq.(5.1)) as a function of the number of parameters for $p = \frac{1}{4}$, both with and without the UEG condition. In both cases the most significant jump in the minimized value occurs between 3 and 6 coefficients. We therefore commenced by generating functionals with 6 expansion coefficients, and then increased this to 9 and 12.

All the expansion coefficients for the optimal functionals are presented in Appendix A.

5.2 Results and discussion

5.2.1 Uniform density scaling (non-crossing) condition

The first part of our investigation involved determining functionals whose enhancement factors f'_{XC} satisfied the uniform density scaling (non-crossing) condition in Eq.(5.2). Perdew *et al.* [62] have demonstrated that, in addition to not crossing, enhancement factor curves should converge at large s (i.e.

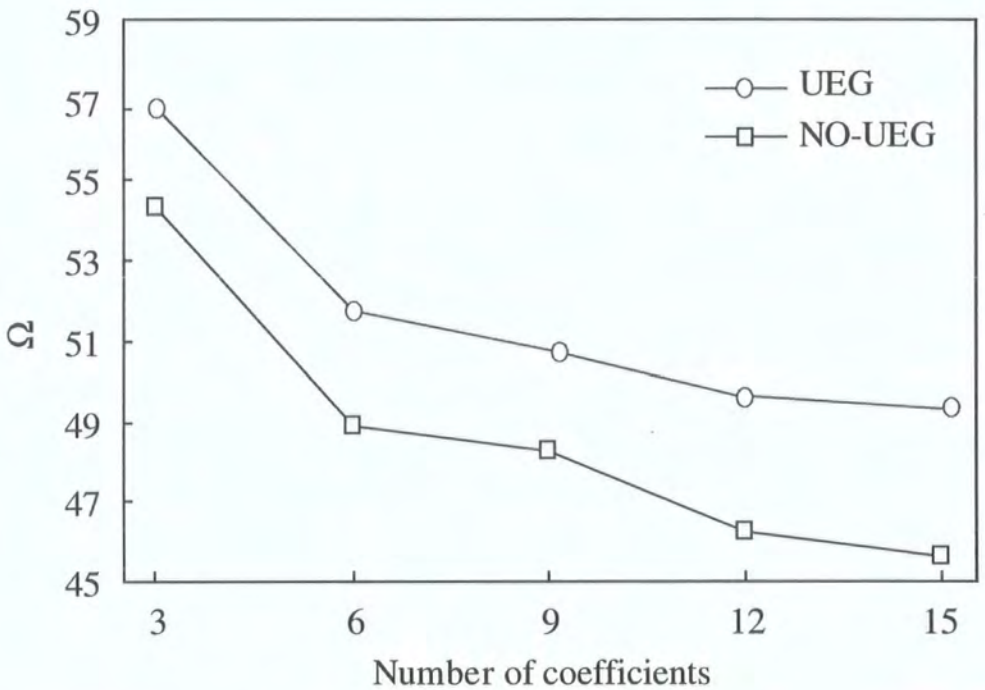

Figure 5.2: The two different trends of the minimization process with and without the imposition of the uniform electron gas condition (UEG)

correlation vanishes). An initial value of p was therefore chosen, for which the curves did not cross. p was then increased in increments of 0.1, causing the curves to approach one another. The largest value of p for which there was no crossing defined our optimal functional.

To determine whether the enhancement factor curves crossed it was necessary to know their values as $s \to 0$ and $s \to \infty$. These were obtained using

$$\lim_{s\to 0} f'_{\mathrm{XC}}(r_s, s) = c_{\mathrm{X}\sigma,0} \cdot f'_{\mathrm{X}\sigma,\mathrm{LDA}}(r_s) + c_{\mathrm{C}\sigma\sigma,0} \cdot f'_{\mathrm{C}\sigma\sigma,\mathrm{LDA}}(r_s) + c_{\mathrm{C}\alpha\beta,0} \cdot f'_{\mathrm{C}\alpha\beta,\mathrm{LDA}}(r_s) \tag{5.12}$$

and

$$\begin{aligned} \lim_{s\to\infty} f'_{\mathrm{XC}}(r_s, s) \;=\; & (\sum_i c_{\mathrm{X}\sigma,i}) f'_{\mathrm{X}\sigma,\mathrm{LDA}}(r_s) + \\ & (\sum_i c_{\mathrm{C}\sigma\sigma,i}) f'_{\mathrm{C}\sigma\sigma,\mathrm{LDA}}(r_s) + \\ & (\sum_i c_{\mathrm{C}\alpha\beta,i}) f'_{\mathrm{C}\alpha\beta,\mathrm{LDA}}(r_s) \end{aligned} \tag{5.13}$$

where $c_{\mathrm{X}\sigma,i}$, $c_{\mathrm{C}\sigma\sigma,i}$ and $c_{\mathrm{C}\alpha\beta,i}$ are the functional expansion parameters and $f'_{\mathrm{X}\sigma,\mathrm{LDA}}$, $f'_{\mathrm{C}\sigma\sigma,\mathrm{LDA}}$ and $f'_{\mathrm{C}\alpha\beta,\mathrm{LDA}}$ are the enhancement factors of the LDA exchange, $\sigma\sigma$ and $\alpha\beta$ correlation functionals.

Figure 5.3 shows the enhancement factor plots of our optimal 6, 9 and 12 coefficient functionals, obtained with the inclusion of the uniform electron gas condition, Eq. (5.4). The values of p used to determine the functionals are also presented. Mean absolute errors are presented for the geometries (Δr), energies (ΔE) and polarizabilities ($\Delta\alpha$) of the systems in Table 3.2 and for isotropic shielding constants ($\Delta\sigma$) of the systems in Table 3.12. There is no clear trend. The 12 coefficient functional yields high quality energies (comparable to PBE) and shieldings are also reasonable (comparable to HCTH-93). However, geometries are very poor with a MAE of 0.019 Å.

Relaxing the UEG condition gives the three functionals whose enhancement factors are presented in Figure 5.4. The best MAE for energies in this case is 19.02 kcal/mol associated with the 6 coefficient functional, which is

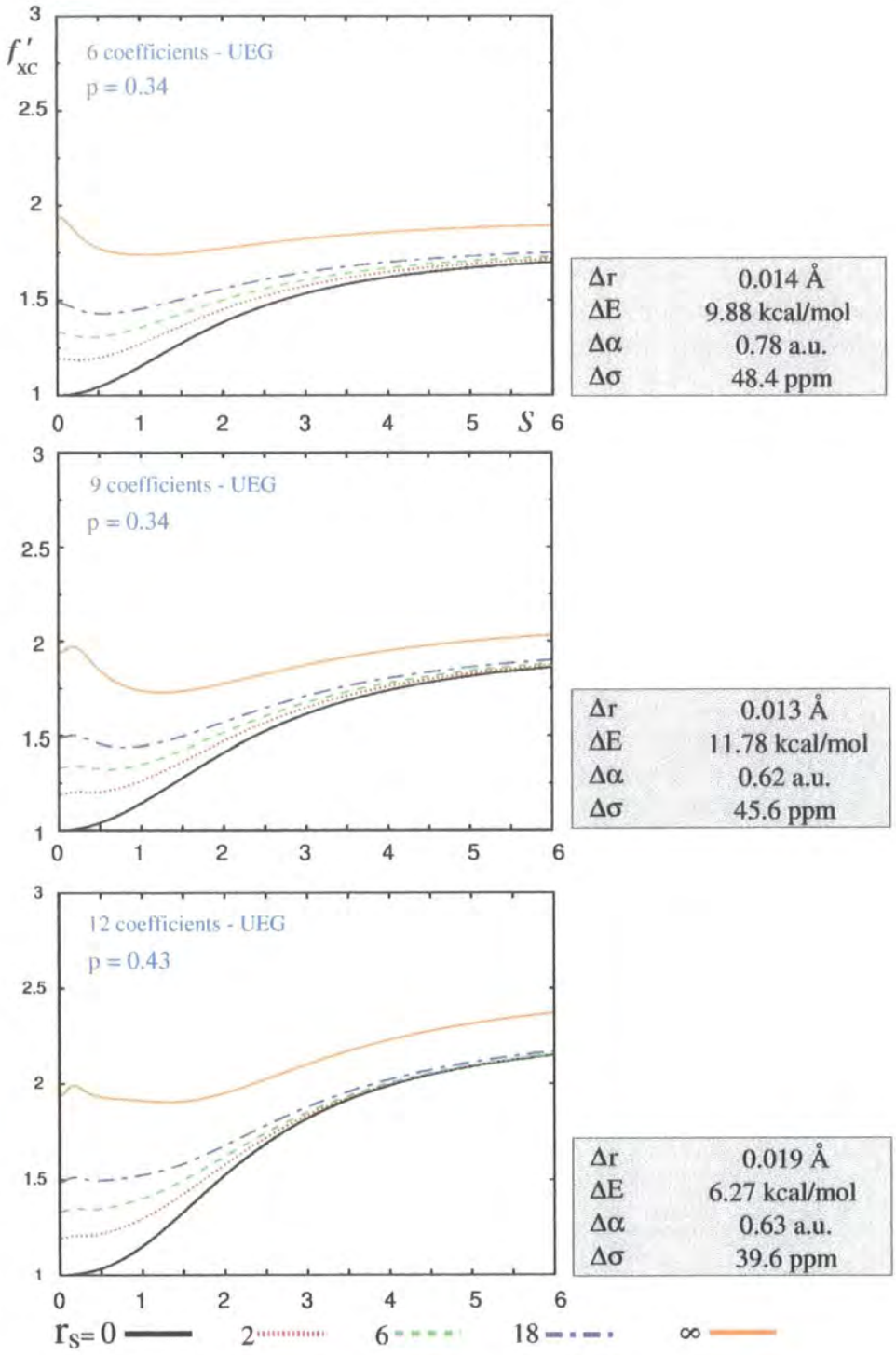

Figure 5.3: Exchange-correlation enhancement factors $f'_{xc}(r_s, s)$ plotted as a function of s for the three optimal functionals satisfying the non-crossing and the uniform electron gas conditions.

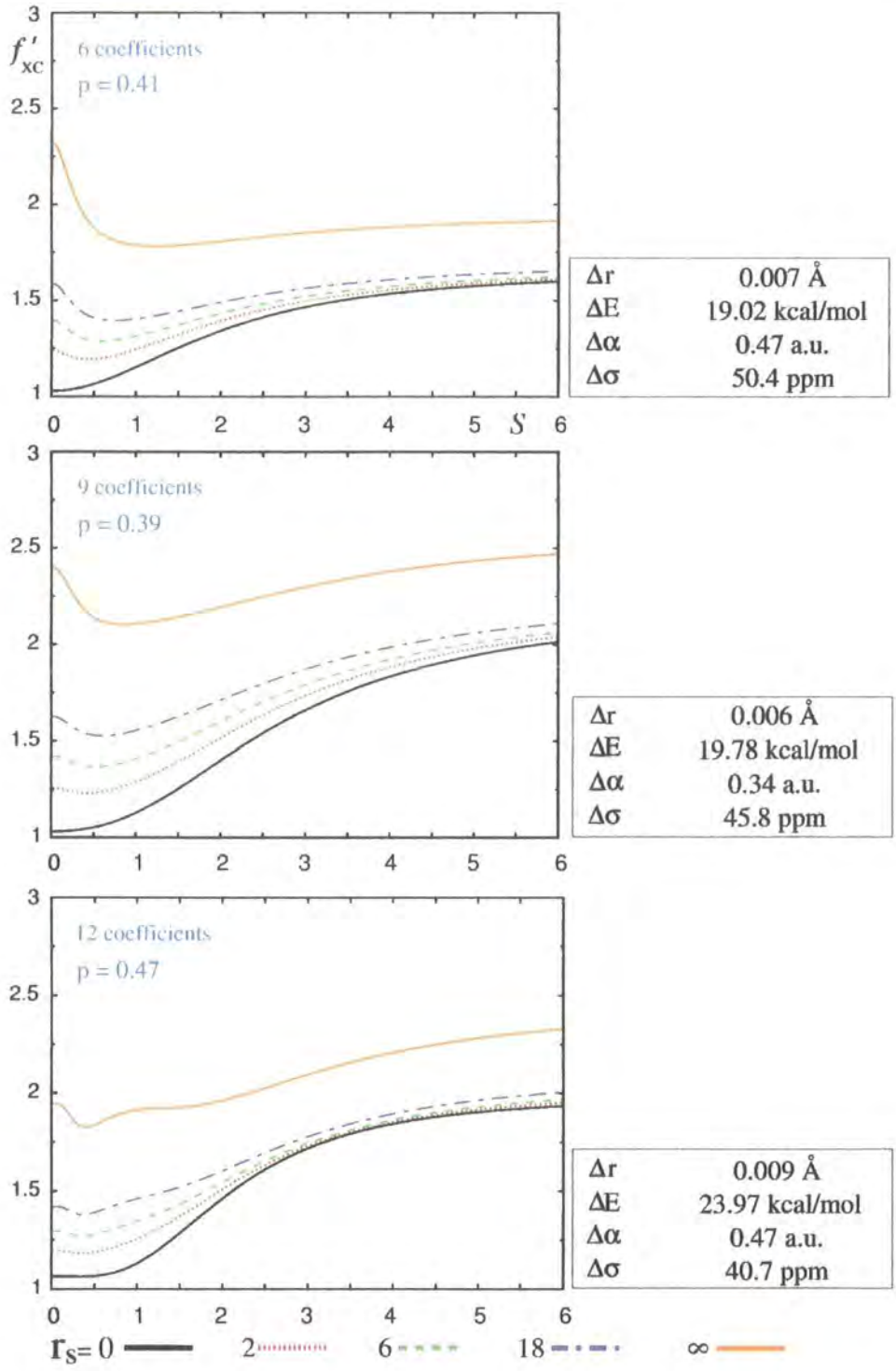

Figure 5.4: Exchange-correlation enhancement factors $f'_{\mathrm{xc}}(r_s, s)$ plotted as a function of s for the three optimal functionals satisfying the non-crossing condition without the uniform electron gas condition.

much less accurate than the UEG case. However, a significant improvement in the molecular structures and polarizabilities is observed. The MAE for the geometries is just 0.007 Å which is close to our $\frac{1}{4}$ functional.

5.2.2 Modified Lieb-Oxford bound condition

The second part of our investigation involved determining functionals whose enhancement factors satisfy the modified Lieb-Oxford bound (Eq. (5.3)). As before, p was varied, but this time the optimal functional was the first one for which all the r_s curves had values below 2.2143 for all values of s. Figure 5.5 presents the enhancement factors of our best 6 and 9 coefficient functionals, obtained with the UEG condition. The enhancement factor of the best 6-coefficient functional consists of almost straight lines. Hence, its behaviour is similar to the enhancement factor in the Local Spin Density Approximation [62], even if the small curvature at small s indicates the presence of a small local density gradient correction. However, a very poor MAE of 30.91 kcal/mol is obtained, which is surprising given that the UEG condition led to better energies in Section 5.2.1.

In moving from 6 to 9 coefficients, i.e. increasing the flexibility of the functional, the curves remain quite flat for small s but cross at approximately $s = 3.5$. The energetics, polarizabilities and shielding constants improve significantly, although molecular structures remain poor.

Figure 5.6 presents the optimal functionals obtained with the relaxation of the UEG condition. The best 6 coefficient functional has a completely different enhancement-factor compared to the 6-coefficient functional obtained under the UEG condition. The curves cross near $s = 2.5$. This functional is a uniform improvement over the 6-coefficient functional developed under the UEG condition.

The next step was to consider the optimal 9 and 12 coefficient functionals. However, it was impossible to find any functional satisfying the Lieb-Oxford

bound condition. This is demonstrated in the last plot of Figure 5.6 where the large s behaviour of the $r_s = \infty$ curve stays above the Lieb-Oxford bound. Hence, we concluded that it is impossible to find optimal 9 and 12 coefficient functionals.

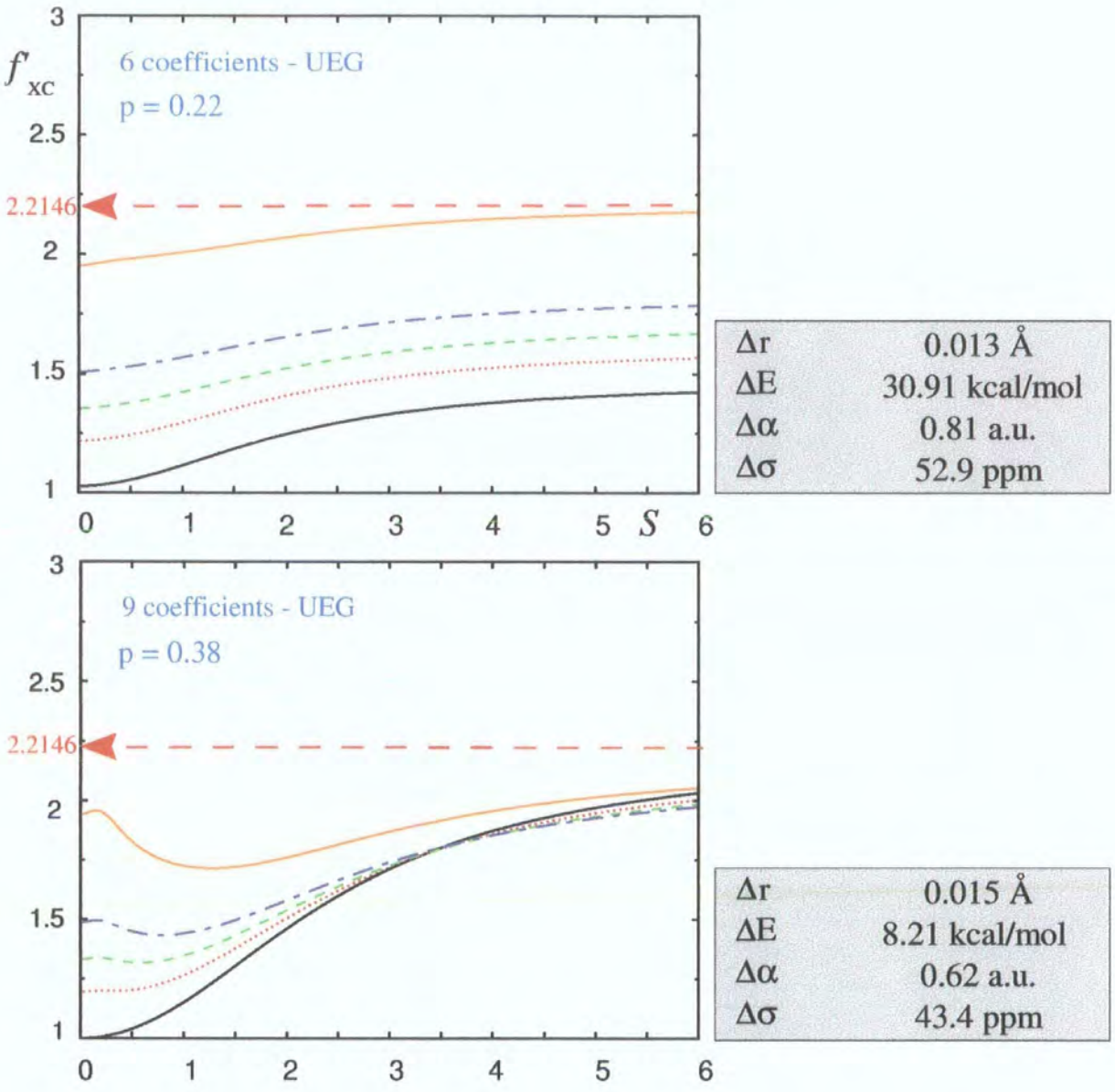

Figure 5.5: Exchange-correlation enhancement factors $f'_{\mathrm{xc}}(r_s, s)$ plotted as a function of s for the two optimal functionals satisfying the Lieb-Oxford bound and the uniform electron gas conditions.

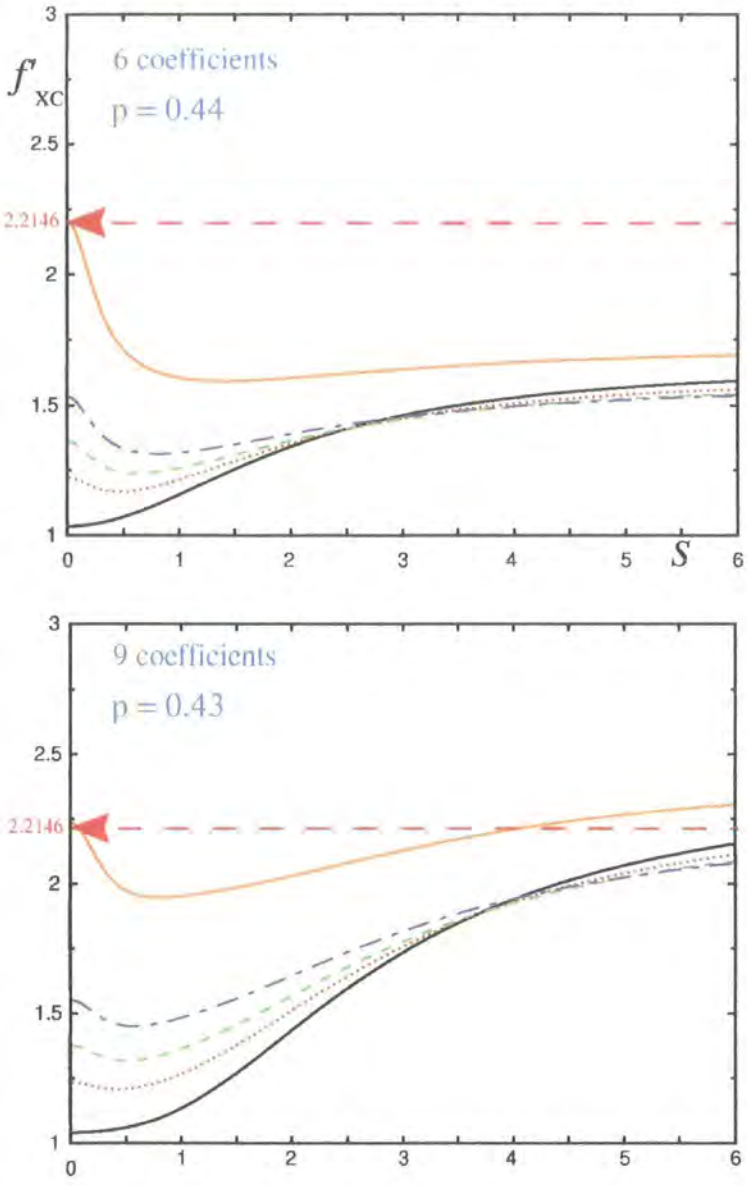

Δr	0.007 Å
ΔE	22.41 kcal/mol
Δα	0.52 a.u.
Δσ	50.3 ppm

It has been impossible to find 9 optimal expansion coefficients without imposing the uniform electron gas (UEG) condition.

Figure 5.6: Exchange-correlation enhancement factors $f'_{\mathrm{xc}}(r_s, s)$ plotted as a function of s for the two optimal functionals satisfying the Lieb-Oxford bound without the uniform electron gas condition.

5.3 The non-crossing HCTH-93

It is well known that the enhancement factor for the HCTH-93 functional does not satisfy the non-crossing condition in Eq.(5.2). To assess the effect of this, we determined a new HCTH-93 functional that does satisfy the condition.

Using the original HCTH-93 functional form and the original fitting procedure involving thermochemical data together with exchange-correlation potentials (See Chapter 3), we investigated the optimal value of p to generate a new non-crossing HCTH-93 functional. The optimal value of p was found to be 0.41 (compared to 0.67 in the original HCTH-93). In Figure 5.7, we present its enhancement factor, together with that of the original HCTH-93. Between $0 \leq s \leq 2.0$ the two plots are almost identical. The effects of the enforcement of the non-crossing condition appear only in the large s region.

We then performed an assessment of this new functional, but did not observe any improvement, apart from the molecular structures where the MAE error decreased from 0.013 Å in the original HCTH-93 to 0.011 Å. This is consistent with the observation in Chapter 3 that relatively diffuse (large s) regions are important for geometries; the new functional improves the large s region. For all the other properties there was a slight reduction in the accuracy, as shown in the tables of Figure 5.7.

The results of this and the previous section demonstrate that, although they are exact conditions, satisfying the uniform scaling and the Lieb-Oxford bound condition does not lead to any overall improvement in the properties considered.

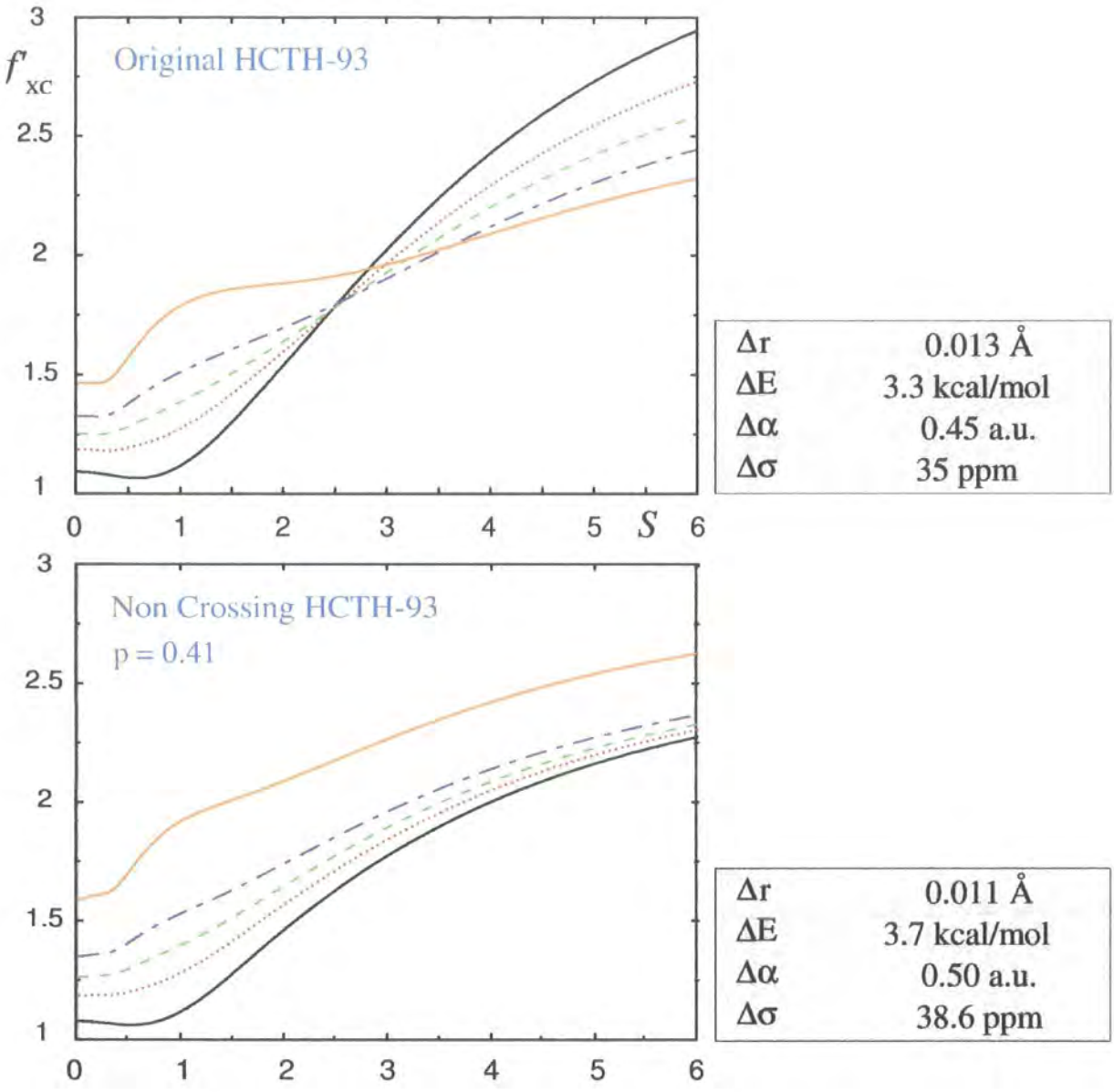

Figure 5.7: Exchange-correlation enhancement factor $f'_{\rm XC}(r_s, s)$ for HCTH-93 and the new non-crossing HCTH-93 plotted as a function of s.(Solid line: $r_s = 0$; dotted line: $r_s = 2$; dashed lines: $r_s = 6$; long-dashed line: $r_s = 18$; dot-dashed line: $r_s = \infty$

5.4 The helium dimer

GGA functionals represent a general improvement over LDA for describing potential energy surfaces [193, 194]. However, it is well known that, like LDA, they provide a poor description of van der Waals systems [195]-[198]. Some GGA functionals predict repulsive interactions with no minimum, whilst others, like LDA, overbind. Zhang, Pan and Yang [79] have demonstrated that the behaviour of the exchange enhancement factor in low density/large gradient (i.e. large s) regions is extremely important to understand quality of GGA predictions in the van der Waals systems. Functionals whose exchange enhancement factors increase rapidly with s tend to predict a repulsive interaction, whilst those whose enhancement factors increase more gradually tend to correctly predict binding. The functionals derived in Chapter 3 provide an excellent opportunity to test this hypothesis.

5.4.1 Results and discussion

In Figure 5.8 we present the exchange enhancement factors of the eight GGA functionals in Chapter 3, and of the $\frac{1}{4}$ functional. For small values of s the differences between the curves are relatively small. For larger values, however the curves become very different. Following Zhang *et al*, we would expect that the functionals associated with smaller values of p should bind the helium dimer, whereas those associated with the larger values should predict repulsive curves.

We have used these functionals to determine potential energy curves of He_2. We used an extensive 7s5p4d3f basis set, corresponding to the nuclear centered part of the DC^+BS (Dc147) basis set of Ref. [199]. We confirmed that BSSE corrections are negligible using this basis set. Results are presented in Figure 5.9. MP2 values are presented as a reference. In plot (a), the curves are exactly as predicted based on the observations of Zhang *et al.* As p increases the curves vary smoothly from attractive to repulsive. Plot

(b) highlights the bonding region for $p = 0, \frac{1}{6}, \frac{1}{4}, \frac{2}{6}$. Beyond these values, the curves are repulsive.

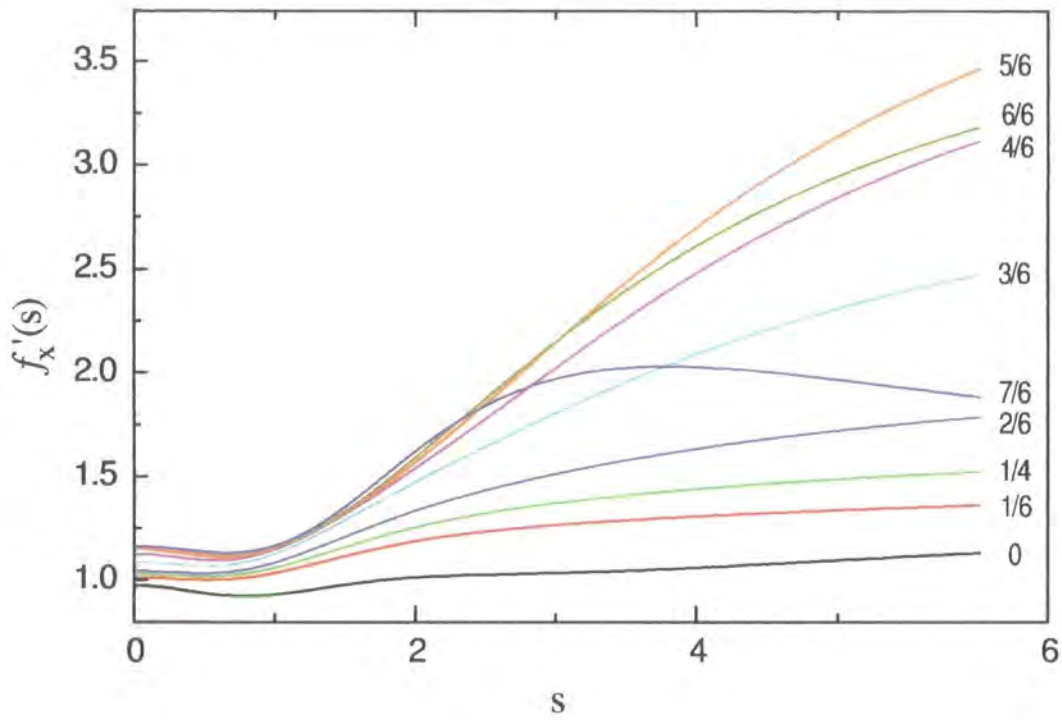

Figure 5.8: Exchange enhancement factor $f_x'(s)$ for $p = \frac{i}{6}$ with $i = 0...7$ and $p = \frac{1}{4}$ plotted as a function of s.

Finally, in Figure 5.10 we present the assessment of the new non-crossing HCTH-93 functional compared to the original HCTH-93. We observe that the new functional binds the helium dimer, whereas HCTH-93 is instead repulsive. This is again consistent with the exchange enhancement factor curves in Figure 5.8. The HCTH-93 curve increases rapidly so the He_2 curve is repulsive. The new functional gives a better behaved curved and correspondingly binds He_2.

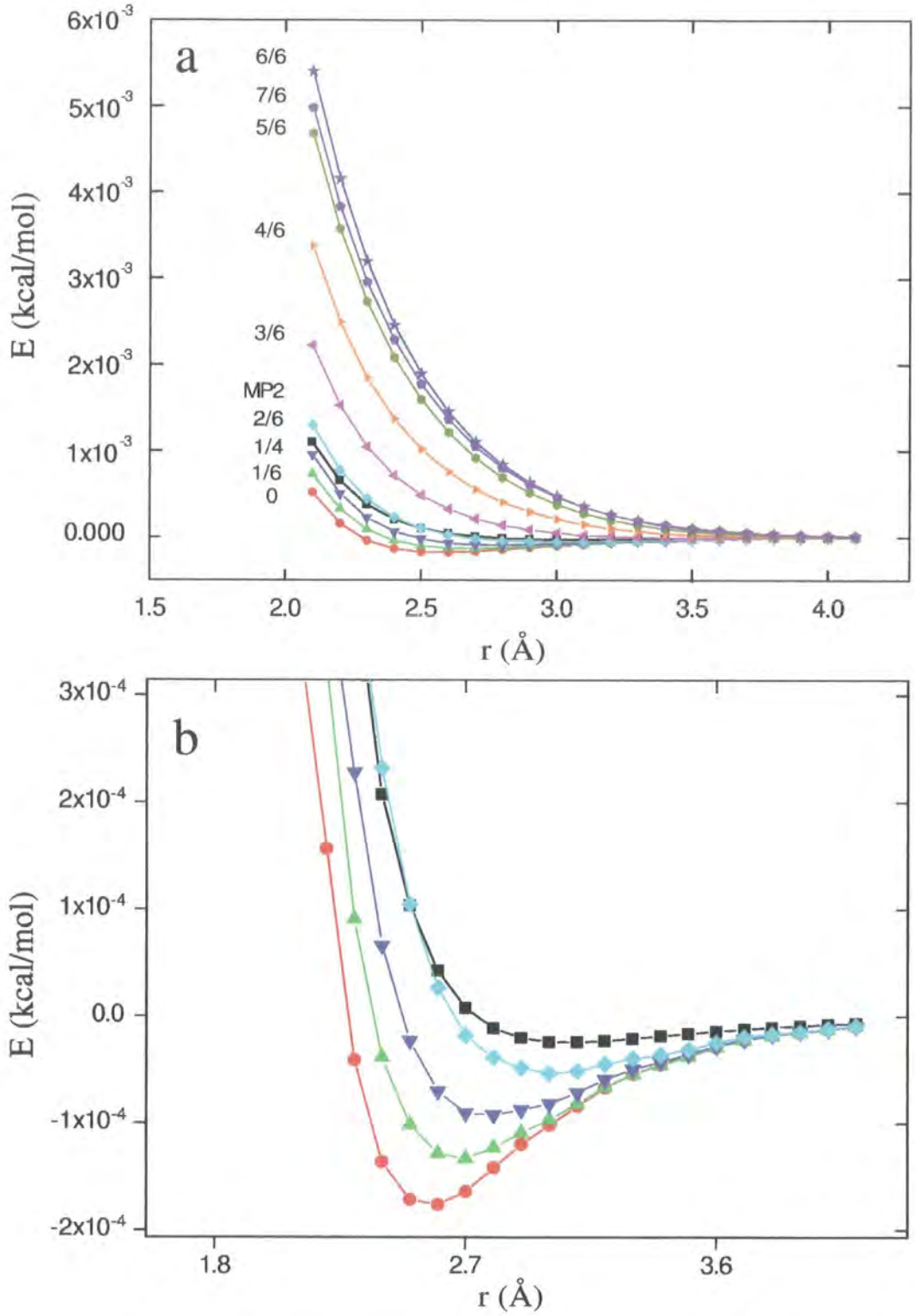

Figure 5.9: Potential energy curves for the helium dimer calculated using the functionals obtained for $p = \frac{i}{6}$ with $i = 0...7$, $p = \frac{1}{4}$, and MP2 plotted as a function of r.

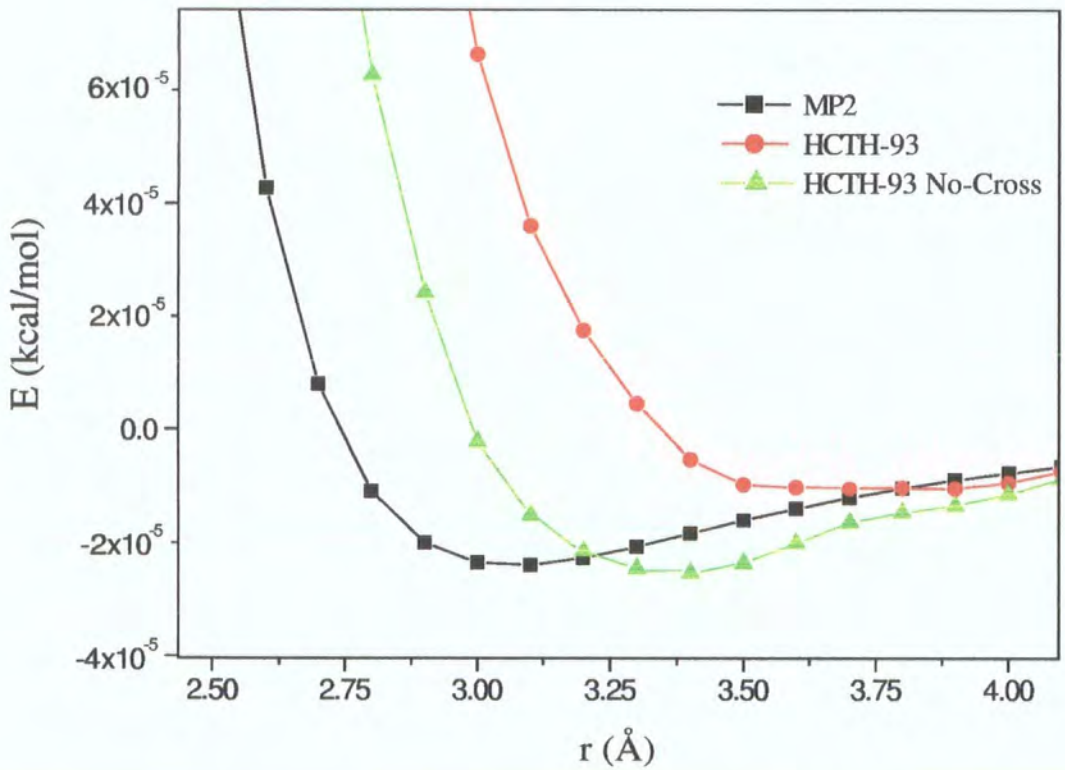

Figure 5.10: Potential energy curves for the Helium dimer calculated using the HCTH-93, HCTH-93 non-crossing functionals and MP2 plotted as a function of r.

Chapter 6

Investigation of hybrid functionals

The diatomic molecule assessment in Chapter 4 highlighted the high quality structural predictions from the PBE0 functional, which contains 25% exact orbital exchange. Other recent studies have also suggested that this fraction is near-optimal. In this chapter we therefore determine a new, highly parameterised functional containing this fraction of exact exchange. By comparing with PBE0 and B97-2 (21%) the influence of parameterisation and fraction of orbital exchange is quantified. Particular attention is paid to chemical reaction barriers and their relationship to self-interaction errors. Following the GGA work in Chapter 3, attempts are also made to determine new hybrid functionals solely from *ab initio* densities.

6.1 The B97-3 hybrid functional

The general expression for a hybrid functional is written as

$$E_{\mathrm{XC}}[\rho_\alpha,\rho_\beta] = E_{\mathrm{XC}}^{\zeta}[\rho_\alpha,\rho_\beta] - \frac{\zeta}{2}\int\int\sum_{\sigma}\frac{\sum_i^{N\sigma}\varphi_i^{\sigma}(\mathbf{r})\varphi_i^{\sigma}(\mathbf{r}')}{|\mathbf{r}-\mathbf{r}'|}d\mathbf{r}d\mathbf{r}' \qquad (6.1)$$

where the first term is a continuum functional and the second is the fraction of exact orbital exchange. Wilson and Tozer [154] recently investigated the

optimal amount of exact exchange to include in a hybrid functional to obtain accurate electron densities. They concluded that the optimal amount is 25%. This is consistent with the PBE0 functional, where 25% was chosen based on a perturbation theory analysis.

Among the most recently developed hybrid functionals we recall the B97-2 functional developed by Wilson *et al* [111] via a fitting procedure involving thermochemical data and exchange-correlation potentials. The procedure is essentially identical to that used to determine HCTH-93 except that
a. no gradient information was used;
b. the potentials were determined using a modified ZMP approach, which accounts for the presence of a fraction of exact orbital exchange.

Its performance is very successful in predicting molecular properties, particularly compared to B97-1 and B3LYP. B97-2 contains 21% exact exchange.

We have therefore determined a new hybrid functional, which we denote B97-3, as it is a natural extension of B97-2. We developed this functional using the same approach that was used to develop B97-2, except we increased the amount of exchange from 21% to 25%. The coefficients defining B97-3 are presented in Appendix B.

6.2 Performance of B97-3

A detailed assessment of the B97-3 functional is now presented comparing with PBE0 [112] and B97-2. Molecular structures, polarizabilities and shielding constants, together with an extensive range of classical reaction barriers are investigated. Unless otherwise stated, all the calculations were performed using the TZ2P basis set and the sets of molecules defined in Chapter 3.

6.2.1 Molecular structures

Table 6.1 presents optimized structures. Increasing the amount of exact exchange does reduce bond lengths; the mean error reduces slightly from

B97-2 to B97-3 although the mean absolute error is unchanged at 0.008 Å. PBE0 gives the most accurate mean absolute error of 0.006 Å.

6.2.2 Thermochemistry

In Table 6.2 we present the MAE for the total energies (E), the ionization potentials (IP) and atomization energies (AE). As for molecular structures, the increase in the amount of exact exchange in B97-3 did not bring any substantial improvement over B97-2. However, both B97-2 and B97-3 are a significant improvement over PBE0. The mean absolute error for the total energies decreases from 25.6 kcal/mol for PBE0 to 3.4-3.5 kcal/mol for B97-2 and B97-3. The mean absolute error for the atomization energies decreases from 3.19 kcal/mol for PBE0 to 2.0-2.2 kcal/mol for B97-2 and B97-3. Mean absolute errors for ionization potentials are comparable for all three functionals.

6.2.3 Static isotropic polarizabilities

In Table 6.3 we present isotropic polarizabilities; zero-point corrections have not been included. BD(T) values are therefore also presented as a reference. PBE0 and B97-2 underestimate experimental polarizabilities by almost the same extent as BD(T), with average errors of 0.07 and 0.13 compared to 0.10 au. B97-3 also underestimates experimental polarizabilities but with an average error of 0.22 a.u. which is consistent with the increased fraction of exact orbital exchange.

6.2.4 Shielding constants

In Table 6.4 we present isotropic shielding constants. The columns headed PBE0, B97-2, B97-3 are the conventional shielding constants, calculated as the second derivatives of the corresponding electronic energies. The mean absolute error is dominated by the error for the ozone molecules, hence we

Table 6.1: Optimised geometries (in Å and degrees) for molecules S using PBE0, B97-2, and B97-3, with the TZ2P basis set

Molecule	Expt[1]	PBE0	B97-2	B97-3
H_2	0.741	0.743	0.739	0.738
LiH	1.596	1.596	1.601	1.598
BeH	1.343	1.349	1.353	1.350
CH	1.12	1.125	1.124	1.122
CH_2	1.078	1.078	1.077	1.076
CH_2S	1.11	1.112	1.11	1.109
CH_3	1.08	1.079	1.077	1.076
CH_4	1.086	1.088	1.087	1.086
NH	1.036	1.038	1.038	1.036
NH_2	1.024	1.025	1.024	1.022
NH_3	1.012	1.012	1.009	1.008
OH	0.97	0.971	0.97	0.968
H_2O	0.957	0.958	0.956	0.954
HF	0.917	0.918	0.916	0.914
Li_2	2.673	2.736	2.754	2.75
LiF	1.564	1.569	1.578	1.575
C_2H_2	1.203	1.196	1.197	1.195
	1.063	1.064	1.062	1.061
C_2H_4	1.331	1.323	1.324	1.322
	1.081	1.084	1.082	1.081
CN	1.172	1.16	1.161	1.159
HCN	1.065	1.068	1.066	1.065
	1.153	1.146	1.146	1.144
CO	1.128	1.124	1.125	1.123
HCO	1.173	1.17	1.171	1.169
	1.123	1.123	1.121	1.119

Cont

Table 6.1: continued.

Molecule	Expt[1]	PBE0	B97-2	B97-3
H_2CO	1.203	1.197	1.197	1.195
	1.102	1.107	1.105	1.104
N_2	1.098	1.09	1.091	1.089
O_2	1.207	1.196	1.198	1.194
H_2O_2	1.456	1.431	1.435	1.43
	0.966	0.963	0.961	0.959
F_2	1.412	1.383	1.387	1.382
CO_2	1.16	1.157	1.158	1.156
HCl	1.275	1.279	1.275	1.274
Na_2	3.079	3.082	3.13	3.121
Si_2	2.246	2.257	2.258	2.254
P_2	1.893	1.884	1.885	1.881
S_2	1.889	1.896	1.898	1.895
Cl_2	1.988	2.001	2.003	1.999
NaCl	2.361	2.363	2.378	2.374
SiO	1.51	1.508	1.509	1.506
CS	1.535	1.532	1.533	1.531
SO	1.481	1.485	1.488	1.485
ClO	1.57	1.576	1.576	1.573
ClF	1.628	1.631	1.633	1.629
Mean r		0.000	0.002	-0.000
Mean abs. r		0.006	0.008	0.008

[1] Ref [115]

Table 6.2: Error assessments of the thermochemistry (kcal/mol) for systems defined in Table 3.2, calculated using PBE0, B97-2 and B97-3.

	PBE0	B97-2	B97-3
Mean abs E	25.6	3.4	3.5
Mean abs AE	3.2	2.0	2.2
Mean abs IP	1.8	1.4	1.3

Table 6.3: Static isotropic polarisabilities (in atomic units) using PBE0, B97-2, and B97-3, with the Sadlej basis set.

	Expt[1]	BD(T)	PBE0	B97-2	B97-3
HF	5.6	5.64	5.68	5.68	5.61
H_2O	9.64	9.71	9.69	9.7	9.6
N_2	11.74	11.75	11.74	11.71	11.66
CO	13.08	13.03	12.98	12.96	12.88
F_2	8.38	8.45	8.56	8.53	8.5
NH_3	14.56	14.33	14.34	14.35	14.21
CO_2	17.51	17.56	17.03	16.99	16.9
CH_4	17.27	16.43	16.74	16.64	16.56
C_2H_4	27.7	26.91	27.61	27.56	27.48
PH_3	30.93	30.44	30.93	30.76	30.64
H_2S	24.71	24.67	24.75	24.61	24.49
SO_2	25.61	26.06	25.3	25.26	25.11
HCl	17.39	17.43	17.53	17.42	17.34
Cl_2	30.35	30.71	30.62	30.46	30.36
Mean (BD(T))			0.03	−0.04	−0.13
Mean abs. (BD(T))			0.24	0.22	0.26
Mean (Expt)		−0.10	−0.07	−0.13	−0.22
Mean abs. (Expt)		0.25	0.18	0.19	0.24

[1]Ref [144] unless otherwise stated

[2]Ref [145]

present the error assessment including and omitting this molecule. All three functionals provide very poor results. The reduction in accuracy in moving from B97-2 to B97-3 is consistent with the work of Wilson and Tozer [154] who demonstrated that the optimal amount of exact exchange is zero for conventional shielding calculations.

The columns headed MKS(PBE0), MKS(B97-2) and MKS(B97-3) are shielding constants calculated using the multiplicative Kohn-Sham approach (MKS) of Wilson and Tozer [201]. In this method the multiplicative ZMP potentials are determined from electron densities. The corresponding Kohn-Sham orbitals and eigenvalues are then used in the conventional uncoupled Kohn-Sham expression for the shielding constants. The MKS(PBE0), MKS(B97-2) and MKS(B97-3) are shielding constants obtained from the PBE0, B97-2 and B97-3 electron densities. In general, there is a significant reduction in the mean absolute errors compared to conventional shielding constant calculations. The MKS(B97-3) results are now an improvement over MKS(B97-2) and the best results are obtained with MKS(PBE0).

6.2.5 Reaction barriers

The calculation of chemical reaction barriers is a significant challenge for DFT. In many cases, GGA and hybrid functionals provide reaction barriers that are significantly below the best *ab initio* values [202]-[204]. Lynch *et al.* [205] have demonstrated that improved results can be achieved by increasing the amount of exact exchange in the functional form. We might therefore expect PBE0 and B97-3 to be more accurate than B97-2, since they include more exact exchange. In Table 6.5, we present 16 classical reaction barriers. The first column indicates the reactants, the second describes the nature of the transition state where in each case the horizontal line is the new bond formed. The next three columns are the reaction barriers calculated with PBE0, B97-2 and B97-3, using the TZ2P basis set. The barriers are

Table 6.4: Isotropic shielding constants (in ppm) using PBE0, B97-2, B97-3, MKS(PBE0), MKS(B97-2) and MKS(B97-3) with the Huzinaga (IGLO IV) basis set.

		Expt[1]	Best *ab initio*[1]	PBE0	B97-2	B97-3	MKS (PBE0)	MKS (B97-2)	MKS (B97-3)
HF	H	419.7	418.6	413.5	412.5	412.8	416	414.4	415.2
H_2O	O	357.6	337.9	330.1	328.3	328.6	332.2	329.8	330.5
CH_4	C	198.4	198.9	192.8	191.3	191.7	192.2	190.7	191
CO	C	2.8	5.6	−16.9	−12.4	−13.6	−3.3	−2.4	−1.1
	O	−36.7	−52.9	−82.5	−74.1	−75.4	−46.2	−45.4	−40.8
N_2	N	−59.6	−58.1	−91.4	−85.9	−87.7	−63.5	−64	−61.1
F_2	F	−192.8	−186.5	−240.5	−243.1	−238.6	−191.8	−202.7	−191.9
O'OO'	O'	−1290	−1208.2	−1736.2	−1660.4	−1707.1	−1143.2	−1174.1	−1133
	O	−724	−754.6	−1168.5	−1099.6	−1151.2	−775	−782.9	−768.4
PN	P	53	86	−54.7	−36.3	−41.2	37	37.1	47.2
	N	−349	−341	−424.4	−408.4	−413.5	−338.9	−340.8	−319.9
H_2S	S	752	754.6	728.5	722.5	723.3	733.3	725.6	727.1
NH_3	N	273.3	270.7	262.8	260.9	261.1	263.6	261.3	261.7
HCN	C	82.1	86.3	70.9	73.4	73	77.6	78.3	79
	N	−20.4	−13.6	−46.9	−39.8	−40.9	−24.2	−22.2	−19.6
C_2H_2	C	117.2	121.8	109.2	111.7	111.6	112.5	113.9	114.4
H_2CO	C	−4.4	4.7	−21.4	−16.6	−16.6	−15	−12.5	−11.3
	O	−375	−383.1	−452.9	−424.9	−428	−354.6	−348.3	−336.9
CO_2	C	58.8	63.5	53.2	55.1	54.7	58.2	58.7	59.2
	O	243.4	236.4	214.1	215.7	215.8	226.2	225.2	227.4
HCl	Cl	952	962.3	956.8	952.4	953.3	957.1	952	953.1
SO_2	S	−126	−134.2	−241	−227.5	−234.4	−171.4	−172.4	−166.8
	O	−205	−170.4	−281.7	−273.8	−275.8	−208.8	−214.7	−205.2
PH_3	P	599.9	594	584.8	580	580.9	585.9	580.4	581.4
Mean			4.6	−69.6	−59.4	−64.4	−3	−5.9	0.16
Mean abs.			12.9	70	59.5	64.5	18.26	18.5	18.8
O_3 omitted									
Mean			2.5	−32.5	−28.3	−29.2	−7	−8.3	10.02
Mean abs.			8.2	32.9	28.4	29.3	10.02	11.21	10.40

[1]Refs [129] and [130]

calculated at the corresponding DFT optimized structures.

Surprisingly we observe that PBE0 provides very poor reaction barriers with a mean absolute error of 4.37 kcal/mol. This is a significant failing. B97-2 and B97-3 are substantially more accurate with mean absolute errors of 2.4 kcal/mol and 2.3 kcal/mol, respectively. The increase in the amount of exact exchange in B97-3 provides only a small improvement in the functional performance. Finally, we note that we did not include any BSSE counterpoise correction in our calculations. The inclusion of this correction would further increase the reaction barriers, although the effect is small for the TZ2P basis set [220].

Increasing the fraction of exact exchange from 21% to 25% does not therefore lead to significant improvements. One of the key observation of this work is the significant failing of PBE0 in describing chemical reaction barriers. B97-2 and B97-3 are substantially more accurate. We now go on to consider the relationship between reaction barrier accuracy and the self-interaction problem.

Table 6.5: Classical reaction barriers (in kcal/mol) using PBE0, B97-2 and B97-3, with the TZ2P basis set.

Reaction	TS	PBE0	B97-2	B97-3	*Abinitio*
$H + H_2$	$H - H_2$	5.52	9.68	10.16	9.61[1]
$CH_4 + CH_3$	$H_3CH - CH_3$	14.34	14.47	14.47	17.5[2], 16.6[3]
$H_2 + CH_3$	$HH - CH_3$	7.92	9.15	8.96	11.81[4]
$H_2 + NH_2$	$HH - NH_2$	4.72	6.28	6.32	9.51[4]
$H_2 + OH$	$HH - OH$	0.9	1.9	2.11	5.62[4], 4.87[3]
$CH_4 + OH$	$H_3CH - OH$	2.27	2.68	3.11	6.62[5], 5.11[3]
$H + N_2$	$H - N_2$	8.78	12.76	13.31	15.2[6], 14.5[7]
$N + O_2$	$N - O_2$	7.74	7.92	8.7	8.8[8], 10.2[9]
$O + HCl$	$O - HCl$	2.68	2.98	3.74	9.78[10], 10.4[11]
$H + N_2O$	$H - N_2O$	6.31	10.36	10.82	9.6[12]
$H + N_2O$	$NNOH$	13.55	16.91	17.02	14.5[12]
$H + N_2O$	$H - ON_2$	14.47	18.75	19.41	17.5[12]
$H + NO$	$H - NO$	0.17	3.73	3.93	4.1[13]
$O + H_2$	$O - H_2$	6.37	8.9	9.10	12.4[14]
$H + HF$	$H - FH$	36.19	42.48	43.57	42.17[3], 46.11[15]
$H + HCl$	$H - ClH$	13.53	18.23	18.89	20.72[15]
Mean		−4.37	−1.77	−1.36	
Mean abs.		4.37	2.37	2.31	

[1]Ref [206]
[2]Ref [207]
[3]Ref [208]
[4]Ref [209]
[5]Ref [210]
[6]Ref [211]
[7]Ref [212]
[8]Ref [213]
[9]Ref [214]
[10]Ref [215]
[11]Ref [216]
[12]Ref [217]
[13]Ref [218]
[14]Ref [219]
[15]Ref [203]

6.3 The H_2^+ molecule

Zhang and Yang [221] have argued that the self-interaction error in approximate exchange-correlation functionals may be responsible for errors in chemical reaction barriers. For all the reactions in Table 6.5 the B97-1 functional (21% exchange) gives a mean absolute error of 3.6 kcal/mol. The B97-2 functional (also 21%) significantly reduces the error to 2.4 kcal/mol. Following Zhang and Yang we would therefore expect self-interaction errors to be smaller for B97-2. Figure 6.1 presents the exact (Hartree-Fock), B97-1 and B97-2 potential energy curves for H_2^+ using the extensive d aug-cc-pV6Z basis set with functions f, g and h removed. No improvement is observed for B97-2 which contradicts the view of Zhang and Yang.

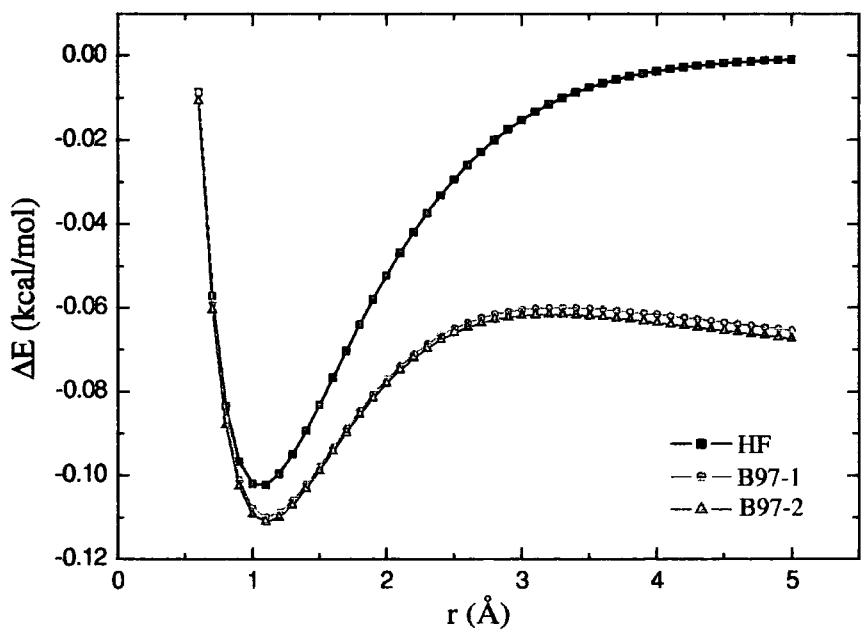

Figure 6.1: Dissociation curves for H_2^+ described by B97-1, B97-2 and HF. $\Delta E = E(H_2^+) - E(H) - E(H^+)$

Figure 6.2 presents H_2^+ potential energy curves for HCTH-93 and $\frac{1}{4}$. The $\frac{1}{4}$ functional provides a much improved description of H_2^+. We view this as a

significant observation, again highlighting the physically interesting nature of $\frac{1}{4}$. However, $\frac{1}{4}$ reaction barriers (not presented in this thesis) are significantly inferior to those of HCTH-93. Once again, this suggests that there is no simple relationship between reaction barriers accuracy and self-interaction errors.

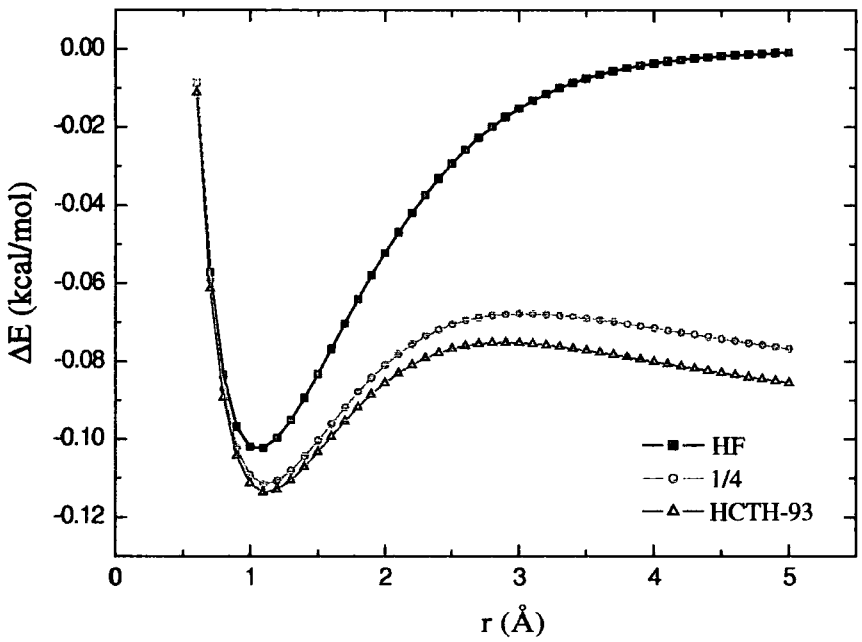

Figure 6.2: Dissociation curves for H_2^+ described by $\frac{1}{4}$, HCTH-93 and HF. $\Delta E = E(H_2^+) - E(H) - E(H^+)$

6.4 Hybrid functionals from v_{xc}

Finally, using the ideas of Chapter 3, we consider the determination of new hybrid functionals by fitting solely to exchange-correlation potentials. Using exactly the same mathematical form and training set used to develop B97-3, again with 25% exact exchange, we determined new functionals by minimizing

$$\Omega = \sum_{T}\sum_{\sigma}\int d\mathbf{r}[v^{\zeta}_{ZMP,\sigma T}(\mathbf{r}) + k^{\zeta}_{\sigma T} - v^{\zeta}_{fit,\sigma T}(\mathbf{r})]^2 \rho^{p}_{\sigma T}(\mathbf{r}) \qquad (6.2)$$

We considered a range of values for p from 0 to $\frac{7}{6}$. Optimal structures and thermochemistry were obtained near $p = 0.21 - 0.25$.

In Table 6.6 we present a detailed analysis of the MAE for the corresponding five functionals. In moving from 0.21 to 0.24 the quality of the bond lengths is constant, comparable to B97-2 and B97-3. Only for $p = 0.25$ does the mean absolute error decrease to 0.007 Å. A different situation is observed for the energy assessment. The removal of the thermochemical data in the fitting procedure leads to a dramatic increase in the mean absolute error for the total energies, as was the case for the GGAs in Chapter 3. Atomization energies and ionization potentials are less accurate than for B97-2 and B97-3. However, they are an improvement over the $\frac{1}{4}$ GGA results. We stress that no thermochemical information was included in the fitting procedure. Unlike in the GGA case, no functional is simultaneously optimal for both structures and thermochemistry.

Table 6.6: Error assessments for self-consistent molecular structures (Å and degrees), thermochemistry (kcal/mol) as a function of the power p in Eq. (6.2).

			p				
	B97-2	B97-3	0.21	0.22	0.23	0.24	0.25
Molecular structures of systems S							
Mean r	0.002	−0.000	−0.004	−0.004	−0.004	−0.004	−0.004
Mean abs. r	0.008	0.008	0.008	0.008	0.008	0.008	0.007
Combined thermochemistry of systems M, A_1, A_1^+, and A_2							
Mean abs E	3.4	3.5	78.3	73.0	67.9	63.1	58.4
Mean abs AE	2.0	2.2	4.4	4.2	4.2	4.7	5.8
Mean abs IP	1.4	1.3	4.8	4.6	4.4	4.3	4.2

Chapter 7

The exchange-correlation charge

This thesis has demonstrated that the exchange-correlation potential $v_{\rm xc}(\mathbf{r})$ is a key quantity in DFT. Another important quantity is the exchange-correlation charge or hole. In this chapter we investigate a new, recently proposed definition of the exchange-correlation charge. We present the first calculations of this charge for molecular systems, paying particular attention to its basis set dependence and its relationship to the exchange correlation potential.

7.1 Definition

The exchange correlation charge (hole) $\rho_{\rm xc}(\mathbf{r},\mathbf{r}')$ has conventionally been related to the exchange-correlation energy $E_{\rm xc}[\rho]$ by the expression

$$E_{\rm xc}[\rho] = \frac{1}{2}\int\int \frac{\rho(\mathbf{r})\rho_{\rm xc}(\mathbf{r},\mathbf{r}')}{|\mathbf{r}-\mathbf{r}'|}d\mathbf{r}d\mathbf{r}' \tag{7.1}$$

The dependence of the charge on both $\mathbf{r}$ and $\mathbf{r}'$ makes it a difficult quantity to visualize. Furthermore it has no simple relationship to the exchange-correlation potential. In light of this, Liu *et al.* [225] have introduced an alternative definition of the exchange-correlation charge. The new charge,

denoted $q_{\mathrm{XC}}(\mathbf{r})$, depends only on a single electronic coordinate and is related to the asymptotically vanishing exchange-correlation potential through the Poisson equation

$$v_{\mathrm{XC}}(\mathbf{r}) = \int \frac{q_{\mathrm{XC}}(\mathbf{r}')}{|\mathbf{r}-\mathbf{r}'|} d\mathbf{r}' \tag{7.2}$$

or

$$\nabla^2 v_{\mathrm{XC}}(\mathbf{r}) = -4\pi q_{\mathrm{XC}}(\mathbf{r}) \tag{7.3}$$

i.e. the new exchange-correlation charge is the charge distribution whose classical Hartree potential is the exchange-correlation potential. Eqns. (7.2) and (7.3) have also been considered by Görling [227].

Within the ZMP approach [72] the exchange-correlation potential is expressed as

$$v_{\mathrm{XC}}(\mathbf{r}) = \lim_{\lambda\to\infty}\left(-\frac{1}{N}\int \frac{\rho^{\lambda}(\mathbf{r}')}{|\mathbf{r}-\mathbf{r}'|} d\mathbf{r}' + \lambda \int \frac{\rho^{\lambda}(\mathbf{r}') - \rho_0(\mathbf{r}')}{|\mathbf{r}-\mathbf{r}'|} d\mathbf{r}'\right) \tag{7.4}$$

Comparing Eq. (7.4) with Eq. (7.2), it follows that the exchange-correlation charge is easily expressed in terms of the ZMP quantities

$$q_{\mathrm{XC}}(\mathbf{r}) = \lim_{\lambda\to\infty}\left(-\frac{\rho^{\lambda}(\mathbf{r})}{N} + \lambda\left[\rho^{\lambda}(\mathbf{r}) - \rho_0(\mathbf{r})\right]\right) \tag{7.5}$$

Given that the trial electron density $\rho^{\lambda}(\mathbf{r})$ and the exact density $\rho_0(\mathbf{r})$ both integrate to N electrons, integration of Eq. (7.5) gives a simple derivation of the sum rule

$$\int q_{\mathrm{XC}}(\mathbf{r}) d\mathbf{r} = -1 \tag{7.6}$$

In practical calculations the exact density $\rho_0(\mathbf{r})$ must be replaced by an accurate *ab initio* electron density, for this reason the exchange-correlation charge and the exchange-correlation potential represent approximations to the exact quantities. In the next section, we solve the ZMP equations and examine the charge for He, Ne, HF, CO and N_2. Diatomic molecules are chosen in order to facilitate graphical analysis of the charges. The method, however, is applicable to any molecule.

7.2 Computational details

BD densities are used for all the calculations. For a finite gaussian basis set the trial density $\rho^{\lambda}(\mathbf{r})$ will never equal the *ab initio* density $\rho_0(\mathbf{r})$ [75]. It follows that as λ approaches infinity, both the potential and the charge will also become infinite, which is unsatisfactory. Two approaches have been proposed to circumvent this problem. One approach [63, 75] is to use a large but finite value for λ; a value of 900 has often been used. An alternative approach is to expand the potential and the charge as Laurent expansions in λ

$$v_{\mathrm{XC}}^{\lambda}(\mathbf{r}) = \sum_{i=n_1}^{n_2} V_i(\mathbf{r})\lambda^i \tag{7.7}$$

$$q_{\mathrm{XC}}^{\lambda}(\mathbf{r}) = \sum_{i=n_1}^{n_2} Q_i(\mathbf{r})\lambda^i \tag{7.8}$$

where $v_{\mathrm{XC}}^{\lambda}(\mathbf{r})$ and $q_{\mathrm{XC}}^{\lambda}(\mathbf{r})$ are the exchange-correlation potential and charge respectively determined for a specific values of λ. From Eq. (7.4) and (7.5)

$$v_{\mathrm{XC}}^{\lambda}(\mathbf{r}) = -\frac{1}{N}\int \frac{\rho^{\lambda}(\mathbf{r})}{|\mathbf{r}-\mathbf{r}'|}d\mathbf{r}' + \lambda \int \frac{\rho^{\lambda}(\mathbf{r}') - \rho_0(\mathbf{r}')}{|\mathbf{r}-\mathbf{r}'|}d\mathbf{r}' \tag{7.9}$$

$$q_{\mathrm{XC}}^{\lambda}(\mathbf{r}) = -\frac{\rho^{\lambda}(\mathbf{r})}{N} + \lambda[\rho^{\lambda}(\mathbf{r}) - \rho_0(\mathbf{r})] \tag{7.10}$$

By calculating the charge and potential at appropriate values of λ, the expansion coefficients $V_i(\mathbf{r})$ and $Q_i(\mathbf{r})$ can be determined and an optimal potential and charge defined.

We performed extensive investigations in order to determine an optimal expansion range (defined by n_1 and n_2) together with optimal values of λ at which the potential and the charge should be calculated. Our criteria were that the calculated potentials should resemble those published previously and that the calculated charge should resemble the published [225] and unpublished results [226] of Liu *et al.* We concluded that the optimal expansion was a five term expansion defined by $n_1 = -3$ and $n_2 = 1$. The final term in this expansion has a linear dependence on λ and represents the basis set deficiency; as λ approaches infinity so to does this term. To determine the

expansion parameters in Eq. (7.7) and (7.8) we calculated the potential and charge at λ values of 32, 64, 128, 256 and 512 and solved the resulting sets of five inhomogeneous linear equations. As $\lambda \to \infty$ the first three terms in the expansion vanish. Given that the fifth term is the basis set error, we define our optimal exchange-correlation potential and charge to be the fourth terms in the expansions

$$v_{\mathrm{XC}}^{\mathrm{opt}}(\mathbf{r}) = V_0(\mathbf{r}) \tag{7.11}$$

$$q_{\mathrm{XC}}^{\mathrm{opt}}(\mathbf{r}) = Q_0(\mathbf{r}) \tag{7.12}$$

The next important consideration is the choice of gaussian basis set. We commenced by using the TZ2P basis set, but observed that the calculated exchange-correlation potential at the nucleus of the Ne atom was about 1 au less negative than the high accuracy Ne potential presented by Zhao *et al.* [72] Furthermore, our potential exhibited a flattening very close to the nucleus, which is not present in the potential of Zhao *et al.* This flattening, which leads to a positive spike in the associated exchange-correlation charge at the nucleus is a consequence of the gaussian basis set. Figures 7.1-7.4 present the charges and the (scaled) potentials for Ne, CO, N_2 and F_2 respectively.

The inclusion of additional high exponent gaussian functions, which are much steeper at the core, completely eliminates this feature and gives a potential which agrees well with that of Zhao *et al.* For C, N, O, F and Ne we therefore augmented the TZ2P basis set with three s and p functions, with exponents 30.0, 90.0 and 270.0; for H and He we add just three s functions with the same exponents. For this basis set, we have confirmed that the behaviour of the exchange correlation charge near the nucleus of the Ne atom closely resembles the charge of Liu *et al.* [226]

Next we consider the quality of this core-augmented TZ2P basis in the valence and asymptotic regions. In Figure 7.5 we present a logarithmic plot of the radial distribution of the Ne exchange-correlation charge $[4\pi r^2 q_{\mathrm{XC}}(\mathbf{r})]$, plotted as a function of distance from the nucleus. For comparison we also

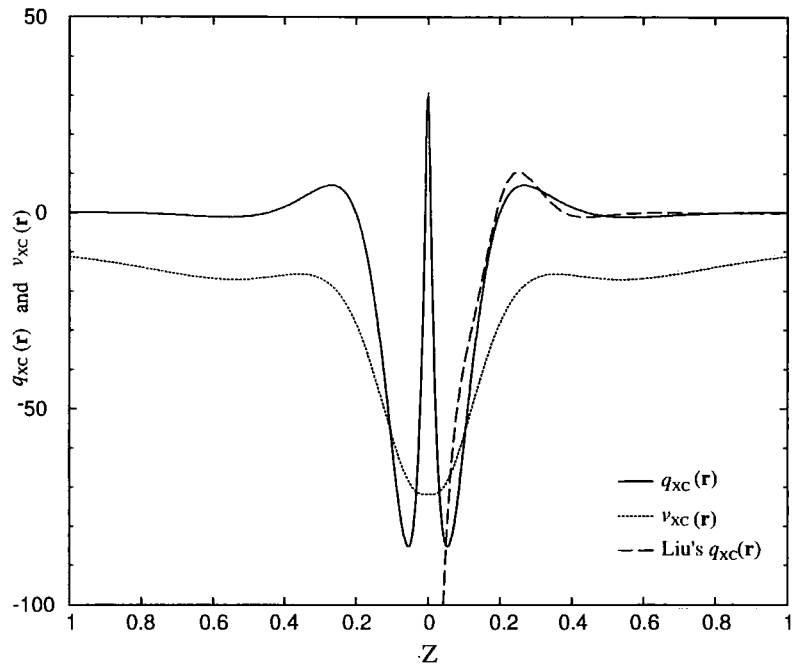

Figure 7.1: Comparison between $q_{\mathrm{XC}}(\mathbf{r})$ and $10 \cdot v_{\mathrm{XC}}(\mathbf{r})$ for Ne atom

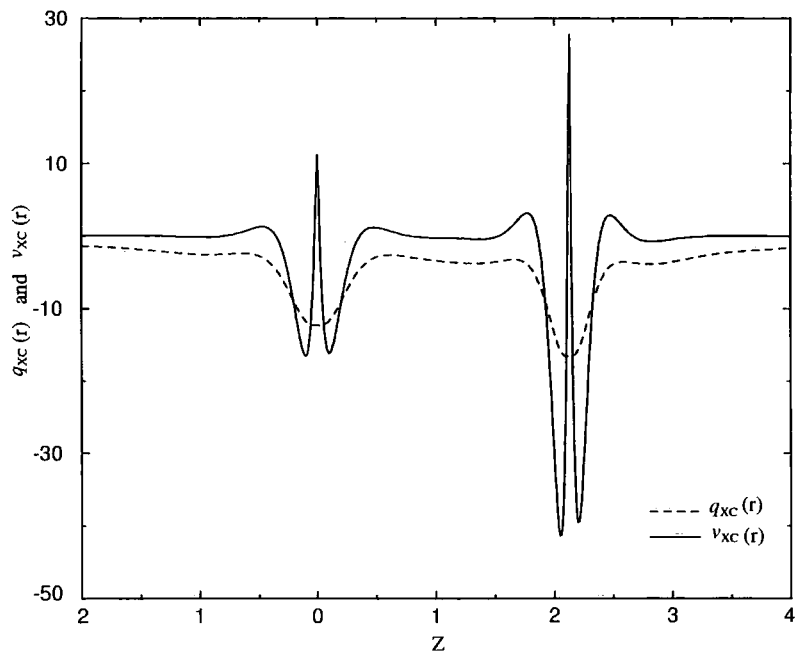

Figure 7.2: Comparison between $q_{\mathrm{XC}}(\mathbf{r})$ and $3 \cdot v_{\mathrm{XC}}(\mathbf{r})$ for CO

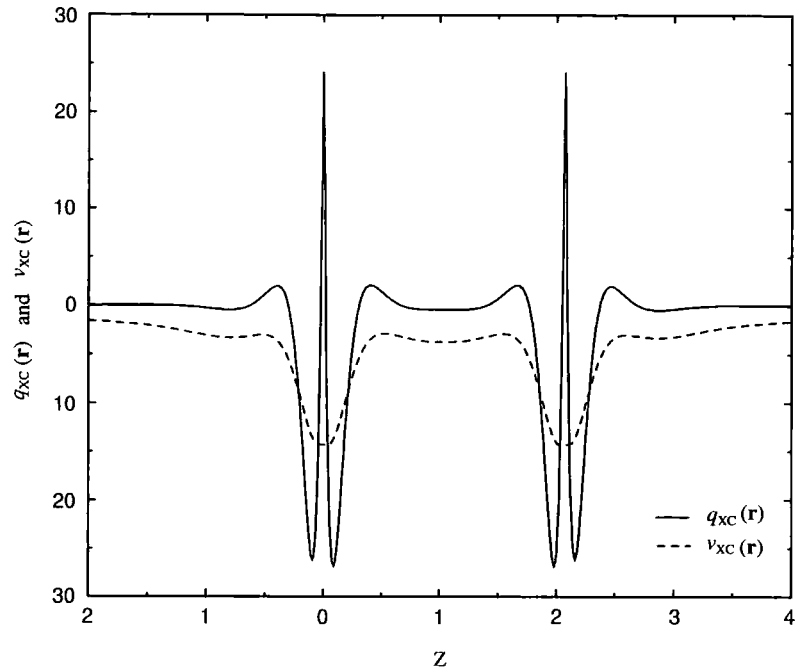

Figure 7.3: Comparison between $q_{\mathrm{xc}}(\mathbf{r})$ and $3 \cdot v_{\mathrm{xc}}(\mathbf{r})$ for N_2

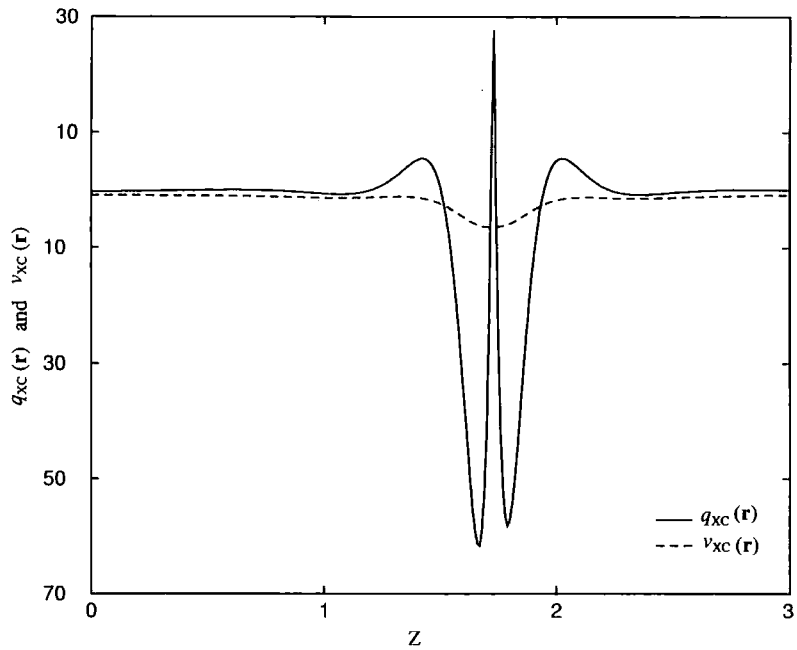

Figure 7.4: Comparison between $q_{\mathrm{xc}}(\mathbf{r})$ and $v_{\mathrm{xc}}(\mathbf{r})$ for HF

present the radial electron density distribution $[4\pi r^2\rho(\mathbf{r})]$. There is a minimum in the radial charge near the first maximum in the radial density and a maximum in the radial charge near the minimum in the radial density. The radial charge exhibits two sub-shell peaks within the second peak of the radial density. These observations are consistent with those of Liu *et al.* except that they observed three, rather than two subshell peaks, as shown in (Figure 7.6). We have investigated this discrepancy and attribute it to the use of a finite gaussian basis set. Adding additional basis functions to the core-augmented TZ2P basis set did not recover the extra subshell peak. However, a calculation using an extremely extensive *sp* even-tempered basis set did recover the peak, although such a basis set is not practical for molecular calculations, nor for determining the BD densities.

Of course, this basis set deficiency is amplified by the r^2 factor in the radial distribution. In Figure 7.8 we present the exchange-correlation charge (not the radial distribution) for the Ne atom, determined using the core-augmented TZ2P basis set. This plot closely resembles the charge of Liu *et al.* [226] It also demonstrates that the dominant structure in the charge lies relatively close to the nucleus, where the core-augmented TZ2P basis-set is adequate. We therefore regard this basis set as acceptable for studying the general structural features of the charge, although inadequate for reproducing the full fine structure in the radial distribution, as was found in the more accurate calculation of Liu *et al.* The core-augmented basis set is used in all the following calculations.

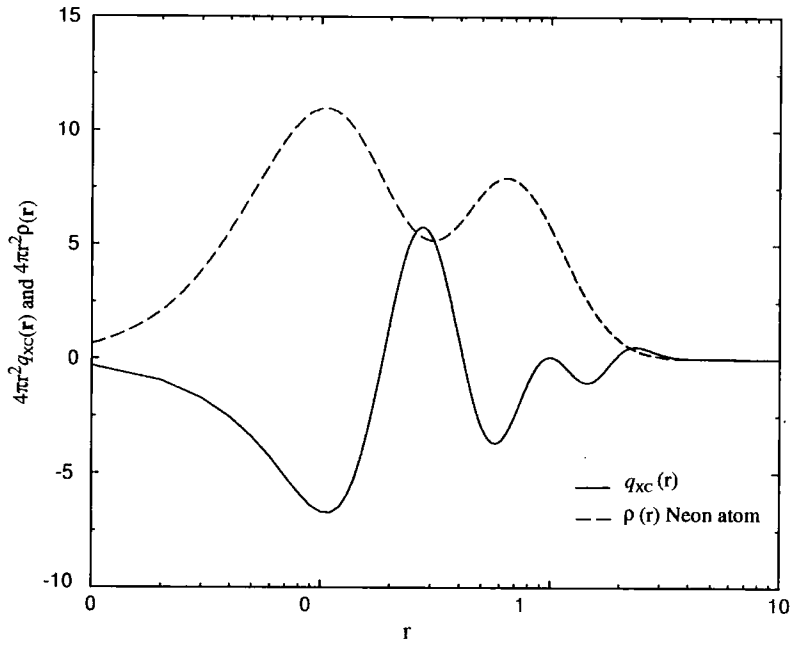

Figure 7.5: Comparison between $4\pi r^2 q_{\mathrm{XC}}(\mathbf{r})$ and $4\pi r^2 \rho(\mathbf{r})$ for Ne atom

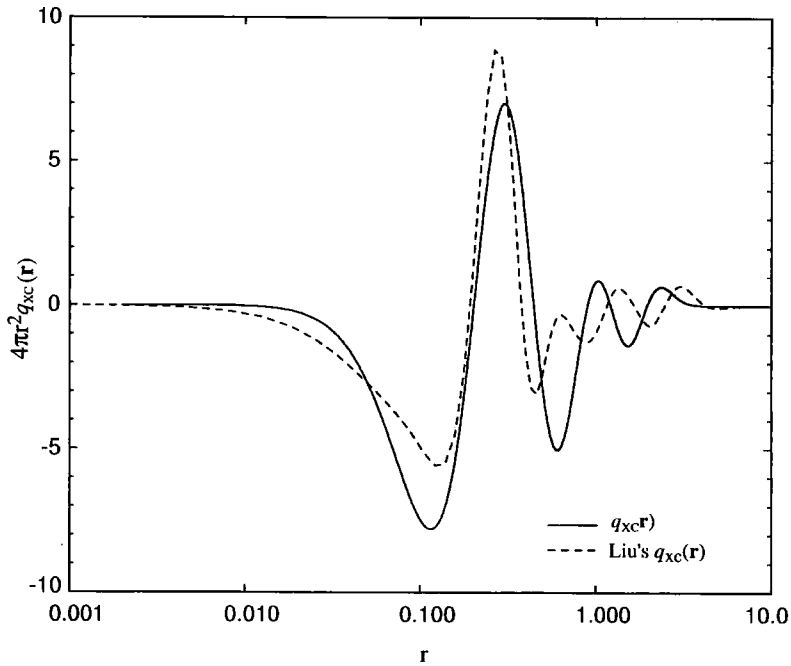

Figure 7.6: Comparison between $4\pi r^2 q_{\mathrm{XC}}(\mathbf{r})$ for Ne atom

7.3 Exchange-correlation charges and potentials

In Figures 7.7-7.11 we present the exchange-correlation charges for He, Ne, HF, CO and N_2, respectively. All nuclei lie on the z-axis. For all systems the distance scale on the plots covers 4 au although the charge scale varies. For the He atom in Figure 7.7 the charge is smooth and negative. Closer examination of the charge does not yield any more structural features. For the Ne atom in Figure 7.8 the charge is large and negative at the nucleus. As the distance from the nucleus increases the charge increases to a maximum and then decreases again. A detailed examination of the charge beyond that point highlights two additional minima and maxima, which is consistent with the structure in Figure 7.5; these additional features are not evident on the scale in Figures 7.7-7.11. The same structure is observed in the vicinity of the C, N, O and F nuclei in the molecular systems.

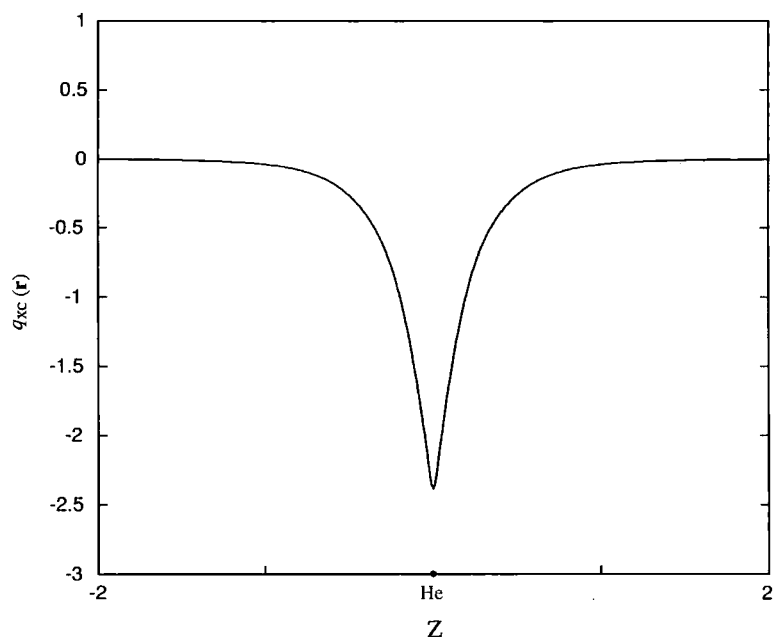

Figure 7.7: Exchange correlation charge $q_{\mathrm{XC}}(\mathbf{r})$ for the He atom, plotted along the z-axis.

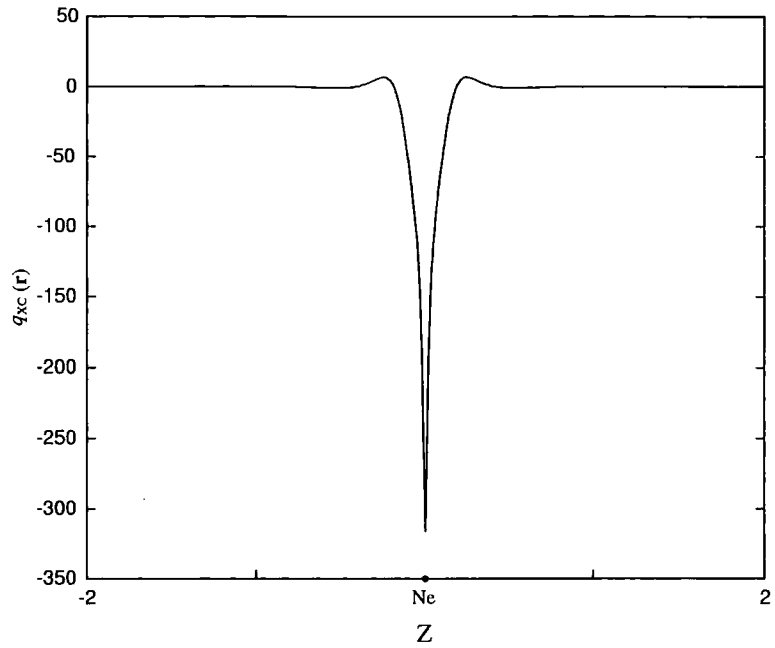

Figure 7.8: Exchange correlation charge $q_{\mathrm{XC}}(\mathbf{r})$ for the Ne atom, plotted along the z-axis.

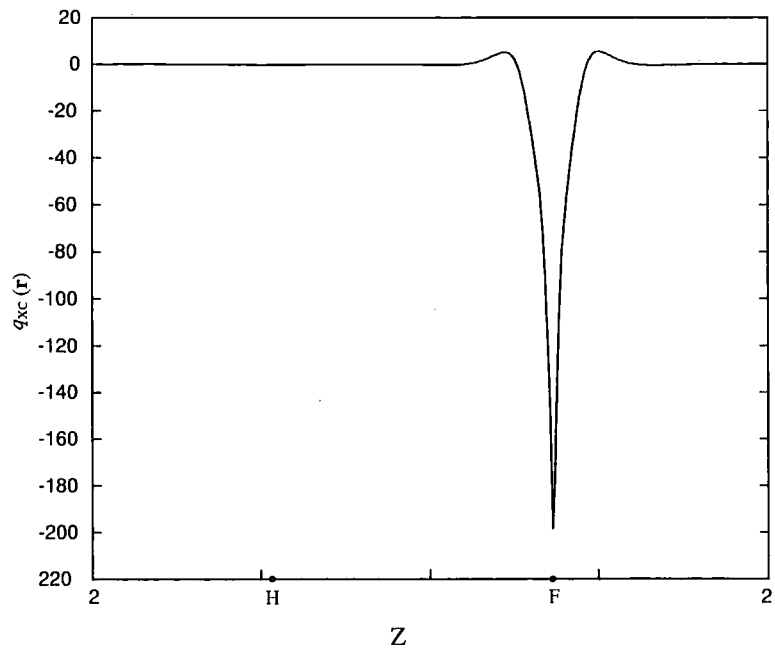

Figure 7.9: Exchange correlation charge $q_{\mathrm{XC}}(\mathbf{r})$ for the HF molecule, plotted along the z-axis.

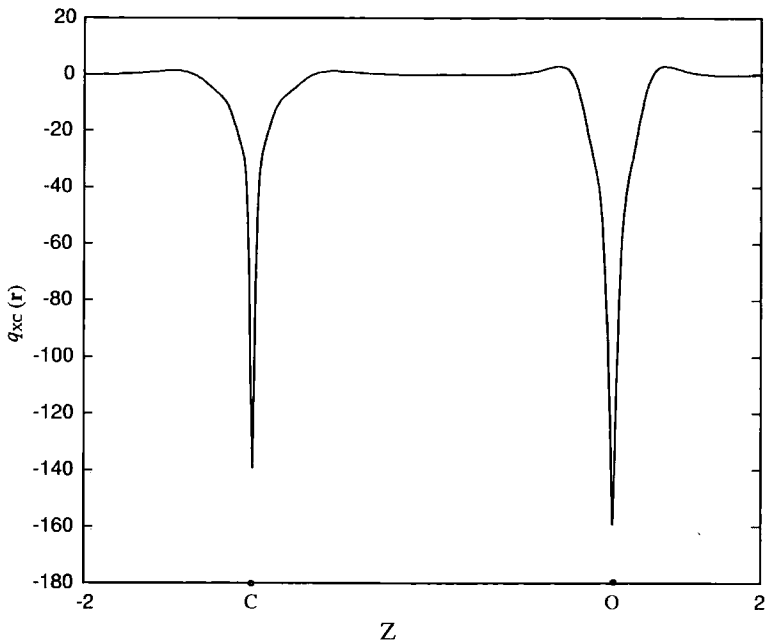

Figure 7.10: Exchange correlation charge $q_{\mathrm{xc}}(\mathbf{r})$ for the CO atom, plotted along the z-axis.

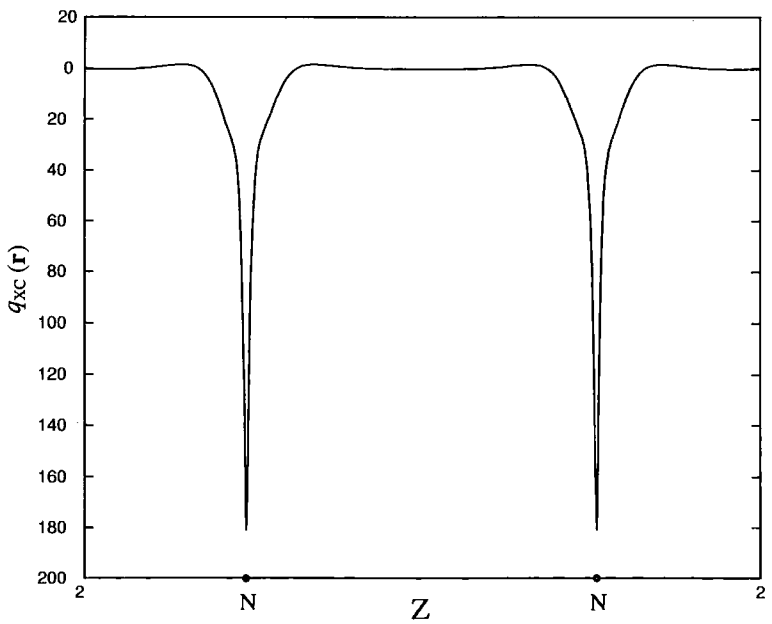

Figure 7.11: Exchange correlation charge $q_{\mathrm{xc}}(\mathbf{r})$ for the N_2 molecule, plotted along the z-axis.

The calculated charges at the nuclei vary significantly with atomic number; the values are also sensitive to the quality of the basis-set in the core region. The molecular charges closely resemble the sum of atomic charges, although for HF the influence of the hydrogen atom is barely visible on this scale.

The exchange-correlation charge and potential are related through Eq. (7.2) and so it is informative to consider these quantities on the same plot. In Figure 7.12 to 7.16 we compare the charge to the exchange-correlation potential. The potential decays much less rapidly with increasing distance from the nuclei and so the distance scale has been increased to 12 au for all systems. To further aid comparison, the same scale is also used throughout on the vertical axes. In order for the potential to be visible, this scale truncates the charge at -10 a.u. For the He atom in Figure 7.12 the exchange-correlation

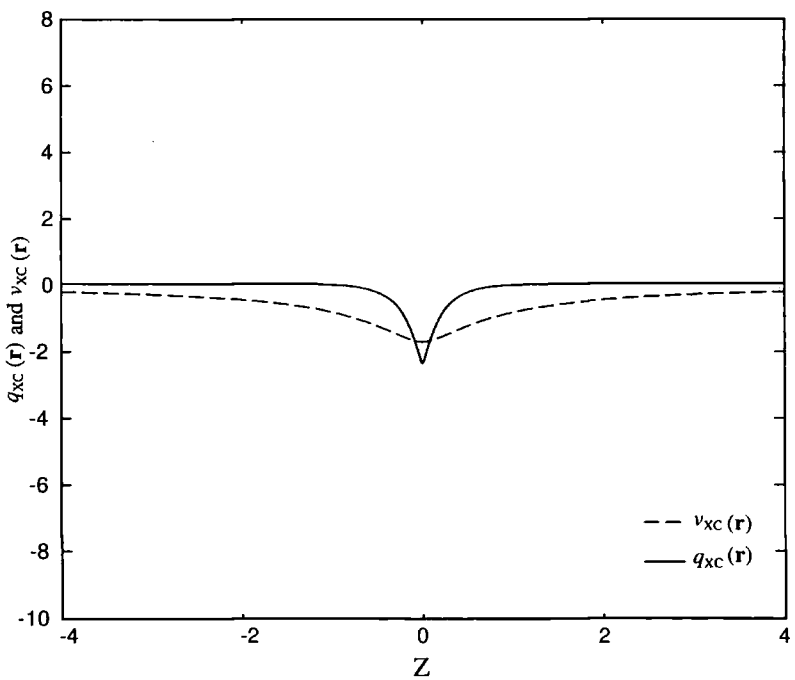

Figure 7.12: Comparison between $q_{\mathrm{xc}}(\mathbf{r})$ and $v_{\mathrm{xc}}(\mathbf{r})$ for He atom

charge is smooth and its associated potential shows no shell structure. In the vicinity of C, N, O, F and the Ne nuclei in Figures 7.13-7.16,the struc-

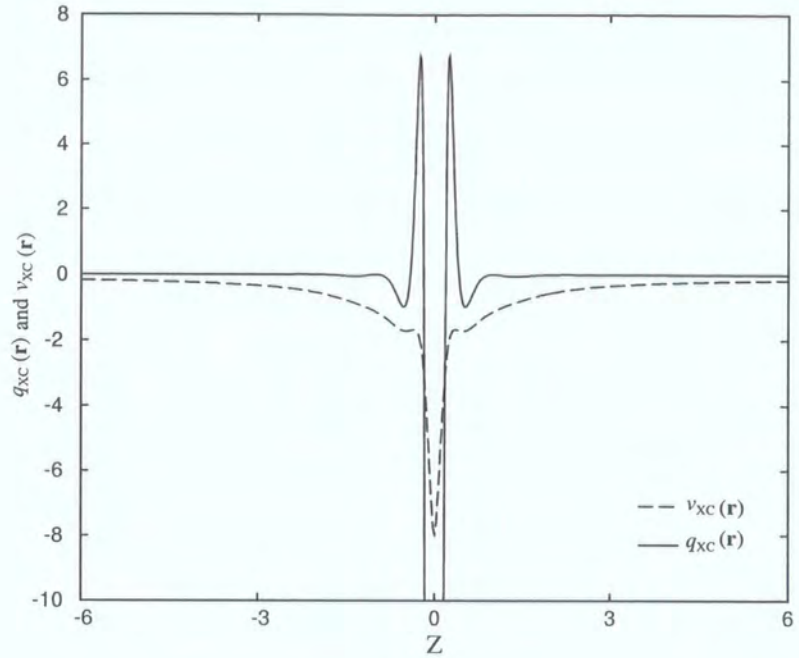

Figure 7.13: Comparison between $q_{\mathrm{XC}}(\mathbf{r})$ and $v_{\mathrm{XC}}(\mathbf{r})$ for Ne atom

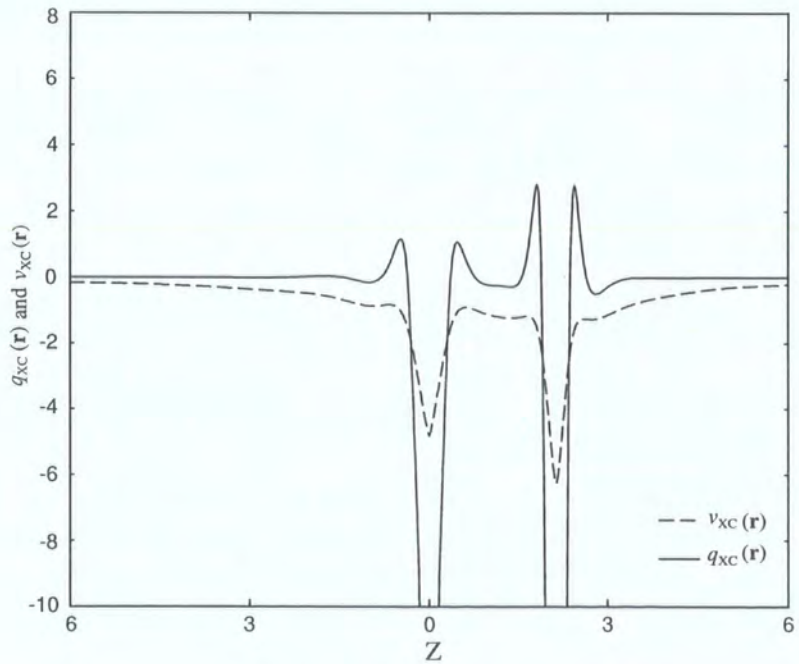

Figure 7.14: Comparison between $q_{\mathrm{XC}}(\mathbf{r})$ and $v_{\mathrm{XC}}(\mathbf{r})$ for CO molecule

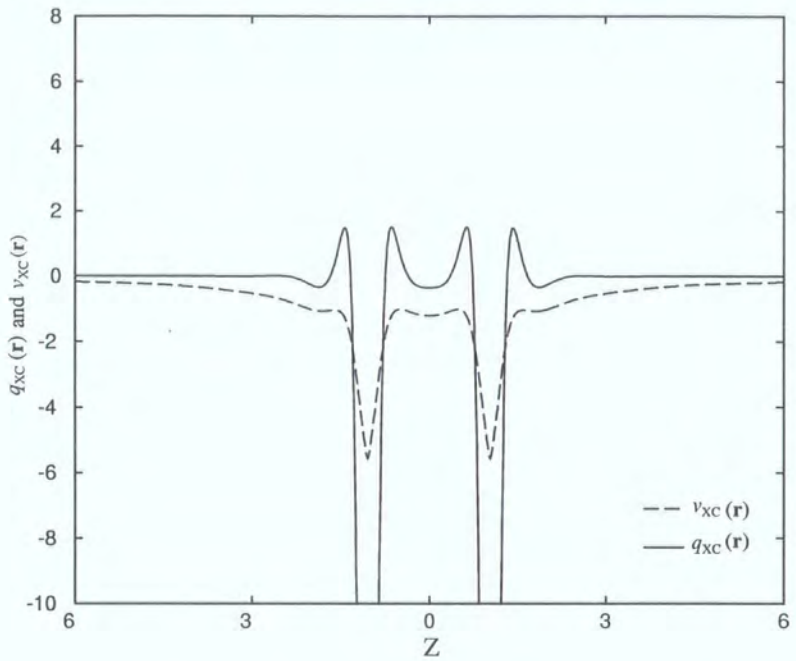

Figure 7.15: Comparison between $q_{\mathrm{XC}}(\mathbf{r})$ and $v_{\mathrm{XC}}(\mathbf{r})$ for N_2 molecule

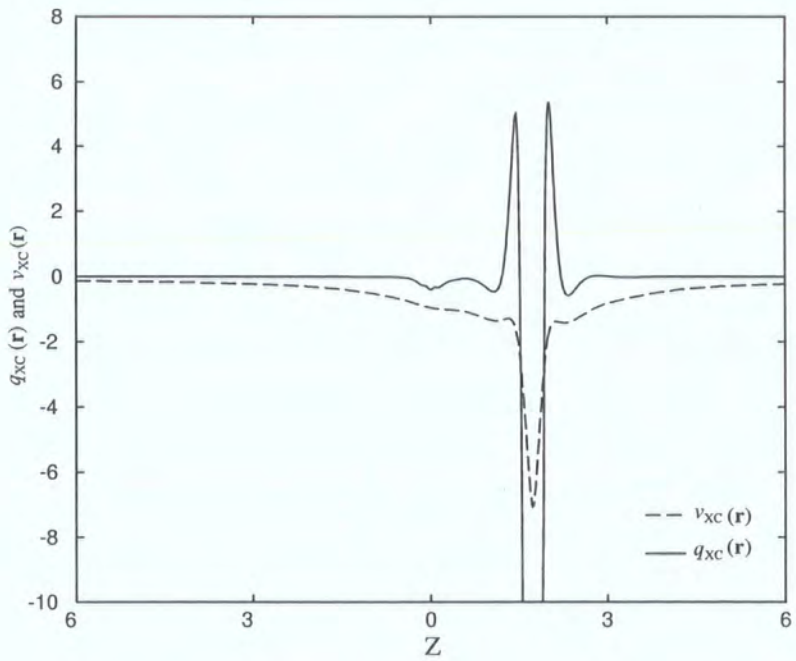

Figure 7.16: Comparison between $q_{\mathrm{XC}}(\mathbf{r})$ and $v_{\mathrm{XC}}(\mathbf{r})$ for HF molecule

ture of the charge is dominated by the characteristic maximum, whose value increases with nuclear charge. An additional minimum is also evident on this scale. The location of these turning points are closely related to those in the exchange-correlation potential. The minimum in the charge is close to the minimum in the potential while the maximum in the charge is close to the well known intershell maximum in the potential. The influence of the hydrogen atom in HF is now clearly visible and the C and O atoms in CO are easily distinguished.

In conclusion, we have demonstrated that the exchange-correlation charge of Liu *et al.* can be calculated for atomic and molecular systems in a gaussian basis set framework. Attention must be paid to the choice of basis set, particularly in the core region. The charges exhibit structure that is closely related to that of the associated exchange-correlation potential. The exchange-correlation charge may be a useful quantity to use in functional development. For example, an approximate charge could be determined by fitting to calculated values; the classical potential of this charge would then represent a new model potential.

Chapter 8

Concluding remarks

The low computational cost and high potential accuracy of Kohn-Sham density functional theory (DFT) makes it the most widely used method in quantum chemistry. Many approximations to the exchange-correlation energy functional have been proposed and further improvements are essential. In this thesis, new approaches to functional development have been investigated, with particular emphasis on the exchange-correlation potential.

A series of exchange-correlation functionals were developed by fitting solely to exchange-correlation potentials from *ab initio* densities. This new method reduced the empiricism and highlighted the spatial dependence of molecular properties. Our initial results demonstrated that the $\frac{1}{4}$ functional gave particularly accurate molecular structures. Its performance was subsequently investigated for a benchmark of theoretically challenging molecules containing sulphur atoms and a new benchmark of diatomic molecules, drawn evenly from the first three rows of the periodic table. To date, the $\frac{1}{4}$ functional provides the highest quality structural predictions of any DFT functional.

The quality of $\frac{1}{4}$ is also evident in its enhancement factor, which satisfies the uniform density scaling condition. By considering the variation of the enhancement factor as a function of spatial weighting and number of parameters, we determined a series of parameterized functionals, satisfying the uniform density scaling condition and the Lieb-Oxford bound. To the best

of our knowledge these are the first parameterised functionals to be determined by enforcing such conditions. We used these functionals to study the helium dimer, confirming the view of Zhang and Yang [79] that the degree of bonding in a van der Waals molecule is dependent on the behaviour of the enhancement factor.

We have also presented a series of investigations on hybrid functionals that, by far, are the most widely used in the chemical literature. We developed a new hybrid functional with 25% of exact exchange, which is believed to be an optimal amount. By comparison with existing functionals, the influence of exact exchange and parametrisation were investigated. We discussed chemical reaction barriers in terms of self-interaction errors. Contrary to the view of Yang [221], we did not observe any relationship between these two quantities. Attempts were also made to derive hybrid functionals directly from exchange-correlation potentials.

Finally, a new definition of the exchange-correlation charge (hole) was investigated, which is closely related to the exchange-correlation potential. The first molecular results were presented. Particular attention was paid to the basis set dependence and extrapolation schemes.

We regard the work presented in this thesis as a useful contribution to exchange-correlation functional development. The existence of the exact functional is a driving force for continuous work in this field.

Appendix A

Functional coefficients

A.1 GGA functionals

Table A.1: The optimal coefficients of the HCTH-93 functional in Chapter 3.

	HCTH-93
$c_{X\sigma,0}$	$+0.109320D+01$
$c_{C\sigma\sigma,0}$	$+0.222601D+00$
$c_{C\alpha\beta,0}$	$+0.729974D+00$
$c_{X\sigma,1}$	$-0.744056D+00$
$c_{C\sigma\sigma,1}$	$-0.338622D-01$
$c_{C\alpha\beta,1}$	$+0.335287D+01$
$c_{X\sigma,2}$	$+0.559920D+01$
$c_{C\sigma\sigma,2}$	$-0.125170D-01$
$c_{C\alpha\beta,2}$	$-0.115430D+02$
$c_{X\sigma,3}$	$-0.678549D+01$
$c_{C\sigma\sigma,3}$	$-0.802496D+00$
$c_{C\alpha\beta,3}$	$+0.808564D+01$
$c_{X\sigma,4}$	$+0.449357D+01$
$c_{C\sigma\sigma,4}$	$+0.155396D+01$
$c_{C\alpha\beta,4}$	$-0.447857D+01$

Table A.2: The optimal coefficients defining the eight functionals developed in Chapter 3 (Section 3.2.1).

	$p=0$	$p=\frac{1}{6}$	$p=\frac{2}{6}$	$p=\frac{3}{6}$
$c_{\mathrm{X}\sigma,0}$	$0.974312D+00$	$0.101596D+01$	$0.104650D+01$	$0.108613D+01$
$c_{\mathrm{C}\sigma\sigma,0}$	$0.416867D+01$	$0.310238D+01$	$0.252332D+01$	$0.109915D+01$
$c_{\mathrm{C}\alpha\beta,0}$	$-0.250375D+00$	$0.109983D+00$	$-0.301155D-01$	$-0.231284D+00$
$c_{\mathrm{X}\sigma,1}$	$-0.884163D+00$	$-0.353246D+00$	$-0.402034D+00$	$-0.591331D+00$
$c_{\mathrm{C}\sigma\sigma,1}$	$0.272896D+00$	$0.727410D-01$	$0.398635D-02$	$-0.312411D-01$
$c_{\mathrm{C}\alpha\beta,1}$	$0.704306D+01$	$0.499776D+01$	$0.402059D+01$	$0.289202D+01$
$c_{\mathrm{X}\sigma,2}$	$0.472730D+01$	$0.319535D+01$	$0.413262D+01$	$0.550849D+01$
$c_{\mathrm{C}\sigma\sigma,2}$	$-0.360448D+01$	$-0.245680D+01$	$-0.963358D+00$	$0.506605D+00$
$c_{\mathrm{C}\alpha\beta,2}$	$-0.193378D+02$	$-0.133929D+02$	$-0.146381D+02$	$-0.169763D+02$
$c_{\mathrm{X}\sigma,3}$	$-0.765091D+01$	$-0.468494D+01$	$-0.579274D+01$	$-0.795703D+01$
$c_{\mathrm{C}\sigma\sigma,3}$	$0.599030D+01$	$0.381560D+01$	$0.683386D+00$	$-0.261334D+01$
$c_{\mathrm{C}\alpha\beta,3}$	$0.224504D+02$	$0.130549D+02$	$0.159908D+02$	$0.225477D+02$
$c_{\mathrm{X}\sigma,4}$	$0.412021D+01$	$0.227487D+01$	$0.301936D+01$	$0.497917D+01$
$c_{\mathrm{C}\sigma\sigma,4}$	$-0.307960D+01$	$-0.194258D+01$	$0.473703D+00$	$0.322313D+01$
$c_{\mathrm{C}\alpha\beta,4}$	$-0.813538D+01$	$-0.298985D+01$	$-0.510287D+01$	$-0.109953D+02$
	$p=\frac{4}{6}$	$p=\frac{5}{6}$	$p=\frac{6}{6}$	$p=\frac{7}{6}$
$c_{\mathrm{X}\sigma,0}$	$0.112917D+01$	$0.115469D+01$	$0.116512D+01$	$0.116525D+01$
$c_{\mathrm{C}\sigma\sigma,0}$	$-0.107721D+01$	$-0.290969D+01$	$-0.398057D+01$	$-0.392143D+01$
$c_{\mathrm{C}\alpha\beta,0}$	$-0.338816D+00$	$-0.261572D+00$	$-0.853154D-01$	$0.192949D+00$
$c_{\mathrm{X}\sigma,1}$	$-0.828164D+00$	$-0.927528D+00$	$-0.842564D+00$	$-0.583033D+00$
$c_{\mathrm{C}\sigma\sigma,1}$	$-0.252626D-01$	$-0.710096D-01$	$-0.304755D+00$	$-0.110098D+01$
$c_{\mathrm{C}\alpha\beta,1}$	$0.202248D+01$	$0.248808D+01$	$0.152803D+01$	$-0.573335D+01$
$c_{\mathrm{X}\sigma,2}$	$0.633989D+01$	$0.624856D+01$	$0.501628D+01$	$0.251769D+01$
$c_{\mathrm{C}\sigma\sigma,2}$	$0.104930D+01$	$0.832740D+00$	$0.719667D-01$	$-0.914050D-01$
$c_{\mathrm{C}\alpha\beta,2}$	$-0.142922D+02$	$-0.840428D+01$	$0.765191D+01$	$0.508757D+02$
$c_{\mathrm{X}\sigma,3}$	$-0.931275D+01$	$-0.873072D+01$	$-0.477947D+01$	$0.381278D+01$
$c_{\mathrm{C}\sigma\sigma,3}$	$-0.427469D+01$	$-0.425342D+01$	$-0.271200D+01$	$-0.859723D+00$
$c_{\mathrm{C}\alpha\beta,3}$	$0.178096D+02$	$0.428368D+01$	$-0.336207D+02$	$-0.135475D+03$
$c_{\mathrm{X}\sigma,4}$	$0.671048D+01$	$0.680977D+01$	$0.337135D+01$	$-0.545906D+01$
$c_{\mathrm{C}\sigma\sigma,4}$	$0.486598D+01$	$0.510580D+01$	$0.397104D+01$	$0.207184D+01$
$c_{\mathrm{C}\alpha\beta,4}$	$-0.994702D+01$	$-0.135816D+01$	$0.259320D+02$	$0.101268D+03$

Table A.3: The optimal coefficients of the $\frac{1}{4}$ functional in Chapter 3 (Section 3.2.1).

	$p = \frac{1}{4}$
$c_{\mathrm{X}\sigma,0}$	$0.103161D + 01$
$c_{\mathrm{C}\sigma\sigma,0}$	$0.282414D + 01$
$c_{\mathrm{C}\alpha\beta,0}$	$0.821827D - 01$
$c_{\mathrm{X}\sigma,1}$	$-0.360781D + 00$
$c_{\mathrm{C}\sigma\sigma,1}$	$0.318843D - 01$
$c_{\mathrm{C}\alpha\beta,1}$	$0.456466D + 01$
$c_{\mathrm{X}\sigma,2}$	$0.351994D + 01$
$c_{\mathrm{C}\sigma\sigma,2}$	$-0.178512D + 01$
$c_{\mathrm{C}\alpha\beta,2}$	$-0.135529D + 02$
$c_{\mathrm{X}\sigma,3}$	$-0.495944D + 01$
$c_{\mathrm{C}\sigma\sigma,3}$	$0.239795D + 01$
$c_{\mathrm{C}\alpha\beta,3}$	$0.133820D + 02$
$c_{\mathrm{X}\sigma,4}$	$0.241165D + 01$
$c_{\mathrm{C}\sigma\sigma,4}$	$-0.876909D + 00$
$c_{\mathrm{C}\alpha\beta,4}$	$-0.317493D + 01$

Table A.4: The optimal coefficients defining the 21 solutions functional in Chapter 3 (Section 3.6)

	21 solns
$c_{\mathrm{X}\sigma,0}$	$0.104182D+01$
$c_{\mathrm{C}\sigma\sigma,0}$	$0.265144D+01$
$c_{\mathrm{C}\alpha\beta,0}$	$0.455703D+00$
$c_{\mathrm{X}\sigma,1}$	$-0.167199D+01$
$c_{\mathrm{C}\sigma\sigma,1}$	$-0.445538D-01$
$c_{\mathrm{C}\alpha\beta,1}$	$0.167602D+01$
$c_{\mathrm{X}\sigma,2}$	$-0.101615D+01$
$c_{\mathrm{C}\sigma\sigma,2}$	$-0.291895D+01$
$c_{\mathrm{C}\alpha\beta,2}$	$-0.438220D+01$
$c_{\mathrm{X}\sigma,3}$	$0.561694D+01$
$c_{\mathrm{C}\sigma\sigma,3}$	$0.556343D+01$
$c_{\mathrm{C}\alpha\beta,3}$	$0.558143D+01$
$c_{\mathrm{X}\sigma,4}$	$-0.265294D+01$
$c_{\mathrm{C}\sigma\sigma,4}$	$-0.386666D+01$
$c_{\mathrm{C}\alpha\beta,4}$	$-0.198258D+01$
$\rho^{\frac{14}{12}}u^1$	$-0.104768D+01$
$\rho^{\frac{14}{12}}u^2$	$0.164314D+01$
$\rho^{\frac{14}{12}}u^3$	$-0.830834D+00$
$\rho^{\frac{18}{12}}u^1$	$-0.685821D+00$
$\rho^{\frac{18}{12}}u^2$	$-0.470281D+01$
$\rho^{\frac{18}{12}}u^3$	$0.651618D+01$

Table A.5: The optimal coefficients defining the three new functionals in Chapter 3 (Table 3.13).

	$(\varphi^2_{\text{HOMO}} + \varphi^2_{\text{LUMO}})$	$(\rho + \varphi^2_{\text{LUMO}})$	$(\rho - \varphi^2_{1s})$
$c_{\text{X}\sigma,0}$	$0.106477D+01$	$0.115493D+01$	$0.115069D+01$
$c_{\text{C}\sigma\sigma,0}$	$0.209763D+01$	$-0.195336D+01$	$-0.463450D+01$
$c_{\text{C}\alpha\beta,0}$	$-0.399165D+00$	$-0.610625D+00$	$0.813898D-01$
$c_{\text{X}\sigma,1}$	$-0.336599D+00$	$-0.884509D+00$	$-0.899743D+00$
$c_{\text{C}\sigma\sigma,1}$	$-0.423024D+00$	$-0.348237D+00$	$-0.120517D-01$
$c_{\text{C}\alpha\beta,1}$	$0.866405D+00$	$0.258221D+01$	$0.210526D+01$
$c_{\text{X}\sigma,2}$	$0.455163D+01$	$0.589771D+01$	$0.624811D+01$
$c_{\text{C}\sigma\sigma,2}$	$0.152788D+01$	$0.732469D-01$	$0.192021D+00$
$c_{\text{C}\alpha\beta,2}$	$-0.919697D+01$	$-0.864182D+01$	$-0.614881D+01$
$c_{\text{X}\sigma,3}$	$-0.724211D+01$	$-0.765314D+01$	$-0.901121D+01$
$c_{\text{C}\sigma\sigma,3}$	$-0.415262D+01$	$-0.256219D+01$	$-0.383410D+01$
$c_{\text{C}\alpha\beta,3}$	$0.145455D+02$	$0.590401D+01$	$0.264955D+01$
$c_{\text{X}\sigma,4}$	$0.499948D+01$	$0.534050D+01$	$0.717413D+01$
$c_{\text{C}\sigma\sigma,4}$	$0.376190D+01$	$0.383473D+01$	$0.531043D+01$
$c_{\text{C}\alpha\beta,4}$	$-0.770806D+01$	$-0.155088D+01$	$-0.158246D-01$

Table A.6: The optimal coefficients defining the three new functionals satisfying the non-crossing and the uniform electron gas conditions in Chapter 5 (Section 5.2.1)

	$p = 0.34$	$p = 0.34$	$p = 0.43$
$c_{X\sigma,0}$	$0.100000D + 01$	$0.100000D + 01$	$0.100000D + 01$
$c_{C\sigma\sigma,0}$	$0.100000D + 01$	$0.100000D + 01$	$0.100000D + 01$
$c_{C\alpha\beta,0}$	$0.100000D + 01$	$0.100000D + 01$	$0.100000D + 01$
$c_{X\sigma,1}$	$0.779568D + 00$	$0.678965D + 00$	$0.506064D + 00$
$c_{C\sigma\sigma,1}$	$-0.385793D + 00$	$0.452972D + 00$	$0.772524D + 00$
$c_{C\alpha\beta,1}$	$-0.151157D + 01$	$-0.171526D + 01$	$-0.582344D + 00$
$c_{X\sigma,2}$		$0.313176D + 00$	$0.145464D + 01$
$c_{C\sigma\sigma,2}$		$-0.863747D + 00$	$-0.201001D + 01$
$c_{C\alpha\beta,2}$		$0.185275D + 00$	$-0.516839D + 01$
$c_{X\sigma,3}$			$-0.657216D + 00$
$c_{C\sigma\sigma,3}$			$0.124913D + 01$
$c_{C\alpha\beta,3}$			$0.382711D + 01$

Table A.7: The optimal coefficients defining the three new functionals satisfying the non-crossing condition without the uniform electron gas condition in Chapter 5 (Section 5.2.1)

	$p = 0.41$	$p = 0.39$	$p = 0.47$
$c_{X\sigma,0}$	$0.102881D + 01$	$0.103077D + 01$	$0.106618D + 01$
$c_{C\sigma\sigma,0}$	$0.228621D + 01$	$0.240022D + 01$	$0.175822D + 01$
$c_{C\alpha\beta,0}$	$0.802715D - 02$	$0.443503D - 01$	$-0.309004D + 00$
$c_{X\sigma,1}$	$0.635265D + 00$	$0.325937D + 00$	$-0.145188D + 00$
$c_{C\sigma\sigma,1}$	$-0.105151D + 01$	$-0.481403D + 00$	$0.520174D - 01$
$c_{C\alpha\beta,1}$	$-0.110869D + 01$	$0.468063D + 00$	$0.353805D + 01$
$c_{X\sigma,2}$		$0.859296D + 00$	$0.275753D + 01$
$c_{C\sigma\sigma,2}$		$-0.278335D + 00$	$-0.173733D + 01$
$c_{C\alpha\beta,2}$		$-0.200990D + 01$	$-0.126820D + 02$
$c_{X\sigma,3}$			$-0.169012D + 01$
$c_{C\sigma\sigma,3}$			$0.144247D + 01$
$c_{C\alpha\beta,3}$			$0.840624D + 01$

Table A.8: The optimal coefficients defining the two new functionals satisfying the Lieb-Oxford bound and the uniform electron gas conditions in Chapter 5 (Section 5.2.2)

	$p = 0.22$	$p = 0.38$
$c_{X\sigma,0}$	$0.100000D + 01$	$0.100000D + 01$
$c_{C\sigma\sigma,0}$	$0.100000D + 01$	$0.100000D + 01$
$c_{C\alpha\beta,0}$	$0.100000D + 01$	$0.100000D + 01$
$c_{X\sigma,1}$	$0.448878D + 00$	$0.673829D + 00$
$c_{C\sigma\sigma,1}$	$0.500058D - 01$	$0.292385D + 00$
$c_{C\alpha\beta,1}$	$-0.582402D + 00$	$-0.174515D + 01$
$c_{X\sigma,2}$		$0.530934D + 00$
$c_{C\sigma\sigma,2}$		$-0.703429D + 00$
$c_{C\alpha\beta,2}$		$-0.247287D + 00$

Table A.9: The optimal coefficients defining the two new functionals satisfying the Lieb-Oxford bound condition without the uniform electron gas condition in Chapter 5 (Section 5.2.2)

	$p = 0.44$	$p = 0.43$
$c_{\mathrm{X}\sigma,0}$	$0.103597D + 01$	$0.104136D + 01$
$c_{\mathrm{C}\sigma\sigma,0}$	$0.210252D + 01$	$0.216345D + 01$
$c_{\mathrm{C}\alpha\beta,0}$	$-0.685795D - 01$	$-0.772438D - 01$
$c_{\mathrm{X}\sigma,1}$	$0.620618D + 00$	$0.263864D + 00$
$c_{\mathrm{C}\sigma\sigma,1}$	$-0.112796D + 01$	$-0.542737D + 00$
$c_{\mathrm{C}\alpha\beta,1}$	$-0.122457D + 01$	$0.847730D + 00$
$c_{\mathrm{X}\sigma,2}$		$0.108915D + 01$
$c_{\mathrm{C}\sigma\sigma,2}$		$-0.209074D + 00$
$c_{\mathrm{C}\alpha\beta,2}$		$-0.282054D + 01$

Table A.10: The optimal coefficients defining the non-crossing HCTH-93 functional in Chapter 5 (Section 5.3)

	non-crossing HCTH-93
$c_{\mathrm{X}\sigma,0}$	$0.107785D + 01$
$c_{\mathrm{C}\sigma\sigma,0}$	$0.492391D + 00$
$c_{\mathrm{C}\alpha\beta,0}$	$0.622261D + 00$
$c_{\mathrm{X}\sigma,1}$	$-0.520534D + 00$
$c_{\mathrm{C}\sigma\sigma,1}$	$0.855389D - 01$
$c_{\mathrm{C}\alpha\beta,1}$	$0.370296D + 01$
$c_{\mathrm{X}\sigma,2}$	$0.471345D + 01$
$c_{\mathrm{C}\sigma\sigma,2}$	$0.199153D + 00$
$c_{\mathrm{C}\alpha\beta,2}$	$-0.149002D + 02$
$c_{\mathrm{X}\sigma,3}$	$-0.575813D + 01$
$c_{\mathrm{C}\sigma\sigma,3}$	$-0.184414D + 01$
$c_{\mathrm{C}\alpha\beta,3}$	$0.157020D + 02$
$c_{\mathrm{X}\sigma,4}$	$0.312925D + 01$
$c_{\mathrm{C}\sigma\sigma,4}$	$0.218076D + 01$
$c_{\mathrm{C}\alpha\beta,4}$	$-0.606736D + 01$

Appendix B

Functional coefficients

B.1 Hybrid functionals

Table B.1: The optimal coefficients defining the B97-3 functional in Chapter 6 (Section 6.1)

	B97-3
$c_{\mathrm{X}\sigma,0}$	$0.782710D+00$
$c_{\mathrm{C}\sigma\sigma,0}$	$0.583888D+00$
$c_{\mathrm{C}\alpha\beta,0}$	$0.104862D+01$
$c_{\mathrm{X}\sigma,1}$	$0.836109D-01$
$c_{\mathrm{C}\sigma\sigma,1}$	$-0.637128D+00$
$c_{\mathrm{C}\alpha\beta,1}$	$0.914349D+00$
$c_{\mathrm{X}\sigma,2}$	$0.159875D+01$
$c_{\mathrm{C}\sigma\sigma,2}$	$0.344944D+00$
$c_{\mathrm{C}\alpha\beta,2}$	$-0.685967D+01$

Table B.2: The optimal coefficients defining the five hybrid functionals developed in Chapter 6 (Section 6.4).

	$p = 0.21$	$p = 0.22$	$p = 0.23$
$c_{X\sigma,0}$	$0.740024D+00$	$0.742280D+00$	$0.744385D+00$
$c_{C\sigma\sigma,0}$	$0.171478D+01$	$0.168957D+01$	$0.166739D+01$
$c_{C\alpha\beta,0}$	$0.717198D+00$	$0.690113D+00$	$0.662486D+00$
$c_{X\sigma,1}$	$0.290147D+00$	$0.296841D+00$	$0.303004D+00$
$c_{C\sigma\sigma,1}$	$-0.152687D+00$	$-0.154569D+00$	$-0.157039D+00$
$c_{C\alpha\beta,1}$	$-0.501937D+00$	$-0.482845D+00$	$-0.464499D+00$
$c_{X\sigma,2}$	$-0.237640D-02$	$0.119607D-01$	$0.282230D-01$
$c_{C\sigma\sigma,2}$	$-0.418198D+00$	$-0.410399D+00$	$-0.401076D+00$
$c_{C\alpha\beta,2}$	$0.282656D+00$	$0.232128D+00$	$0.179684D+00$
	$p = 0.24$	$p = 0.25$	
$c_{X\sigma,0}$	$0.746356D+00$	$0.748209D+00$	
$c_{C\sigma\sigma,0}$	$0.164780D+01$	$0.163036D+01$	
$c_{C\alpha\beta,0}$	$0.634397D+00$	$0.605938D+00$	
$c_{X\sigma,1}$	$0.308602D+00$	$0.313595D+00$	
$c_{C\sigma\sigma,1}$	$-0.160096D+00$	$-0.163735D+00$	
$c_{C\alpha\beta,1}$	$-0.446577D+00$	$-0.428725D+00$	
$c_{X\sigma,2}$	$0.464109D-01$	$0.665032D-01$	
$c_{C\sigma\sigma,2}$	$-0.390277D+00$	$-0.378074D+00$	
$c_{C\alpha\beta,2}$	$0.124923D+00$	$0.674690D-01$	

Appendix C

Publications and Conferences

C.1 Publications

Atomic and molecular exchange-correlation charges in Kohn-Sham theory. Phys. Chem. Chem. Phys. **2**, 3739 (2000)

Emphasizing the exchange-correlation potential in functional development. J. Chem. Phys. **114**, 3958 (2001).

Diatomic bond lengths and vibrational frequencies: assessment of recently developed exchange-correlation functionals. Chem. Phys. Lett. **360**, 38 (2002)

C.2 Conferences and Poster Presentations

University of Cambridge, 23rd June 2000

Afternoon of Computational Chemistry

University of Durham, 23-25th April 2001

Application performance optimisations on Sun Systems. SunTune Training

Course

San Lorenzo de El Escorial, Madrid, 10-14th September 2001

Poster presentation at the *9th International Conference on the applications of the DFT in Chemistry and Physics DFT 2001*

University of Nottingham, 31st July-2nd August 2002

Poster presentation winner at the international meeting *Exploring Modern Computational Chemistry*

Jesus College, University of Oxford, 18-23rd August 2002

Poster presentation at the *Molecular Physics and Quantum Chemistry Summer School*

Bibliography

[1] E. Schrödinger, Ann. Phys. **79**, 361 (1926)

[2] E. Schrödinger, Ann. Phys. **80**, 437 (1926)

[3] E. Schrödinger, Ann. Phys. **81**, 109 (1926)

[4] M. Born and J. R. Oppenheimer, Ann. Phys. **84**, 457 (1927)

[5] D. R. Hartree, Proc. Camb. Philos. Soc. **24**, 89 (1928)

[6] V. Fock, Z. Physik **61**, 126 (1930)

[7] J. C. Slater, Phys. Rev. **81**, 385 (1951)

[8] E. Fermi, Rend. Accad. Lincei **6**, 602 (1927)

[9] M. A. Buijse and E. J. Baerends, *Electronic density functional theory of molecules, clusters and solids*, (D. E. Ellis Ed. Kluwer Academic Publishers Dordrecht, The Netherlands, 1995), page 1

[10] T. A. Koopmans, Physica **1**, 104 (1934)

[11] J. A. Pople and R. K. Nesbet, J. Chem. Phys. **22**, 571 (1954)

[12] C. C. J. Roothan, Rev. Mod. Phys. **23**, 69 (1951)

[13] G. G. Hall, Proc. Roy. Soc. **A205**, 541 (1951)

[14] S. F. Boys, Proc. Roy. Soc. **A200**, 542 (1958)

[15] J. C. Slater, Phys. Rev. **36**, 57 (1930)

[16] E. Clementi and D. R. Davie, J. Comp. Phys. **1**, 223 (1966)

[17] J. L. Whitten, J. Chem. Phys **44**, 359 (1966)

[18] H. Takega, S. Huzinaga and K. O-ohata, J. Phys. Soc. Jpn. **21**, 2313 (1966)

[19] D. Feller and E. R. Davidson, Rev. Comput. Chem **1**, 1 (1990)

[20] T. Helgaker and P. R. Taylor, *Modern Electronic Structure Theory, Part II*, (Yarkony D. R. World Scientific Singapore, 1995)

[21] S. F. Boys and F. Bernardi, Mol. Phys. **19**, 553 (1970)

[22] P. O. Löwdin, Adv. Chem. Phys. **2**, 207 (1959)

[23] N. C. Handy and A. J. Cohen, Mol. Phys. **99**, 403 (2001)

[24] M. Cook and M. Karplus, J. Phys. Chem. **91**, 31 (1987)

[25] A. Szabo and N. S. Ostlund, *Modern Quantum Chemistry: Introduction to advanced electronic structure theory*, (MacMillan Publishing Co., New York, 1996)

[26] M. A. Buijse, *Electron Correlation. Fermi and Coulomb holes, Dynamical and Non-Dynamical correlation.*, (Ph.D. Thesis, Vrije Universiteit, 1991)

[27] A. J. Cohen and N. C. Handy, Mol. Phys. **99**, 607 (2001)

[28] C. Møller and M. S. Plesset, Phys. Rev. **46**, 618 (1934)

[29] J. S. Binkley and J. A. Pople, J. Am. Chem. Soc. **102**, 939 (1980)

[30] R. D. Amos, J. S. Andrews, N. C. Handy and P. J. Knowles, Chem. Phys. Lett. **185**, 256 (1991)

[31] T. H. Dunning Jr. and K. A. Peterson, J. Chem. Phys. **108**, 4761 (1998)

[32] F. Coester, Nucl. Phys. **7**, 421 (1958). F. Coester and H. Kümmel, Nucl. Phys. **17**, 477 (1960). J. Čižek and J. Paldus, Physica Scripta **21**, 251 (1980)

[33] J. Čižek, J. Chem. Phys. **45**, 4256 (1966). J. Čižek, Adv. Chem. **14**, 35 (1969)

[34] R. J. Bartlett, J. Phys. Chem. **93**, 1697 (1989)

[35] G. E. Scuseria and T. J. Lee, J. Chem. Phys. **93**, 5851 (1990)

[36] K. Raghavachari, J. A. Pople, E. S. Replogle and M. Head-Gordon, J. Phys. Chem. **94**, 5579 (1990)

[37] R. J. Bartlett, J. D. Watts, S. A. Kucharsky and J. Noga, Chem. Phys. Lett. **165**, 513 (1990)

[38] K. A. Brueckner, Phys. Rev. **96**, 508 (1954)

[39] J. F. Stanton, J. Gauss and R. J. Bartlett, J. Chem. Phys. **97**, 5554 (1992)

[40] T. J. Lee, R. Kobayashi, N. C. Handy and R. D. Amos, J. Chem. Phys. **96**, 8931 (1992)

[41] E. R. Davidson, *Reduced density matrices in quantum chemistry*, (Academic Press, New York, 1976)

[42] E. Bright-Wilson *Structural Chemistry and Molecular Biology*, (Freeman, San Francisco, 1968), pages 753760

[43] L. H. Thomas, Proc. Camb. Phil. Soc. **23**, 542 (1927). Reprinted in 1975

[44] E. Fermi, Rend. Accad. Lincei **6**, 602 (1927)

[45] E. Fermi, Z. Phys. **48**, 73 (1928)

[46] E. Fermi, Rend. Accad. Lincei **7**, 117 (1928)

[47] P. A. M. Dirac, Proc. Camb. Phil. Soc. **26**, 376 (1930)

[48] E. Teller, Rev. Mod. Phys. **34**, 627 (1962)

[49] P. Hohenberg and W. Kohn, Phys. Rev. **136**, B864 (1964)

[50] W. Kohn and L. J. Sham, Phys. Rev. **140**, A1133 (1965)

[51] W. Kohn, A. D. Becke and R. G. Parr, J. Phys. Chem. **100**, 12974 (1996)

[52] E. J. Baerends and O. V. Gritsenko, J. Phys. Chem. A **101**, 5383 (1997)

[53] R. Stowasser and R. Hoffmann, J. Am. Chem. Soc. **121**, 3414 (1999)

[54] E. J. Baerends, Theo. Chem. Acc. **103**, 0265 (1999)

[55] J. P. Perdew, R. G. Parr, M. Levy and J. L. Balduz, Phys. Rev. Lett. **49**, 1691 (1982)

[56] C. O. Almbladh and U. Von Barth, Phys. Rev. B **31**, 3231 (1985)

[57] J. Katriel and E. R. Davidson, Proc. Natl. Acad. Sci. USA **77** 4403 (1980)

[58] A. Savin, C. J. Umrigar and X. Gonze, Chem. Phys. Lett. **288**, 391 (1998)

[59] S. A. C. McDowell, R. D. Amos and N. C. Handy, Chem. Phys. Lett. **235**, 1 (1995)

[60] M. E. Casida, C. Jamorski, K. C. Casida and D. R. Salahub, J. Chem. Phys. **108**, 4439 (1998)

[61] J. P. Perdew and M. Levy, Phys. Rev. Lett. **51**, 1884 (1983)

[62] J. P. Perdew and K. Burke, Int. J. Quantum Chem. **57**, 309 (1996)

[63] D. J. Tozer and N. C. Handy, J. Chem. Phys. **108**, 2545 (1998)

[64] D. J. Tozer and N. C. Handy, J. Chem. Phys. **109**, 10180 (1998)

[65] M. Levy, J. P. Perdew and V. Sahni, Phys. Rev. A **30**, 2745 (1984)

[66] C. O. Almbladh and A. P. Pedroza, Phys. Rev. A **29**, 2322 (1984)

[67] À. Nagy, J. Phys. B **26**, 43 (1993); Philos. Mag. B **69**, 779 (1994)

[68] P. Süle, O. V. Gritsenko, À. Nagy and E. J. Baerends, J. Chem. Phys. **103**, 10085 (1995)

[69] F. Arysetiawan and M. J. Stott, Phys. Rev. B **38**, 2974 (1988); J. Chen and M. J. Stott, Phys. Rev. A **44**, 2816 (1991); J. Chen, R. O. Esquivel and M. J. Stott, Philos. Mag. B **69**, 1001 (1994)

[70] A. Görling and M. Ernzerhof, Phys. Rev. A **51**, 4501 (1995)

[71] O. V. Gritsenko, R. van Leeuwen and E. J. Baerends, Phys. Rev. A **52**, 1870 (1995)

[72] Q. Zhao, R. C. Morrison and R. G. Parr, Phys. Rev. A **50**, 2138 (1994)

[73] M. Levy and J. Perdew, *Density Functional Methods in Physics*, (R. M. Dreizler and J. da Providencia, Plenum, New York, 1985), pp. 11-30

[74] E. Fermi and E. Amaldi, Mem. R. Acad. Italia **6**, 117 (1934)

[75] D. J. Tozer, V. Ingamells and N. C. Handy, J. Chem. Phys. **105**, 9200 (1996)

[76] J. P. Perdew and A. Zunger, Phys. Rev. B **23**, 5048 (1981)

[77] J. P. Perdew and M. Ernzerhof, *Electron density functional theory. Recent Progress and new directions*, (J. F. Dobson, G. Vignale and M. P. Das editors, Plenum Press, New York, 1998)

[78] R. Merkle, A. Savin and H. Preuss, J. Chem. Phys. **97**, 9216 (1992)

[79] Y. Zhang, W. Pan and W. Yang, J. Chem. Phys. **107**, 7921 (1997)

[80] F. Bloch, Z. Physik **57**, 545 (1929)

[81] D. M. Ceperley and B. J. Alder, Phys. Rev. Lett. **45**, 566 (1980)

[82] S. J. Vosko, L. Wilk and M. Nusair, Can. J. Phys. **58**, 1200 (1980)

[83] J. P. Perdew and Y. Wang, Phys. Rev. B **45**, 13244 (1992)

[84] M. Rasolt and H. L. Davis, Phys. Lett. A **86**, 45 (1981)

[85] M. Rasolt and D. J. W. Geldart, Phys. Rev. B **34**, 1325 (1986)

[86] L. Kleinman and S. Lee, Phys. Rev. B **37**, 4634 (1988)

[87] D. C. Langreth and S. H. Vosko, Adv. Quantum Chem. **21**, 175 (1990)

[88] J. P. Perdew and Y. Wang, Phys. Rev. B **33**, 8800 (1986); Erratum: Phys. Rev. B **40** 3399 (1989)

[89] A. D. Becke, Phys. Rev. A **38**, 3098 (1988)

[90] J. P. Perdew, *Electronic Structure of Solids* P. Ziesche, H. Eschrig (eds.), Akademie Verlag, Berlin.

[91] K. Burke, J. P. Perdew and Y. Wang, *Electronic Density Functional Theory. Recent Progress and New Directions*, (J. F. Dobson, G. Vignale, M. P. Das editors, Plenum Press, New York).

[92] J. P. Perdew, K. Burke and M. Ernzerhof, Phys. Rev. Lett. **77**, 3865 (1996). Erratum: Phys. Rev. Lett. **78**, 1396 (1997)

[93] J. P. Perdew, Phys. Rev. B. **33**, 8822 (1986)

[94] C. Lee, W. Yang and R. G. Parr, Phys. Rev. B **37**, 785 (1988)

[95] R. Colle and O. Salvetti, Theor. Chem. Acta **37**, 329 (1975)

[96] K. Molawi, A. J. Cohen and N. C. Handy, Int. J. Quantum Chem. **89**, 86 (2002)

[97] F. A. Hamprecht, A. J. Cohen, D. J. Tozer and N. C. Handy, J. Chem. Phys. **109**, 6264 (1998)

[98] A. D. Becke, J. Chem. Phys. **107**, 8554 (1997)

[99] A. D. Boese, N. L. Doltsinis, N. C. Handy and M. Sprik, J. Chem. Phys. **112**, 1670 (2000)

[100] A. D. Boese, N. C. Handy, J. Chem. Phys. **114**, 5497 (2001)

[101] J. Perdew, S. Kurth, A. Zupan and P. Blaha, Phys. Rev. Lett. **82**, 2544 (1999).

[102] J. Perdew, J. A. Chevary, S. H. Vosko, K. A. Jackson, M. R. Pederson, D. J. Singh and C. Fiolhais, Phys. Rev. B **46**, 6671 (1992)

[103] J. P. Perdew, K. Burke, Int. J. Quantum Chem. **19** 427 (1996)

[104] M. Levy and J. Perdew, Phys. Rev. A **32**, 2010 (1985)

[105] E. H. Lieb and S. Oxford, Int. J. Quantum Chem. **19**, 427 (1981)

[106] G. K.-L. Chan and N. C. Handy, Phys. Rev. A **59**, 3075 (1999)

[107] A. D. Becke, J. Chem. Phys. **98**, 1372 (1993)

[108] A. D. Becke, J. Chem. Phys. **98**, 5648 (1993)

[109] P. J. Stevens, J. P. Devlin, C. F. Chabalowsi and M. J. Frisch, J. Phys. Chem. **98**, 11623 (1994)

[110] A. D. Becke, J. Chem. Phys. **107**, 8554 (1997)

[111] P. J. Wilson, T. J. Bradley and D. J. Tozer, J. Chem. Phys. **115**, 9233 (2001)

[112] C. Adamo and V. Barone, J. Chem. Phys. **110**, 6158 (1999)

[113] M. Ernzerhof and G. E. Scuseria, J. Chem. Phys. **110**, 5029 (1999)

[114] H. Stoll, C. M. E. Pavlidou and H. Preuss, Theor. Chem. Acc. **49**, 143 (1978); H. Stoll, E. Golka and H. Preuss, *ibid* **55**, 29 (1980)

[115] N. C. Handy and D. J. Tozer, Mol. Phys. **94**, 707 (1998)

[116] R. van Leeuwen and E. J. Baerends, Phys. Rev. A **51**, 170 (1995)

[117] D. J. Tozer, J. Chem. Phys. **112**, 3507 (2000)

[118] R. van Leeuwen and E. J. Baerends, Phys. Rev. A **49**, 2421 (1994)

[119] P. R. T. Schipper, O. V. Gritsenko, S. J. A. van Gisbergen and E. J. Baerends, J. Chem. Phys. **112**, 1344 (2000)

[120] M. E. Casida, K. C. Casida and D. R. Salahub, Int. J. Quantum Chem. **70**, 933 (1998)

[121] T. H. Dunning, J. Chem. Phys. **55**, 716 (1971); S. Huzinaga, *ibid* **42**, 1293 (1965)

[122] D. J. Tozer, N. C. Handy and W. H. Green, Chem. Phys. Lett. **273**, 183 (1997)

[123] D. J. Tozer and N. C. Handy, J. Phys. Chem. **102**, 3162 (1998)

[124] R. D. Amos, I. L. Alberts, J. S. Andrews *et al*, CADPAC6.5 The Cambridge Analytic Derivatives Package (1998)

[125] C. J. Umrigar and X. Gonze, Phys. Rev. A **50**, 3827 (1994)

[126] A. J. Sadlej, Collect. Czech. Chemm. Commun. **53**, 1995 (1988); Theor. Chem. Acta **79**, 123 (1991)

[127] A. J. Russell and M. A. Spackman, Mol. Phys. **84**, 1239 (1995); **90**, 251 (1997)

[128] S. Huzinaga, *Approximate Atomic Functions*, (University of Alberta, Edmonton, 1971)

[129] P. J. Wilson, R. D. Amos and N. C. Handy, Chem. Phys. Lett. **312**, 475 (1999)

[130] T. Helgaker, P. J. Wilson, R. D. Amos and N. C. Handy, J. Chem. Phys. **113**, 2983 (2000)

[131] K. P. Huber and G. Herzberg, *Constants of diatomic molecules*, (Van Nostrand Reinhold, New York, 1979)

[132] H. Bredohl, I. Dubois, Y. Houbrechts and P. Nzohabonayo, J. Mol. Spectrosc. **112**, 430 (1985)

[133] J. B. Burkholder, P. D. Hammer, C. J. Howard and A. R. W. McKellar, J. Mol. Spectrosc. **118**, 471 (1986)

[134] R. P. Tuckett, A. R. Dale, D. M. Jaffey, P. S. Jarret and T. Kelly, Mol. Phys. **49**, 475 (1983)

[135] A. J. H. Wachters, J. Chem. Phys. **52**, 1033 (1970)

[136] R. H. Jackson, J. Chem. Soc. **1962**, 4585 (1962); K. C. Kim and G. M. Campbell, J. Mol. Struct. **129**, 263 (1985)

[137] R. R. Smardzewski and W. B. Fox, J. Chem. Phys. **60**, 2980 (1974)

[138] T. Tanaka and Y. Morino, J. Mol. Spectrosc. **33**, 538 (1970); A. Barber, C. Secroun and S. A. Clough, *ibid.* **49**, 171 (1974)

[139] K. Yamada and E. Hirota, J. Chem. Phys. **80**, 4694 (1984)

[140] A. Jost, B. Rees and W. B. Yelon, Acta Crystallogr., Sect. B: Struct. Crystallogr. Cryst. Chem. **31**, 2649 (1975)

[141] B. Rees and A. Mitschler, J. Am. Chem. Soc. **98**, 7918 (1976)

[142] L. Hedberg, T. Iijima and K. Hedberg, J. Chem. Phys. **70**, 3224 (1979)

[143] D. Braga, F. Grepioni and A. G. Orpen, Organometallics **12**, 1481 (1993)

[144] C. V. Caillie and R. D. Amos, Chem. Phys. Lett. **328**, 446 (2000)

[145] M. A. Spackman, J. Chem. Phys. **94**, 1288 (1991)

[146] P. A. M. Dirac, Proc. Cambridge Philos. Soc. **26**, 376 (1930); S. J. Vosko, L. Wilk and M. Nusair, Can. J. Phys. **58**, 1200 (1980)

[147] D. J. Tozer, J. Chem. Phys. **104**, 4166 (1996)

[148] S. A. C. McDowell, R. D. Amos and N. C. Handy, Chem. Phys. Lett **235**, 1 (1995)

[149] N_2: S. B. Ben-Shlomo and U. Kaldor, J. Chem. Phys. **92**, 3680 (1990); H_2CO: D. J. Clouthier and D. A. Ramsay, Annu. Rev. Phys. Chem. **34**, 31 (1983); S. Taylor, D. G. Wilden and J. Comer, Chem. Phys. **70**, 291 (1982); C_6H_6: J. Lorentzon, P. -A. Malmquist, M. Fulscher and B. O. Roos, Theo. Chim. Acta **91**, 91 (1995)

[150] M. E. Casida, C. Jamorski, K. C. Casida and D. R. Salahub, J. Chem. Phys. **108**, 4439 (1998)

[151] W. Koch and M. C. Holthausen, *A Chemist's Guide to Density Functional Theory* (Wiley-VCH, Weinheim, 1999)

[152] M. Bühl, M. Kaupp, O. L. Malkina and V. G. Malkin, J. Comput. Chem. **20**, 91 (1999)

[153] P. J. Wilson, R. D. Amos and N. C. Handy, Mol. Phys. **97**, 757 (1999)

[154] P. J. Wilson and D. J. Tozer, J. Chem. Phys. **116** 10139 (2002)

[155] P. J. Wilson, R. D. Amos and N. C. Handy, Phys. Chem. Chem. Phys. **2**, 187 (2000)

[156] P. J. Wilson, R. D. Amos and N. C. Handy, J. Mol. Struct: Theochem **506**, 335 (2000)

[157] T. Keal and D. J. Tozer, Unpublished Results

[158] M. J. Allen and D. J. Tozer, J. Chem. Phys. **113**, 5185 (2000)

[159] J. A. Altmann, N. C. Handy and V. E. Ingamells, Int. J. Quantum Chem. **57**, 533 (1996)

[160] J. A. Altmann, N. C. Handy and V. E. Ingamells, Mol. Phys. **92**, 339 (1997)

[161] J. A. Altmann and N. C. Handy, Phys. Chem. Chem. Phys. **1**, 5529 (1999)

[162] T. H. Dunning Jr., J. Chem. Phys. **90**, 1007 (1989)

[163] D. E. Woon and T. H. Dunning Jr., J. Chem. Phys. **98**, 1358 (1993)

[164] G. Herzberg, *Molecular Spectra and Molecular Structure, Infrared and Raman Spectra of Polyatomic Molecules*, (Van Nostrand, New York, 1945) Vol. II

[165] T. H. Edwards, N. K. Moncur and L. E. Snyder, J. Chem. Phys. **46**, 2139 (1967)

[166] G. Winnewisser and K. M. T. Yamada, Vib. Spectrosc. **1**, 263 (1991)

[167] N. J. Lucas and J. G. Smith, J. Mol. Spectrosc. **43**, 327 (1972)

[168] A. Kaldor and A. G. Maki, J. Mol. Spectrosc. **45**, 123 (1973)

[169] G. Blanquet, J. Walrand and C. P. Courtroy, An. Soc. Bruxelles **88**, 87 (1974)

[170] D. R. Johnson, F. J. Lovas and W. H. Kirchhoff, J. Phys. Chem. Ref. Data **1**, 1001 (1972)

[171] Y. Morino and C. Matsumuta, Bull. Chem. Soc. Jpn. **40**, 1095 (1967)

[172] L. R. Pierce and M. Hayashi, J. Chem. Phys. **35**, 479 (1961)

[173] Y. Endo, S. Saito, E. Hirota and T. Chikaraishi, J. Mol. Spectrosc. **77**, 222 (1979)

[174] M. W. Chase, C. A. Davies, J. R. Downey, D. R. Frurip, R. A. Macdonald and N. Syverud, *JANAFF Thermochemical Tables*, 3rd Edn.; J. Phys. Chem. Ref. data **14**, (1985) Suppl. 1

[175] D. C. McKean and P. McQuillang, J. Mol. Struct. **49**, 275 (1978)

[176] J. E. Ellwood, D. Steele and D. Gerrard, Spectrochim. Acta A **50**, 913 (1994)

[177] S. D. Ross, *Inorganic and Raman Spectra*, (MacGraw-Hill, New York, 1972)

[178] K. Nakamoto, *Infrared and Raman Spectra of Inorganic and Coordination Compounds*, (Wiley, New York, 1986)

[179] R. D. Brown and G. P. Pez, Spectrochim. Acta A **26**, 1375 (1970)

[180] J. Phys. Chem. Ref. Data, **6**, 1011 (1977)

[181] R, J. Glinski, C. D. Taylor and F. W. Kutzler, J. Phys. Chem. **94**, 6196 (1990)

[182] W. B. Person, J. S. Kwiatkowski and R. J. Bartlett, J. Mol. Struct. **157**, 237 (1987)

[183] N. P. Machara and B. S. Ault, J. Mol. Struct. **172**, 129 (1988)

[184] L. Andrews, T. C. McInnis and Y. Hannachi, J. Chem. Phys. **96**, 4248 (1992)

[185] R. R. Smardzewski and M. C. Lin, J. Chem. Phys. **66**, 3197 (1977)

[186] M. A. Spackman, J. Phys. Chem. **93**, 7594 (1989)

[187] M. A. Spackman, J. Chem. Phys. **94**, 1288 (1991)

[188] M. P. Bogaard, A. D. Buckingham, R. K. Pierens and A. H. J. White, J. Chem. Soc. Faraday Trans I **74**, 3008 (1978)

[189] F. Engelke, G. Ennen, K. H. Meiwes, Chem. Phys. **66**, 391 (1982)

[190] V. Bednarska, I. Jackowska, W. Jastrzebsky, P. Kowalczyk, J. Mol. Spectrosc. **189**, 244 (1998)

[191] A. J. Ross, C. Effantin, J. D'Incan, R. F. Barrow, Mol. Phys. **56**, 903 (1985)

[192] C. Amiot, J. Mol. Spectrosc. **147**, 370 (1991)

[193] T. Ziegler, Chem. Rev. **91**, 651 (1991)

[194] B. G. Johnson, P. M. W. Gill and J. A. Pople, J. Chem. Phys. **98**, 5612 (1993)

[195] D. J. Lacks and R. G. Gordon, Phys. Rev. A **47**, 4681 (1993)

[196] S. Kristyán and P. Puláy, Chem. Phys. Lett. **229**, 175 (1994)

[197] J. M. Pérez-Jordá and A. D. Becke, Chem. Phys. Lett **233**, 134 (1995)

[198] M. B. Nardelli, Solid State Commun. **97**, 215 (1996)

[199] T. Korona, H. L. Williams, R. Bukowski, B. Jeziorski and K. Szalewicz, J. Chem. Phys. **106**, 5109 (1997)

[200] R. van Leeuwen and E. J. Baerends, Phys. Rev. A **49**, 2421 (1994)

[201] P. J. Wilson and D. J. Tozer, Chem. Phys. Lett. **337**, 341 (2001)

[202] S. Skokov and R. A. Wheeler, Chem. Phys. Lett. **271**, 251 (1997)

[203] M. Filatov and W. Thiel, Chem. Phys. Lett. **295**, 467 (1995)

[204] J. L. Durant, Chem. Phys. Lett. **256**, 595 (1996)

[205] B. J. Lynch, P. L. Fast, M. Harris and D. G. Truhlar, J. Chem. Phys. A **104**, 4811 (2000)

[206] Y. -S. M. Wu, A. Kuppermann and J. B. Anderson, Phys. Chem. Chem. Phys. **1**, 929 (1999)

[207] C. Musgrave, J. K. Perry, R. C. Merkle and W. A. Goddard III, Nanotechnology **2**, 187 (1991)

[208] D. K. Malick, G. A. Petersson and J. A. Montgomery Jr., J. Chem. Phys. **108**, 5704 (1998)

[209] E. Kraka, J. Gauss and D. Cremer, J. Chem. Phys. **99**, 5306 (1993)

[210] K. D. Dobbs, D. A. Dixon and A. Komornicki, J. Chem. Phys. **98**, 8852 (1993)

[211] S. P. Walch, J. Chem. Phys. **93**, 2384 (1990)

[212] J. Gu, Y. Xie and H. F. Schaefer III, J. Chem. Phys. **108**, 8029 (1998)

[213] G. Suzzi Valli, R. Orru, E. Clementi, A. Lagana and S. Crocchianti, J. Chem. Phys. **102**, 2825 (1995)

[214] S. P. Walch and R. L. Jaffe, J. Chem. Phys. **86**, 6946 (1987)

[215] B. Ramachandran, E. A. Schrader III, J. Senekowitsch and R. E. Wyatt, J. Chem. Phys. **111**, 3862 (1999)

[216] J. L. Durant and C. M. Rohlfing, J. Chem. Phys. **98**, 8031 (1993)

[217] S. P. Walch, J. Chem. Phys. **98**, 1170 (1993)

[218] S. P. Walch and C. M. Rohlfing, J. Chem. Phys. **91**, 2939 (1989)

[219] S. P. Walch, J. Chem. Phys. **86**, 5670 (1987)

[220] D. J. Tozer and N. C. Handy, J. Phys. Chem. A **102**, 3162 (1998)

[221] Y. Zhang and W. Yang, J. Chem. Phys. **109**, 2604 (1998)

[222] J. P. Perdew and M. Levy, Phys. Rev. B **56**, 16021 (1997)

[223] R. Merkle, A. Savin and H. Preuss, J. Chem. Phys. **97**, 9216 (1992)

[224] A. Savin, *Recent Developments and Applications of Modern Density Functional Theory*, (J. M. Seminario, Elsevier, Amsterdam, 1996), page 327

[225] S. Liu, P. W. Ayers and R. G. Parr, J. Chem. Phys. **111**, 6197 (1999)

[226] Unpublished results from Ref. [225]

[227] A. Görling, Phys. Rev. Lett. **83**, 5459 (1999)

[228] N. C. Handy, J. A. Pople, M. Head-Gordon, K. Raghavachari and G. W. Trucks, Chem. Phys. Lett. **164**, 185 (1989)

[229] D. J. Tozer, K. Somasundram and N. C. Handy, Chem. Phys. Lett. **265**, 614 (1997)

[230] M. Levy and J. Perdew, *Density Functional Methods in Physics*, (Plenum, New York, 1985) pages 11-30

[231] S. Liu, P. W. Ayers and R. G. Parr, unpublished results (1999)